Reprinted from

Volume 17, Number Chapter 8 **1987**

REVIEWS in MINERALOGY & GEOCHEMISTRY

Ore Fluids: Magmatic to Supergene

George H. Brimhall and David A. Crerar

Chapter 8

George H. Brimhall and David A. Crerar

ORE FLUIDS: MAGMATIC TO SUPERGENE

INTRODUCTION

A diverse spectrum of fluids exists in the Earth which is responsible for the transport and enrichment of ore-forming constituents including both metals and essential non-metallic species such as water, sulfur and halogens. Through their mobility and peculiar solvent characteristics, silicate magmas, aqueous fluids, and gasses may all, under particular circumstances, contribute to the mass and heat transfer involved in ore deposition. Such transport fluids, be they magmatic, gaseous, or aqueous, not only interact with wall rocks encountered along paths of migration by assimilation, thermal exchange, or hydrochemical reaction, but mutually interact themselves by phase separation as with boiling or exsolution of salt– and metal-rich magmatic water from a melt. Such release of solute-rich aqueous fluids promotes intense physical and chemical interaction of solids, aqueous fluids, and gasses and, because of enhancement of chemical mobility by complexing, results in selective metasomatic effects unsurpassed elsewhere in the Earth's crust.

In our treatment here, we have chosen to emphasize the continuum in nature in chemical and physical ore-forming processes and to develop relationships to those of common petrogenesis. Consequently, rather than writing separate chapters, we have combined our efforts into a single chapter, subdivided in three parts, beginning with the origin of ore-forming magmas and aqueous fluids in the context of crustal processes. We then develop the systematics in the physical chemistry of hydrothermal ore fluids, and end with the formation of primary ore deposits and their chemical weathering products. Metasomatic behavior is stressed.

In part, the high level of metasomatism is due to the chemical fractionation effects peculiar to fluid/fluid, fluid/rock, and fluid/solute interactions which efficiently extract ore elements from large source regions and quantitatively concentrate them in relatively small physical domains which are preserved for geological periods of time. It is the potential for such repetitive chemical focussing in the vicinity of available sources of thermal energy that drives ore-forming systems to extreme values of reaction progress and fluid-dominance. The attainment of end stages of chemical fractionation separates ores from the more common products of petrogenesis. The Earth as a thermally active planet surrounded by an oxygenated atmosphere provides ample opportunities for fractionation processes to begin internally; these ultimately are taken to completion by migrating fluids at shallow depths at or near the interface of the lithosphere and atmosphere, where chemical gradients are steep and disequilibrium common.

Many characteristics of these highly metasomatic systems such as rock permeability, porosity, redox state, and solution acidity may reach extreme values. In fact, it is now becoming obvious that constructive, that is mutually enhancing interrelationships, between such coupled factors as overall volume changes due to chemical reaction and rock permeability may be critical to attainment of ore-grade metasomatism. One reason why much more common crustal assemblages as in metamorphic rocks, indeed once considered isochemical products, have a more limited compositional spectrum than ores is that the heat and mass transport processes are themselves exceedingly more restricted in terms of time-integrated fluid and heat fluxes, solute load, permeability, and reactivity than in ore-forming systems, or at least less intense near the final stages of thermal or chemical dissipation. These ordinary crustal systems may in fact be self-limited while ore-forming systems may be runaway in comparison. Nevertheless, in many other respects the principles are identical to those governing igneous, metamorphic, and sedimentary processes within the Earth, but differ mainly in extent.

It is only now becoming possible to address rigorously such complex and interrelated physiochemical phenomena. First-principle forward modeling has largely been limited to consideration of either the chemical evolution or the fluid mechanics involved in ore transport and deposition, but not both simultaneously. Here we use the term "modeling" in a general sense, meaning any conceptualization of process based upon fundamental analytical considerations. This includes formulation of hypotheses from field, experimental, and theoretical perspectives. Given the complexity of ore deposits, recent modeling studies for the most part have had a limited scope, focussing on explaining central phenomena contributing to enrichment of metals at certain stages of the thermal, mechanical, or chemical evolution of specific types of ore deposits. While modeling has proceeded through such gross simplification, the results are nevertheless illuminating. Still, a challenging frontier remains in understanding fluid flow with chemical reaction from a theoretical, experimental, or field perspective. It is likely that insights from all three approaches will be necessary to meet the ultimate demands of the rich problems remaining in understanding ore fluids.

In this chapter we take a broad sweep through some of the processes responsible for deposition of ore and mineral deposits. We have out of necessity limited our treatment here considerably. Reviews of many relevant topics omitted here may be found in Brimhall (1987a), including magmatic ore deposits (Irvine et al., 1983), a topic neglected here altogether but one in which elegant thermo-mechanical-chemical modeling techniques have been developed. Instead, the focus here is on deposition from aqueous solutions, ranging from high-temperature fluids associated with felsic magmas, through hydrothermal systems at intermediate temperatures, down to near-surface oxidative weathering processes. We limit our analysis in this way so as to present the most complete, overall treatment of a single class of ore deposits, rather than err on the side of superficiality with a broader treatment. As a common thread, you might regard this as the local history of water-related deposits associated with a particular crystallizing pluton, from melting giving rise to a magma, its intrusion, primary mineralization, to final supergene or residual enrichment of ore metals. Metals, rather than being simply used as tracers to infer the nature of geochemical processes, are themselves the primary focus.

PART I. THE GENERATION OF MAGMAS AND ORE FLUIDS

PRE-METALLOGENIC HISTORY OF MAGMAS

It is important to keep in mind in the scenario which follows that metal enrichment does not simply begin with the emplacement of a parent pluton in the upper levels of the crust. Such localization of ore-grade concentrations of metallic compounds represents only the most recent metasomatic stage in a 4.5 billion-year history of selective enrichment of useful primordial elements in the form of ore deposits contained in preserved supracrustal environments (Hutchinson, 1981; Sawkins, 1984; Meyer, 1985). These supracrustal environments have themselves evolved considerably over geological time from the earliest Archean granite-submarine greenstone terranes through a variety of developing continental cratonic settings, up to the present plate tectonic environments at active subduction zones, continent-continent collision zones, passive continental margins, and submarine rift settings.

Ores occurring in these localized enriched states have as progenitors still earlier transport processes affecting large regions within the Earth. Within the first few hundred million years of Earth history, core/mantle interaction depleted the mantle in moderately siderophile transition metals (Fe, Co, Ni, Ag, Mo, and W) and highly siderophile metals (Au, and Pt-group metals) (Ringwood, 1979). The subsequent growth of the continental crust from the primitive mantle over a period of geological time spanning more than 3 Ga enriched the crust in incompatible rock-forming elements and ore metals (Brimhall, 1987b).

In this context ores are the outgrowths of efficient crustal fractionation processes beginning with the extraction of crustal components from the primitive mantle. Derivation and ascent of basaltic liquids enriched in incompatible elements by crystal/liquid partitioning results in formation of the oceanic crust. The relatively small mass of the crust in

relation to the mantle yields maximum enrichment factors of approximately 100 which are limited essentially by mass balance constraints. For example, consider a highly incompatible element such as Cs which is thoroughly fractionated into the magmas giving rise to oceanic crust which ultimately is reprocessed through subduction to make continental crust. Figure 1 outlines bulk continental fractionation factors from the primitive mantle from Brimhall (1987b) using estimates of the composition of the primitive mantle by Wanke et al. (1984) and continental crust by Taylor and McLennan (1985). Most ore metals are enriched in the continental crust relative to the mantle by factors which vary systematically with Period and Group in the Periodic Table, as are all the incompatible elements, indicating a clear commonality of process and governing thermodynamic control. It is clear then that crust-forming processes, specifically magma generation in the mantle is the first order control on fractionation not only of rock-forming elements, but ore metals as well. Thus the conditions under which melting occurs in the mantle become the starting point for understanding fractionation of ore metals during crustal evolution. Subsequent remelting of continental crust gives rise to highly differentiated igneous products, which extends the spectrum of ore metal enrichment to still greater extremes. Many of the fractionation processes which ultimately produce near-surface ore deposits begin with the large-scale tectonic activity of the upper mantle and crust.

GENERATION OF MAGMAS AND PLUTONS AT SUBDUCTION ZONES

It has been known for a long time now that andesitic volcanoes and porphyry copper/molybdenum ore bodies tend to occur at a relatively uniform distance from oceanic trenches and subduction zones (e.g., Sillitoe, 1972; Turcotte and Schubert, 1973). The Circum-Pacific andesitic volcanoes, for example, form the well-known "ring of fire." Figures 2 and 3 outline a commonly accepted geochemical model for this feature. We will see that water plays an all-important role at every step. Our discussion is drawn largely from a paper by Burnham (1979) which you should consult for complete details.

Oceanic zones

Oceanic crust descending in a subduction zone carries with it some water in interstitial pores and vesicles, as well as the hydroxyl component in clays and chlorites. At pressures and temperatures represented approximately by point A on Figure 2, a subducting slab should have metamorphosed to the amphibolite facies with 2.0 to 3.0 wt % water bound in amphiboles. This descends further along the average P-T conditions for subduction zones illustrated as A→B on this figure. The solidus (beginning of melting) curves labeled S(a_W = 1.0 to 0.1) show the great effect water has on the melting temperature of amphibolite: Increasing water activity from 0.1 to 1.0 (saturation) decreases the melting temperature by roughly 500°C above 10 kbar. If this rock contains no pore fluid, it will not begin to melt until it intersects the "fluid-absent" hornblende solidus (Hb-S) at B. Here hornblende reacts to produce garnet peridotite and a silicate melt of water activity ≥ 0.3 (which you can read from the solidus curve for amphibolite). For this water activity, the melt must contain ≥ 6.4 wt % H_2O; this can be achieved by melting roughly 20% of an amphibolite containing 1.5 wt % H_2O.

This melange of solid + melt might continue on down the subduction zone for several more kilometers, perhaps to point C, melting further at greater depths. Somewhere over the narrow interval between B and C the melt will begin to rise (C→D) into hotter overlying lithosphere. Because it contains more water, it will melt or assimilate the low-melting fraction of overlying rocks and will crystallize more refractory minerals (pyroxene, olivine, garnet), becoming more felsic as it rises. Burnham (1979) estimates that by the time this syntectic melt rises to point D, it will have assimilated an additional 80% of overlying lithosphere, contain about 3% water and be roughly dioritic (andesitic) in composition. Since the initial melting at point C occurs within a very narrow depth range of 75-80 km, this overall process produces hydrous calc-alkaline magmas at a uniform distance from the oceanic trench. These magmas contain sufficient water to produce explosive island arc

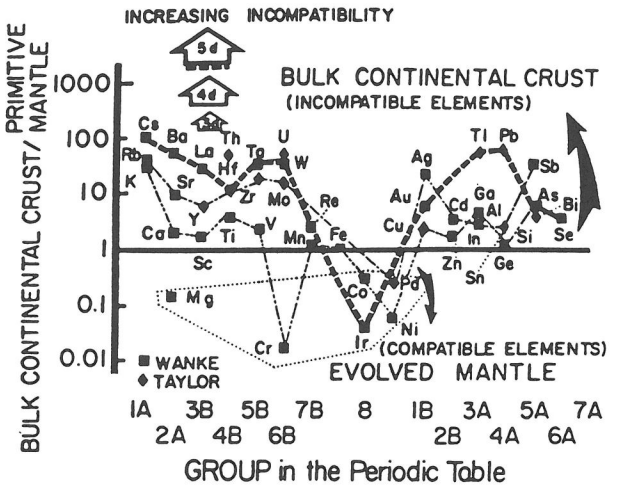

Figure 1. Bulk continental crust fractionation curves relative to the primitive mantle. Most metals are enriched in the crust by factors varying systematically with Group and Period in the Periodic Table. From Brimhall (1987b).

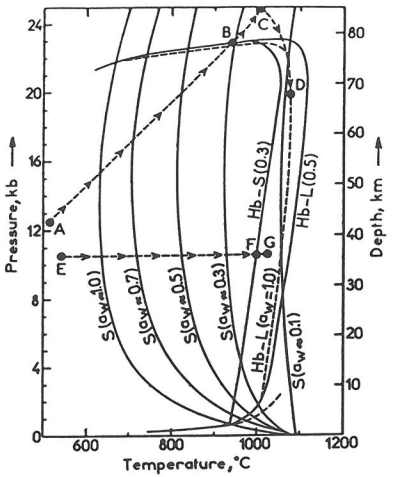

Figure 2. Melting relations for an amphibolite of olivine tholeiite composition. Curves marked S are the beginning of melting (solidus) for the water activities shown. Hb-S(0.3) is the beginning of melting for amphibolite for a mole fraction 0.3 of water in the melt. Hb-L(0.5) is the maximum stability of hornblende at a mole fraction 0.5 of water in the melt. Hb-L(a_w = 1.0) is the maximum stability of water-saturated hornblende. From Burnham (1979).

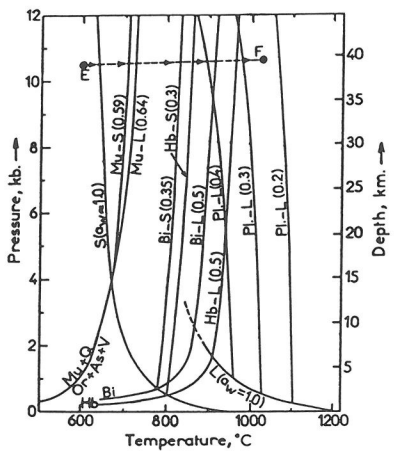

Figure 3. Melting relations for average hornblende-biotite-granodiorite composition. The curve Mu + Q = Or + As + V is the upper stability of muscovite + quartz. S(a_w = 1.0) and L(a_w = 1.0) are the water-saturated solidus and liquidus (plagioclase), respectively. Curves Mu-S, Bi-S and Hb-S are the fluid-absent solidi for assemblages containing muscovite, biotite and hornblende, respectively. The curves Mu-L, Bi-L, Hb-L and Pl-L are approximate thermal stabilities (liquidi) of muscovite, biotite, hornblende and plagioclase, respectively. Numbers in parentheses on each curve are the mole fraction of water in the melt. From Burnham (1979).

volcanism and associated hydrothermal deposits, as we shall see below.

Continental zones

The above process occurs under oceanic lithosphere. By contrast, the path E-F-G on Figure 2 represents intrusion of mafic magma at 1200°C into amphibolites underlying continents. Here the primary role of mantle-derived mafic magmas is simply to provide the heat to partially melt and assimilate deep crustal rocks. A mafic, water-poor magma intruded at 1200°C into lower amphibolitic crust at 40 km and 600°C can raise the temperature of equal proportions of magma plus (crustal) amphibolite above 1025°C (point G)—just above the solidus (F) for dry amphibolite. This can produce an anatectic melt (of roughly 50% the mass of the intruding magma) containing 3% H_2O, with the composition of a quartz diorite. Once again, the melt will rise while olivine, pyroxene and calcic plagioclase crystallize and sink, and H_2O-rich amphibolite melts at the top of the magma chamber.

Figure 3 illustrates what happens if the same mafic magma (at 1200°C) rises into a felsic granodioritic gneiss in deep continental crust (containing quartz, muscovite, biotite, plagioclase, orthoclase and amphibole). Starting at the same P-T conditions (point E), melt will appear at 710°C (muscovite solidus) containing 0.59 wt % water. If this melt rises without significant cooling, it could reach depths as shallow as 10-15 km before crystallizing (at the intersection with the solidus for water saturation, $a_W = 1.0$). Because the melt is water-saturated ($a_W = 1.0$) when it crystallizes, it could produce pegmatites (where large silicate crystals appear to have grown into immiscible aqueous bubbles in the silicate liquid). This is our first example of an aqueous ore fluid of magmatic origin. Pegmatites are frequently mined for elements which are incompatible in crystallizing silicates and are left behind to crystallize out in residual aqueous phases: examples are the rare earths (lanthanides), the actinides, and other anomalies such as tantalum minerals, boron in tourmaline, beryllium in beryl, and lithium-rich micas and pyroxenes.

If heating continues in Figure 3 on to point F, biotite, hornblende and plagioclase will melt in succession. This magma could reach a depth of less than 2.0 km before crystallizing (if it rises without significant cooling); for example, a magma at the intermediate temperature of 820°C will have melted muscovite, then biotite, and if it rises adiabatically it will not intersect the solidus (S for $a_W = 1.0$) until about 2 km; note that at this point it becomes water saturated ($a_W = 1.0$). Thus, granitic to dioritic magmas containing 3.0-9.0 wt % H_2O can be generated by intrusion of mafic mantle melts into lower crustal rocks. If these felsic magmas rise without significant cooling, they will not crystallize (intersect the solidus) until depths of several km, at which point they may become water saturated.

Figure 4 provides a closer look at the specific conditions which release water from a cooling felsic magma. This comes from the experimental phase equilibrium studies of Whitney (1975), and the figure represents a quartz monzonite system containing 3 wt % total water. Notice that at pressures greater than P2, aqueous vapor (V) and silicate liquid can coexist only over the very narrow temperature range of the field labeled Pl+Af+Q+L+V. Between P2 and P1 vapor and liquid coexist over a slightly wider field (including Pl+Af+L+V). However, below P1, aqueous vapor and silicate liquid coexist over the entire range of temperatures from approximately 720°C on up beyond 1200°C; under these conditions a felsic magma can be expected to become saturated in water and to exsolve or give off water as it crystallizes. A monzonitic magma containing 3 wt % water rising from depth will begin to exsolve copious water at P1 = 1 kbar, at a depth of about 3.5 km. The same thing will happen to a similar magma containing 4 wt % water at 1.3 kbar or about 4.5 km.

We emphasize that this evolution of water only occurs at fairly shallow depth, within the upper few kilometers of the Earth's crust. Also, most of the water originally contained in the magma must be given off as the system cools and crystallizes, because most felsic rocks contain <1 wt % water (as hydroxyl in micas and amphiboles). This means that an absolutely enormous quantity of water can be given off by a cooling magma. For example,

a felsic magma of 1 km^3 volume containing 3 wt % water would exsolve approximately 10^8 metric tons of water as it solidified at shallow depth.

CLASSES OF ORE-FORMING PLUTONS

A critical question to ask about the aqueous magmatic fluids released from crystallizing plutons is whether or not there is significant diversity in their composition. There are certainly distinctive groups of base metal ores related to felsic magmas, indicating the existence of some major differences in overall processes between families of ore deposits. This may be attributable to essential differences in plutons and the ore-forming fluids specific to them.

In general, base metal ores related to plutons fall into three types. First, porphyry copper deposits related to granodiorites or diorites may have either molybdenum or gold as byproduct metals, depending upon whether the local tectonic setting is predominantly continental or oceanic, the former being relatively evolved chemically, the latter, primitive (Kesler, 1973; Hollister, 1978). Secondly, porphyry molybdenum deposits, often accompanied by a suite of highly lithophile trace metals W, Sn, Be, Zn, and Li, are related to highly differentiated silicic rhyolitic magmas of totally continental derivation (White et al., 1981, Barton, 1987; Christiansen and Lee, 1986). Thirdly, tin or tungsten deposits often form in association with true granites (Lehmann, 1982; Taylor, 1979).

These three types of mineralization are fundamentally distinct, raising the question whether the differences are due to the respective inheritance of metal suites or to other factors subsequent to formation of the magma body, such as composition of exsolved magmatic aqueous fluids and gasses. The latter possibility may depend on earlier processes affecting magmas on their ascent, such as assimilation or fractional crystallization. It is therefore essential to recognize and accurately interpret the salient differences between parent magmas for the three main types of base metal ore deposits related to plutons. It is logical to begin the analysis of this complex problem by examining the characteristics of magmatic source rocks as these attributes may constitute the primary difference, not only in terms of metal endowment, but physiochemical effects which are peculiar to pluton types.

Magmatic source rocks

Burnham (1981) outlined a number of physiochemical factors relating hydrothermal mineralization to intrinsic characteristics of parent magmas. These factors included water content, temperature or heat content, metal content, chlorine content, sulfur content, and oxidation state. He argued that each of these constraints is imposed differently on porphyry magmas by each of three magmatic source rocks assumed to exist in the source regions of partial melting. The critical source rocks are interpreted to be (1) hornblende-bearing mafic rocks, (2) biotite-bearing rocks of intermediate composition, and (3) muscovite-bearing metasedimentary rocks.

Utility of biotite mineral chemistry. Further support for Burnham's interpretation has come from mineral chemistry studies, particularly those of biotite, a hydrous mineral which reflects the relative fugacities of HF, HCl, O_2, H_2 and water during crystallization (Wones and Eugster, 1965; Munoz and Swenson, 1981; Munoz, 1984; Brimhall et al., 1985; Ague and Brimhall, 1987, 1988a,b; Brimhall and Ague, 1988), thereby contributing simultaneously to understanding several of the factors expressed by Burnham. The prime utility of biotite in this context is that it enters into equilibrium relationships with other common rock-forming minerals such as alkali feldspar and magnetite and thus buffers O_2 fugacity (Wones and Eugster, 1965), and hence oxidation state, while simultaneously reflecting the concentration of halogen species and water (Munoz, 1984). As a complex solid solution crystallizing from both magmas and high-temperature hydrothermal fluids, the substitution of F and Cl for OH which surround Mg and Fe in close octahedral coordination, makes biotite ideally-suited to serve this useful purpose in monitoring intensive variables in magmas and exsolved aqueous fluids from the magmatic stage to early hydrothermal processes

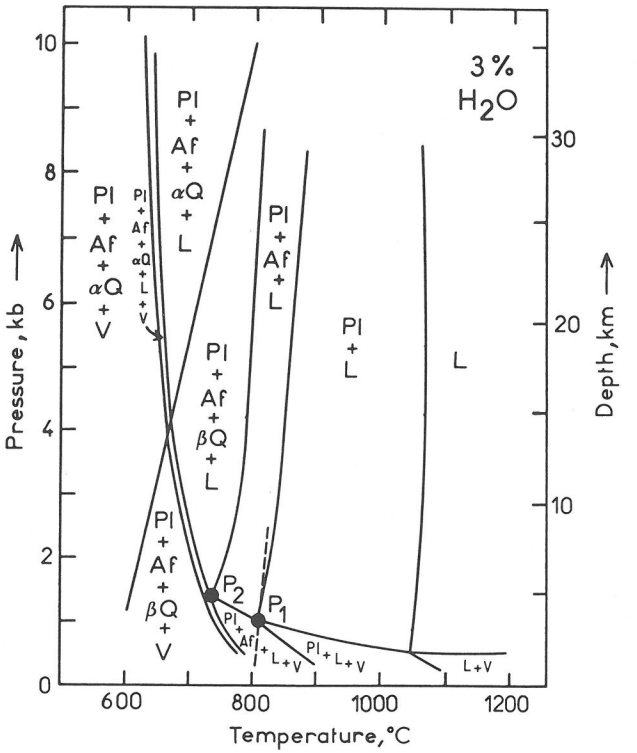

Figure 4. Phase diagram for synthetic quartz monzonite composition with magmatic water content of 3 wt %. The symbols Pl, Af, Q, L and V refer to plagioclase, alkali feldspar, quartz, liquid silicate, and water vapor, respectively. From Whitney (1975).

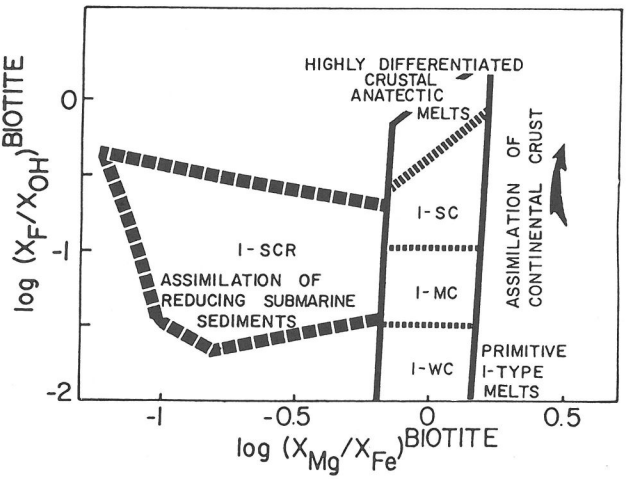

Figure 5. Summary of igneous biotite compositions within the batholiths of California. Highly differentiated crustal anatectic melts are from Colorado. From Brimhall and Ague (1988). Classification scheme of plutons uses biotite composition. I-scr type plutons are strongly contaminated and reduced through the assimilation of graphitic metasediments. The I-wc to I- sc trends are normal plutonic types from primitive oceanic crust-derived melts to strongly contaminated magmas derived from the pre-Cambrian crust or highly contaminated with continental crust.

responsible for the initial release of ore metals from the parent magma.

Using the X_{Mg} and X_F of alteration hydrothermal biotite in this capacity, Munoz and Swenson (1981) proved that there were in fact substantial differences in the HF/HCl fugacity between porphyry copper and porphyry molybdenum deposits pointing out, for the first time, quantitative thermodynamic differences between the geochemical evolution of such magmatic-hydrothermal systems at the hydrothermal stage. By considering biotite compositions more broadly in terms of X_F/X_{OH} and X_{Mg}/X_{Fe} it was demonstrated by Brimhall et al. (1985) that igneous biotite compositions, in distinction to hydrothermal products, are grouped into three main classes which each correlate with a distinct type of base metal ore deposit.

Hornblende, biotite, and muscovite. Both porphyry molybdenum deposits and porphyry Cu deposits have igneous biotites with nearly equal mole fractions of Mg and Fe, but the former have a much higher X_F/X_{OH} in biotite. In contrast, tungsten and tin deposits have magmatic biotites with much lower Mg contents reflecting relatively low oxygen fugacity. This correspondence of ore metal type and biotite composition serve to illuminate the source rocks involved in the genesis of ore-forming magmas. F-rich biotites probably reflect the melting of biotite-bearing gneisses in the pre-Cambrian craton of North America which gives rise to porphyry molybdenum deposits derived exclusively from highly fractionated radiogenic continental materials. Melting of mafic amphibolites with a correspondingly lower F content may form the parent magmas of porphyry copper deposits. The ferruginous nature of biotites in tungsten and tin deposits indicates relatively reducing conditions which have been ascribed to anatexis of pelitic metasedimentary rocks, often containing graphite. Burnham and Ohmoto (1980) have demonstrated that the redox lines of descent of these magma types are distinct, and accompanied by differences in the concentration of carbon and sulfur species.

A single orogenic belt in which major ore deposits occur can contain plutons of several types differing markedly in their biotite mineral chemistry. Field relationships are necessary to interpret the significance of the differences. Granitic batholiths of the Circum-Pacific region have received intense study and serve a useful purpose in illustrating the fundamental differences between pluton types and the controlling geological factors.

Classification by redox state and biotite halogen composition

Figure 5 shows the spectrum of biotite compositions from the granitic batholiths of California which range in composition from quartz diorites on the western oceanic side to true granites on the eastern continental side where plutons have intruded great thicknesses of pre-Cambrian continental crust. The primary variable in biotite composition used in this classification (Brimhall et al., 1985; Ague and Brimhall, 1987, 1988a,b) is $\log(X_F/X_{OH})$ which increases from a value of −2.0 in biotite from primitive mafic rocks (quartz diorites) to a high of 0.0 for the most felsic granites, with a range of a factor of 100 variation in X_F/X_{OH}, from 0.01 to 1.0. In reference to the inferred amount of interaction or derivation from the pre- Cambrian craton, the variations in these I-type plutons have been referred to as I-wc (weakly contaminated), I-mc (moderately contaminated), and I-sc (strongly contaminated). I-wc, I-mc, and I-sc pluton types define elongate belts parallel to the edge of the pre-Cambrian craton of North America (Ague and Brimhall, 1987). Well within the craton, for example in Colorado, highly differentiated crustal anatectic melts contain biotites with the highest F content studied.

The ratio $\log(X_{Mg}/X_{Fe})$ in biotite in I-wc, I-mc, and I-sc plutons remains essentially constant at a value near zero. However, a distinct type of pluton, I-scr (strongly contaminated and reduced) contains biotite with much lower ratios. Such plutons in California and elsewhere, for example Japan, occur only where plutons intrude graphite-bearing pelitic metasedimentary wall rocks. These special plutons are generally peraluminous, bearing muscovite and, rarely, garnet, and often contain ilmenite as the main Fe-Ti oxide in contrast to magnetite and ilmenite in the I-wc to I-sc series. The distribution of I-scr types is con-

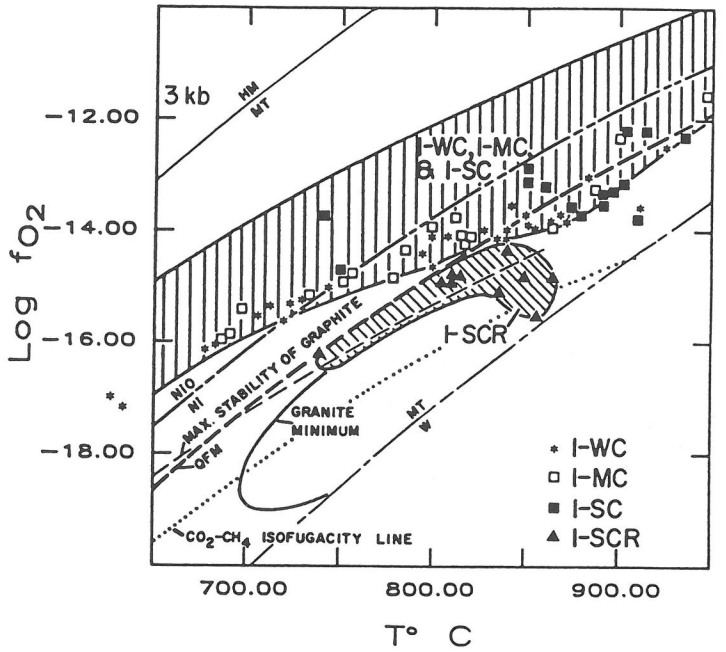

Figure 6. Calculated variation cf oxygen fugacity with temperature for I-wc to I-sc plutons in comparison to I-scr types. Based upon the ilmenite- granite buffer equilibria of Ague and Brimhall (1988b).

trolled solely by the nature of pre-batholitic wall rocks.

Classification of granitic plutons by intensive variables

Use of biotite mineral chemistry to subdivide distinct types of granitic plutons provides a simple means of extending their characterization to include ranges in intensive variables of importance to interpreting controls on mineralization. Through equilibrium rock-forming mineral assemblages and experimental activity-composition relations for biotite (Munoz, 1984), Ague and Brimhall (1988b) transform observed igneous biotite compositions in terms of X_{Mg}/X_{Fe} and X_F/X_{OH} into calculated values of oxygen fugacity and fugacity ratio of HF to H_2O. Thus a direct comparison between plutons may be made based on fugacities of HF/H_2O and O_2, intensive variables of thermodynamic significance.

Oxygen fugacity. Granitic plutonic rocks, in contrast to their extrusive equivalents which cool rapidly upon air quenching after eruption, have Fe-Ti oxide compositions which are affected by sub-solidus re-equilibration during slow cooling. Plutonic magnetite is generally pure Fe_3O_4, having lost its Ti content through diffusion during cooling. However, ilmenite is affected much less severely than magnetite by re-equilibration, and may be used to estimate oxygen fugacity of plutons. This is accomplished by modifying the granitic rock oxygen buffer equilibria of Wones and Eugster (1965) to use the hematite (Fe_2O_3) component of ilmenite instead of magnetite (Fe_3O_4). The equilibrium from (Ague and Brimhall, 1988b) is:

$$\text{annite} + 0.75\,O_{2(gas)} = \text{alkali feldspar} + 1.5\ \text{hematite} + \text{water}$$

Compositional data on biotites and ilmenites from plutons of the batholiths of California provide both oxygen fugacity and temperature estimates shown in Figure 6 from Ague and Brimhall (1988b). I-scr plutons crystallize at much lower oxygen fugacities than I-wc, I-mc, or I-sc plutons. The latter three types generally cluster along the Ni-NiO buffer,

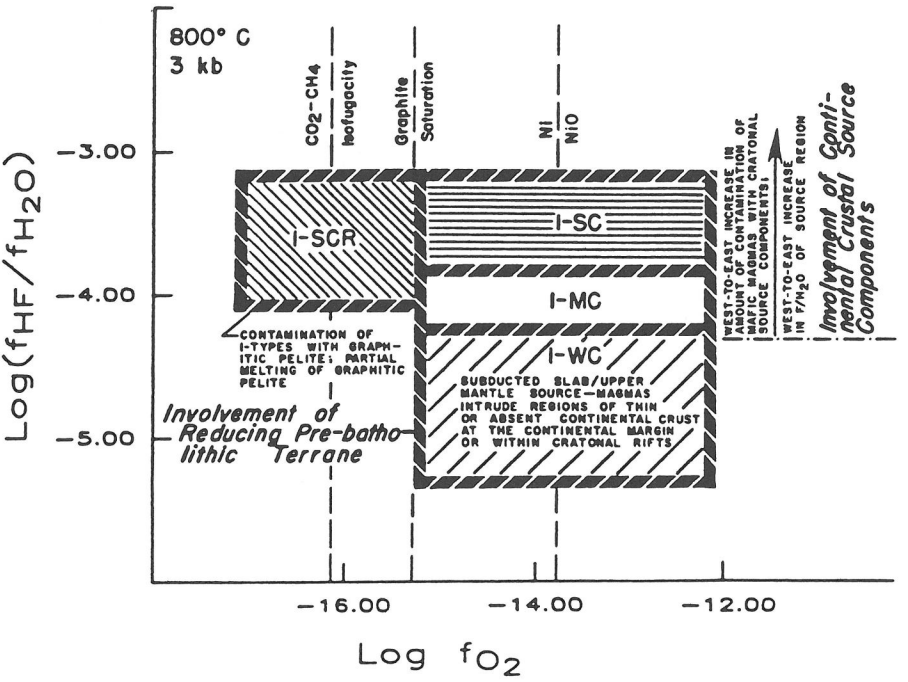

Figure 7. Calculated gas fugacities assuming a total pressure of 3 kbar and 800°C. From Ague and Brimhall (1988b).

below magnetite-hematite and above quartz-fayalite-magnetite. I-scr plutons have oxygen fugacities between quartz-fayalite-magnetite and the isofugacity curve of CO_2-CH_4, falling generally in the realm of the granite melting minimum in the presence of graphite as calculated by Ohmoto and Kerrick (1977); this supports the conclusions of Burnham and Ohmoto (1980) that some S-type (sediment-derived) granites cool along the latter gas buffer curve. I-scr type plutons are distinct from I-wc, I-mc, and I-sc types in terms of oxygen fugacity trends, and crystallize at much lower values, probably in equilibrium with graphite. It is likely that at least some of the I-scr plutons are in fact derived by partial melting of graphitic and pelitic wall rocks which gives rise to the peraluminous character of these plutons.

HF/H_2O fugacity. Using activity-composition relations of Munoz (1984), biotite compositions expressed in terms of X_F/X_{OH} may be interpreted as fugacity ratios of HF/H_2O. In Figure 7 we present these calculations (from Ague and Brimhall, 1988b) at crystallization conditions of 3 kilobars and 800°C. The separation of pluton classes in terms of fugacities of HF/H_2O and O_2 is clear. The oxygen fugacity trend of the I-wc to I-sc plutons along the Ni-NiO buffer is similar to common temperature-oxygen fugacity curves derived for volcanic rocks using magnetite-ulvospinel and ilmenite-hematite Fe-Ti oxides (Carmichael et al., 1974). It is clear then that with the exception of the reduced I-scr plutons, the I-wc to I-sc types do have extrusive equivalents. The I-scr plutons are distinct from the main igneous trends.

Correlation of ores with plutonic classes

In Figure 8 we show the compositions of biotites from mineralized plutons. Igneous and hydrothermal biotites from the three ore types Cu, Mo, and W are depicted (Brimhall and Ague, 1988). Included are data for porphyry copper deposits: Santa Rita, New Mexico (Jacobs and Parry, 1979) and Butte, Montana, the Henderson Colorado porphyry molybdenum deposit (Gunow et al., 1980), and two tungsten deposits (Pine Creek and Strawberry). For comparison, the biotite data from the unmineralized plutons of the California batholiths, and the Magnetite and Ilmenite Series of Japan (Ishihara et al., 1979) using data from

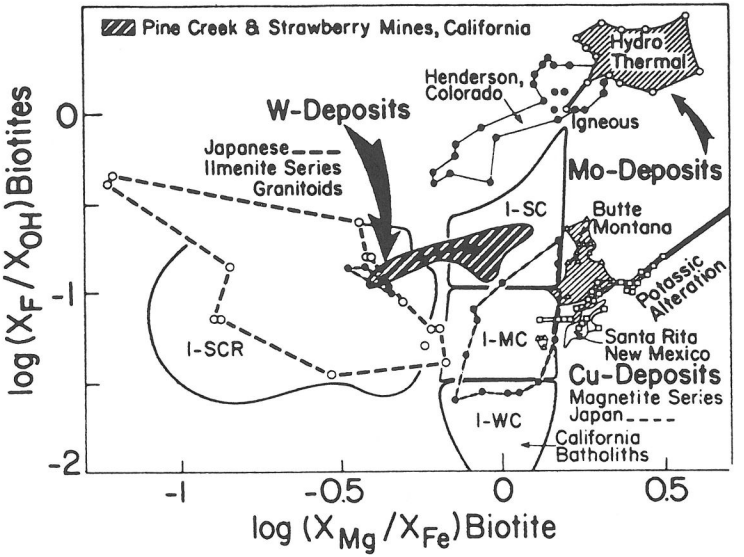

Figure 8. Comparison of hydrothermal biotite compositions with igneous biotites. Hydrothermal biotites form arrays with a positive slope extending away from the composition of the local igneous biotite composition. Hydrothermal biotites are shown for three types of base metal ore deposits related to porphyries; W, Mo, and Cu. The Japanese Ilmenite and Magnetite Series plutons are shown in comparison to the California batholiths. From Brimhall and Ague (1988).

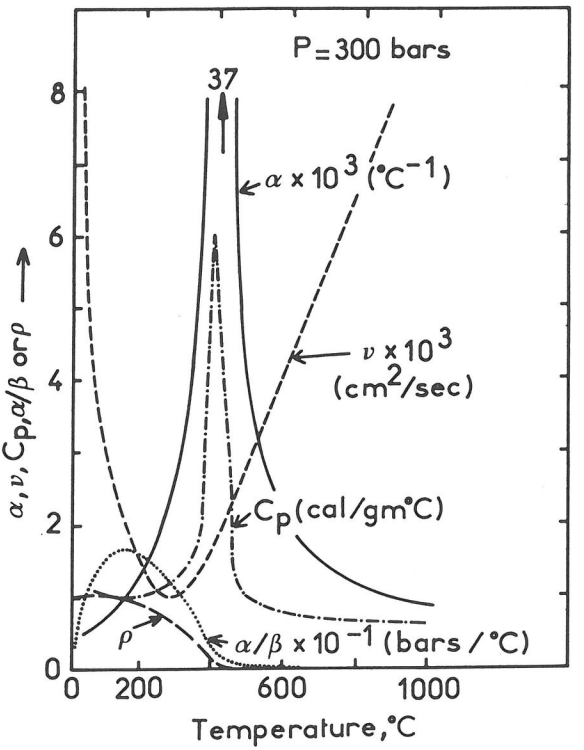

Figure 9. Physical properties of pure water at 300 bars versus temperature. The symbols α, β, ρ, C_p, and ν refer to coefficients of thermal expansion and compressibility, density, heat capacity and viscosity, respectively. From Norton (1984).

Czamanske et al. (1981) are shown. It is clear that assuming similar crystallization conditions, Cu, Mo, and W deposits are characterized by distinctive igneous biotite compositions, and hence by distinct values of oxygen and HF/H_2O fugacity. Both Mo and Cu systems are in general much more oxidizing than W deposits, a conclusion consistent with recent experimental studies indicating inverse dependence of scheelite and cassiterite solubilities with oxygen fugacity (Wilson and Eugster, 1984; Haselton and D'Angelo (1986). While having generally the same redox state, Mo systems are more fluorinated than Cu deposits, consistent with the radiogenic character of the parent rhyolitic intrusives derived from biotite gneiss of the pre-Cambrian craton.

Hydrothermal biotites form arrays extending away from the compositions of local igneous biotites, and in general are richer in magnesium and fluorine. Interpretation of this effect will follow a consideration of the composition of magmatic water and its release from plutons.

Physical implications of magmatic water

Energy release. The range of water concentrations of felsic magmas as estimated by Burnham (1979) is 2.5 to 6.5 wt % with a median close to 3.0%. The lower limit is necessary to produce biotite or hornblende, and the upper limit corresponds to saturation at 2.1 kbar or 8 km depth. As water exsolves from a melt, it undergoes a considerable change in volume. For example the partial molar volume of water in a silicate (albite) melt as measured by Burnham and Davis (1971) is 22 cm^3 $mole^{-1}$ at 800°C, 1kbar, while the molar volume of pure water at the same T and P is 78 cm^3 $mole^{-1}$ (Burnham et al., 1969); under these conditions, water expands 3.5 times as it exsolves from a magma. The total change in volume of the reaction H_2O-saturated melt $\rightarrow$ crystals + vapor generates tremendous P-V mechanical energy, on the order of 10^{16} J km^{-3} of magma. This is the approximate explosive energy of a 10 megaton bomb for each km^3 of magma -- for details, see Burnham (1979, 1985). The most spectacular consequence is explosive volcanism, such as the Mount St. Helens blast of May 18, 1980 which was equivalent to a 400 megaton explosion (Decker and Decker, 1981). More important for ore emplacement, less cataclysmic release can cause intense fracturing, brecciation, void volumes, and extensive comminution of the solidifying magma. Ore deposits (such as porphyries) associated with large plutons are commonly mineralized at scales ranging from large veins and breccia zones down to microscopic dissemination in finely comminuted host rock. Explosive volcanism is rare relative to this latter type of fracture release because the tensile strength of typical igneous wall rocks is only on the order of 100 bars (corresponding roughly to 1000 J kg^{-1}).

Hydrothermal convection. The intrusion of any heat source such as a magma into fluid-rich crustal rocks will generate convection cells, irrespective of whether magmatic fluid is released or not. The energetic release of magmatic water will intensify convection by increasing permeability and acting as an upward-moving, high-temperature plume. Some of the properties of pure water that guide its behavior in such systems are summarized in Figure 9, from Norton and Knight (1977) and Norton (1984). This is particularly interesting because it shows a near coincidence of conditions favorable for convection in the vicinity of 300°-400°C: maximum heat capacity and minimum density (promotes buoyant force and heat-carrying ability); minimum viscosity; and a maximum ratio of thermal expansivity to compressibility (develops maximum pressure per unit increase in temperature). This demonstrates that a hydrothermal fluid exerts considerable control over its own P-V-T conditions in a convecting system. It also suggests that the temperature range 300°-400°C provides optimal convective behavior, and might partly explain why temperatures measured in the most active ocean ridge vents often fall within this range.

There is certainly no dearth of hydrologic models for hydrothermal convection around magmatic systems (see, for example, Cathles, 1977; Norton and Knight, 1977; Norton, 1978; Henley and McNabb, 1978; and Norton, 1984, on convection around plutons; and Fehn, 1986; and Fehn and Cathles, 1986, on multiple convection cells at oceanic spreading centers). These models all have in common the entrainment of groundwaters within the

convection cell, and some do not consider magmatic waters at all. Other models include provision for boiling or vapor formation, and we illustrate one of these by Cathles (1977) in Figure 10. This represents the behavior of a pluton 0.75 km in half-width, 2.25 km high, intruded at 700°C to a depth 2.75 km below the surface assuming a uniform permeability of 0.25 millidarcies. Free flow of water is permitted at the surface (as hot springs and as groundwater recharge). Initial discharge of magmatic water is not considered, so the model is conservative. The diagram shows a cap of vapor above the pluton which reaches a maximum for these conditions after 5000 years. This is formed by boiling if the fluid is sufficiently NaCl-rich to remain subcritical. This vapor phase rises and disappears after 10,000 years for these conditions and convection dies out in less than 100,000 years. The convection cell includes considerable entrained groundwater and total flow would be 250 kg water/cm^2 through the top of the pluton in the 10^4 year lifetime of this system. Cathles shows by simple mass balance that this flow is sufficient to leach 0.05 wt % Cu from the intrusive and concentrate it in an ore shell 1 km deep and 200 m thick of grade 0.43 wt % Cu, provided solubility exceeds 1000 ppm Cu, and suitable deposition mechanisms can be invoked. We will see below that these conditions are not unreasonable, particularly if initial magmatic water is included in the picture.

Active hydrothermal convection has now been observed at many sites along oceanic spreading centers, as illustrated, for example, by upwelling vents such as the celebrated 21°N "Black Smokers." Recently, downward circulation of hot, chloride– and metal-rich brines has been observed in crater lakes of active volcanoes, providing a potential for ore generation within volcanic stockworks (Brantley et al., 1987).

Lifetimes of hydrothermal systems

The general lifetime of hydrothermal ore-forming systems is not well known because radiometric dating techniques are insufficiently precise to date the beginning and end of deposition. Skinner (1979) suggests that 10^6 years is an upper limit for porphyry coppers, simply because some known deposits in the Pacific are about that old. He notes that seafloor hydrothermal deposits of the Kuroko and Cyprus type probably formed in several thousand years because they contain little sedimentary detritus. Observation of active seafloor vents seems to indicate that these change almost daily, but that large systems such as the Guaymas basin and Red Sea brines may persist for periods of 10^2 to 10^3 years at least. Theoretical models of convection also indicate relatively rapid formation ($<10^4$ years) as we have just seen.

SOURCES AND GENERAL COMPOSITIONS OF HYDROTHERMAL SOLUTIONS

Sources of water

The question of source has been debated by economic geologists for over a century. In fact, Skinner (1979) managed to find comments on the subject by Agricola (who favored meteoric water) and Descartes (a magmatist of sorts).

Aside from magmatic and entrained groundwater, it is also certain that seawater convects at oceanic spreading centers, perhaps to depths on the order of 7–10 km (the thickness of the oceanic crust). There is also considerable evidence in metamorphosed terrains suggesting that hydrothermal waters could have been produced by metamorphic dehydration reactions (Henley et al., 1976; Fyfe and Kerrich, 1984; Henley, 1985).

The greatest success in differentiating magmatic and meteoric water sources has come from oxygen and hydrogen isotope analyses. Figure 11 is a now quite familiar compilation of data for different ore deposits by Taylor (1979) showing the fields of meteoric and primary magmatic water. A complication with these diagrams is that many groundwaters of meteoric origin react with rock-forming minerals to become enriched in ^{18}O, which moves them to the right of the meteoric line. However, you can see from this diagram that some deposits such as the Kuroko ores must have formed predominantly from heated seawater;

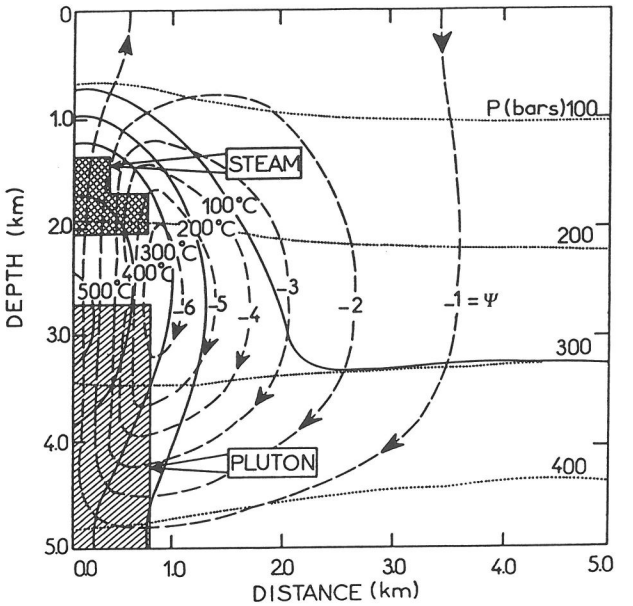

Figure 10. Convective behavior of pure water around a pluton 0.75 km in half-width, 2.25 km high, intruded at 700°C to a depth 2.75 km beneath the surface, assuming uniform permeability of 0.25 millidarcies, and calculated for a period 5000 years after intrusion. Free flow of water is permitted in and out of the surface. The shaded area above the pluton represents a region of vapor-like fluid, and would be generated by boiling in systems containing >10 wt % total dissolved salts. Temperature and hydrostatic pressure are contoured, and streamlines are given in units of cm^2/sec flow. From Cathles (1977).

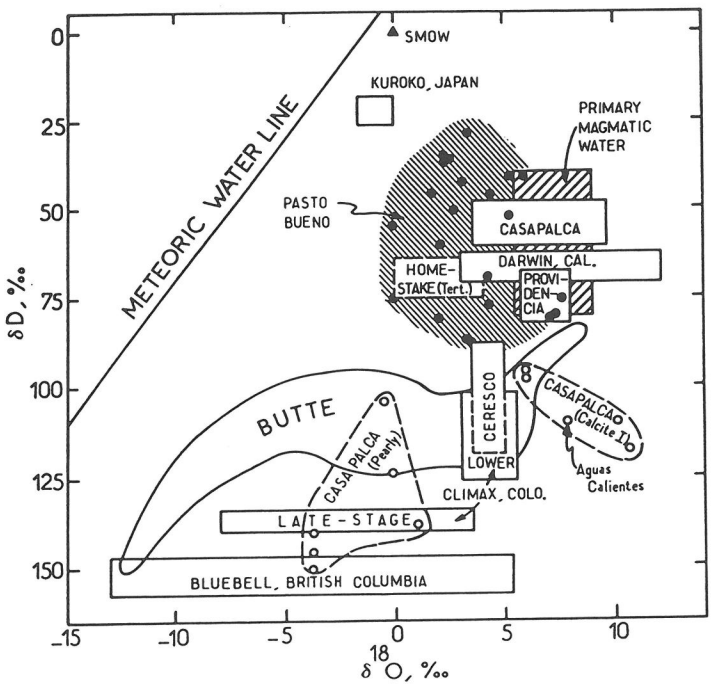

Figure 11. Hydrogen versus oxygen isotope plot showing observed values of hydrothermal fluids in a variety of ore deposits. SMOW is standard mean ocean water, and the fields of meteoric and magmatic water are delineated. Compilation by Taylor (1979).

Bluebell appears to have formed from a meteoric source; other deposits such as Homestake and Providencia were predominantly magmatic; and a third class started as predominantly magmatic and evolved to late-stage hydrothermal waters of meteoric origin (Casapalca, Climax, Butte).

Because of this variety of possible sources it is inappropriate to associate the term "hydrothermal solution" with waters of any one origin. Instead, take the word in its literal sense to mean any natural hot water.

Composition

The compositions of ore-forming hydrothermal solutions vary widely, but all can be thought of as brines with total dissolved solids ranging from roughly 1 to 50 wt %. The major components are generally Na, K, Ca and Cl, with lesser concentrations of Mg, Br, SO_4, H_2S, CO_2 and possibly NH_3 at concentrations frequently exceeding 1000 ppm. Ore-forming metals may be present in concentrations ranging from <1 ppm to >1000 ppm. The pH generally falls within 1-2 units of neutral; more acidic conditions predominate for many ore deposits, while many active geothermal systems are slightly basic. Barnes (1979) suggests that the most common, idealized ore-forming solution might have the following properties: 1m Cl^-, 0.1m carbonate, <0.1m total dissolved sulfur (H_2S or HSO_4^-), 0.01m NH_4^+ and pH 1 unit acid from neutral. It is commonly presumed that such solutions must contain at least 1 to 10 ppm of a dissolved metal to deposit potential ore. Very high concentrations (>10,000 ppm) of metals such as Fe, Cu, Mn and Zn have occasionally been observed in fluid inclusions (Roedder, 1979; Kwak et al., 1986), usually in more saline and/or higher temperature samples.

The observed compositions of hydrothermal solutions have been compiled by: Skinner (1979) and Barnes (1979) (hydrothermal, ore-forming); Ellis and Mahon (1977), Ellis (1979), Weissberg et al. (1979), Henley et al. (1984) and Henley (1985) (geothermal, typically sub-economic); and Von Damm et al. (1985 a,b) (hydrothermal vents at oceanic spreading centers).

COMPOSITION OF MAGMATIC WATER

As a hydrothermal solution exsolves from a cooling magma it will take with it any components that preferentially concentrate in aqueous rather than silicate fluids. This includes most highly volatile species, all electrolytic salts and many transition (and other) metals. Experimental data so far indicate that this is an extremely important fractionation process, capable of transporting many ore-forming components.

Water solubility in silicate melts

The primary volatile components of late-stage magmas include H_2O, H_2S, HCl, HF, CO_2, CH_4, SO_2 and H_2. Preliminary experimental results quoted by Burnham (1979) suggest that the solubilities of H_2O, H_2S and HCl in granitic melts are comparable and high. These should all be expected to fractionate strongly into an exsolving aqueous phase, because they are similar, strongly polar small molecules, fundamentally different from the large, polymerized structural units of silicate melts.

The first, obvious question is whether water is really significantly soluble in silicate melts. If so, then presumably other volatile, polar molecules important to ore-formation such as HCl and H_2S may behave similarly. In fact, water is extremely soluble in magmas covering the entire composition range from basaltic to pegmatitic as shown in Figure 12 from Burnham (1975). The larger plot expresses water solubility in these different rock types normalized against the molecular weight of albite (according to rules described by Burnham). The surprising feature here is that a silicate melt can actually contain more moles of water than silicate since 14 wt % H_2O (maximum measured solubility on the insert) is 70 mole % relative to albite. Note the strong pressure dependence; as pressure

drops, water solubility falls causing exsolution at near-surface pressures as already observed in Figures 2 to 4.

Partitioning of ore components between magmas and exsolving water

Fractionation of different components between felsic melts and exsolving aqueous fluids has been studied by Kilinc (1969), Kilinc and Burnham (1972), Holland (1972), Flynn and Burnham (1978), Webster and Holloway (1980), Carron and Lagache (1980), Manning (1981), and Candela and Holland (1984, 1986).

Chloride and sulfur. The early experimental work by Kilinc (1969) and Kilinc and Burnham (1972) showed that chloride partitions very strongly from felsic silicate melts into coexisting aqueous fluids. They observed molal partitioning coefficients ($m_{Cl,aq}/m_{Cl,melt}$) of 43, 85, and 13 at 2, 6 and 8 kbar, respectively. Unpublished results by Kilinc (1969) show a similar fractionation of H_2S. If the granodioritic gneiss of our previous example (Fig. 3) with 3.0 wt % H_2O contains a conservative 0.1 wt % Cl, the first-formed aqueous fluid (0.6 kbar, 2 km depth, 90% melt) would contain 4.6 wt % Cl; at 8 km depth (2.1 kbar) exsolution of water begins only when the magma is 53% crystallized, and first-formed waters here should contain 7.5 wt % Cl (Burnham, 1979).

The quenched pH of these and similar experiments by Holland (1972) were very low with median values about pH=2. This is presumably due to strong fractionation of HCl from melt to aqueous fluid. This fractionation has been interpreted by Eugster (1985, 1986) as hydrolysis of NaCl dissolved in the melt:

$$2NaCl_{melt} + H_2O_{fluid} \rightarrow HCl_{fluid} + Na_2O_{melt} \quad .$$

As we shall see below, HCl and other electrolytic components are highly associated as neutral species (HCl°) at magmatic temperatures, and under these conditions, the solutions are probably not far from neutral pH. However, as temperature falls HCl and similar components ionize, becoming strong acids. Thus, chloride partitioning into the aqueous fluid provides a complex-forming ligand for metal transport as well as acid potential. We will see that this acidity increases metal solubility at higher temperatures, and as temperature falls it causes wall rock alteration and concomitant metal precipitation. The partitioning of sulfur is important for similar reasons: it too becomes acidic at lower temperatures, can serve as a possible complex-forming ligand, and is obviously necessary for deposition of metallic sulfides (and sulfates such as barite and anhydrite).

Cations and metals. Experiments by Holland (1972) showed that partitioning of both Na and K from melt to aqueous vapor varies linearly with the total Cl concentration of the vapor. The molal partitioning coefficients for melts of granitic composition are: $m_{Na,aq}/m_{Na,melt} = 0.46\ m_{Cl,aq}$, and $m_{K,aq}/m_{K,melt} = 0.34\ m_{Cl,aq}$. A similar result was obtained by Candela and Holland (1984) for monovalent Cu, for which $m_{Cu,aq}/m_{Cu,melt} = 9.21\ m_{Cl,aq}$.

The divalent cations Ca, Mg, Zn and Mn also partition into the aqueous phase with Mn and Zn being most strongly concentrated (Holland, 1972). For these four cations, the partitioning coefficients increase more rapidly than the first power of Cl concentration: $m_{i,aq}/m_{i,melt} = k\ (m_{Cl,aq})^x$ (for $x > 1$).

Finally, Candela and Holland (1984) showed that Mo partitioning is independent of Cl: $m_{Mo,aq}/m_{Mo,melt} = 2.5$. The chloride dependence is necessary to maintain an electrical charge balance between chloride (the predominant anion) and all cations. At these magmatic temperatures the predominant aqueous species are associated, neutral molecules such as $CuCl°$, $NaCl°$, $CaCl°_2$ and $ZnCl°_2$. The 1:1 proportionality between univalent cations and Cl follows from these stoichiometries, and the 1:2 relations between divalent cations and Cl, from equilibria such as

$$CaCl_{2(aq)} + 2Na^+_{(melt)} = Ca^{2+}_{(melt)} + 2NaCl_{(aq)}$$

where $NaCl_{(aq)}$ varies directly with $Cl_{(aq)}$. Equilibrium constants for such reactions derived from the partitioning coefficients fit the observed data relatively well, suggesting that these

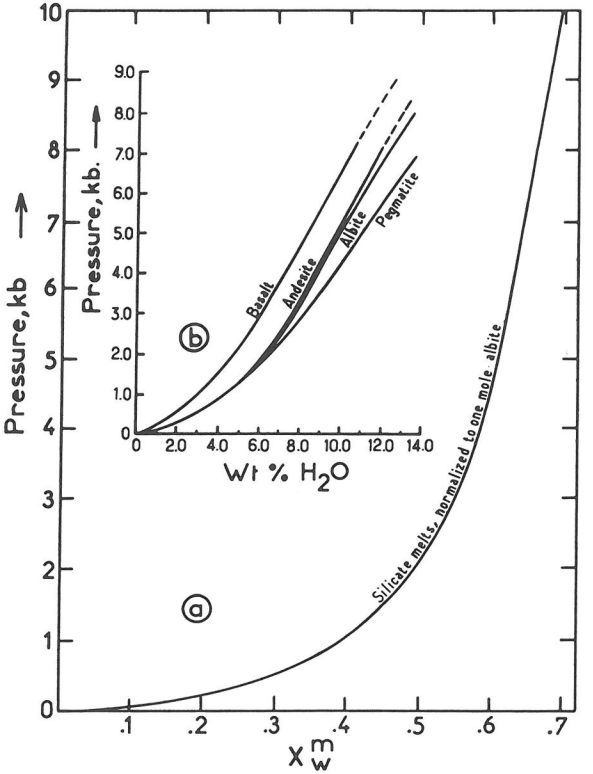

Figure 12. Observed solubility of water in silicate melts including basalt, andesite, Li-pegmatite and albite. The insert plots wt % solubility, and the larger figure gives the mole fraction of water in all four melt compositions normalized against albite composition. From Burnham (1979).

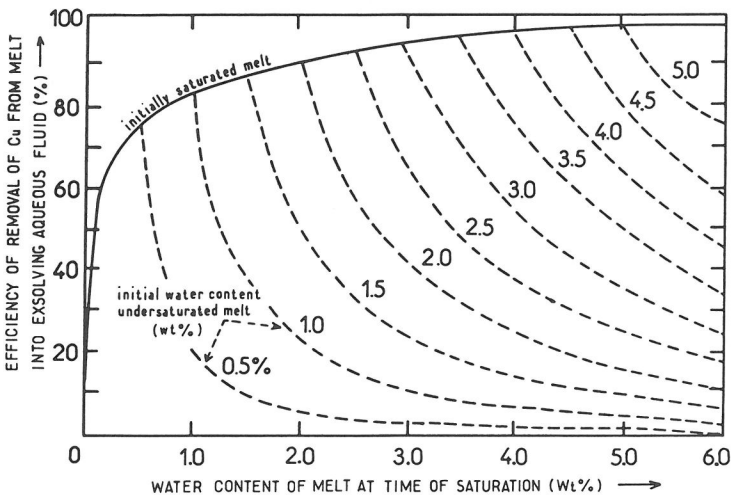

Figure 13. The percent efficiency of removal of Cu from a felsic silicate melt into an exsolving aqueous fluid as a function of both wt % water in the melt at saturation and of the initial wt % water in the melt. Calculated for a solid/melt Cu partition coefficient of 0.3 and an initial concentration ratio (chloride/water) in the melt of 0.1. From Candela and Holland (1986).

kinds of exchange reactions control the distribution of cations between the aqueous and silicate phases. Mo, which is Cl-independent, may be a special case which does not form appreciable chloride compounds , but instead partitions as mixed H_2O-OH^- complexes such as molybdic acid, $MoO_2(OH)_2$.

The partitioning coefficient for Cl, coupled with those for Zn, Mo, Cu and Mn, can be used to calculate the metal concentrations of hydrothermal solutions exsolving from felsic magmas as a function of initial Cl, H_2O and metal concentrations. This depends on the water content of the melt at the time of water saturation, and on the degree of crystallization of the melt. A representative calculation by Candela is included here as Figure 13, and many of the possible variations are discussed by Holland (1972) and Candela and Holland (1986). All metals studied so far can be very efficiently extracted from a melt into an exsolving aqueous phase, provided water concentrations at the time of melt saturation are sufficiently high. In Figure 13, for example, the fractionation of Cu into exsolving water is nearly complete (95%) for the 3 wt % water concentrations used in our representative felsic magmas above. Based on his own experimental work, Burnham (1979) calculated that an aqueous vapor coexisting with a granodioritic magma containing magnetite and 0.1 wt % Cl at 900°C and 1 kbar would have the following composition: roughly 1m total Cl, 0.40m Na, 0.23m K, 0.1m total dissolved Fe, 0.09m H (as H+) and 0.02m Ca. The very high concentration of iron has been borne out by more recent solubility studies mentioned below. In addition, the exsolving HCl-charged vapor phase will leach metals from the cooling, solid carapace of the pluton and from adjacent wall rocks.

Magmatic to hydrothermal transition: the biotite sensor

The phase separation accompanying the transition from magmatic to early hydrothermal processes affects considerable fractionation of ore metals and dissolved salts manifested in precipitation of abundant ore sulfides and the presence of solute-rich fluid inclusions in quartz in biotitic igneous- hydrothermal breccias occurring near the tops of plutons or dikes. Since biotite crystallizes both from magmas and as a reaction product in the potassic alteration assemblage, it serves a critical function of monitoring the earliest stages of hydrothermal fluid circulation. Hydrothermal biotite is easily recognized petrographically on the basis of its shreddy habit and occurrence in veinlets, and in their alteration halos. Fortunately hydrothermal biotites form in all three ore deposit types (Cu, Mo, and W-Sn) and from its composition and the associated mineral assemblages the nature of the magmatic to hydrothermal transition can be compared between systems. See Brimhall and Ague (1988) for more details on the thermodynamic arguments which follow.

Compositions of hydrothermal biotites. Figure 14 presents a generalized version of Figure 8, showing the compositions of hydrothermal biotites accompanying mineralization. In all three cases (Cu, Mo, and W deposits) biotite compositions form regular linear data arrays extending away from the specific composition of igneous biotite in the parent pluton, I-scr for W, I-mc for Cu, and crustal anatectic melt for Mo. The slopes of these arrays are positive, near a value of 3/2 shown with a solid bar in Figure 8, such that systematic F and Mg enrichment occur simultaneously during potassic alteration. One possible explanation of this positive slope is simply that it is due to the Fe-F avoidance principle (Munoz, 1984). Ague and Brimhall (1988b) have shown that this effect would produce a slope of only 0.6 in contrast to the observed 3/2 and have concluded that other processes are responsible for the Mg and F enrichment observed. Fe-OH and Mg-Fe exchange equilibria for chemical components in biotite in equilibrium with aqueous ions in solution can be used effectively for this purpose:

$$KMg_3AlSi_3O_{10}(OH)_2 + 2F^- + 3Fe^{2+} = KFe_3AlSi_3O_{10}(F_2) + 2OH^- + 3Mg^{2+} \quad . \qquad (1)$$

This expression is one of two possible mineral-solution equilibria which defines the exchange of F, OH, Mg, and Fe end-member components in biotite. The alternative set of exchange components is Mg-F and Fe-OH which we will return to later. The equilibrium constant for this reaction is:

$$K(p,t) = \frac{a^{biotite}_{KFe_3AlSi_3O_{10}(F_2)}\ a^{2\,fluid}_{(OH)^-}\ a^{3\,fluid}_{Mg^{2+}}}{a^{biotite}_{KMg_3AlSi_3O_{10}(OH)_2}\ a^{2\,fluid}_{F^-}\ a^{3\,fluid}_{Fe^{2+}}} \qquad (2)$$

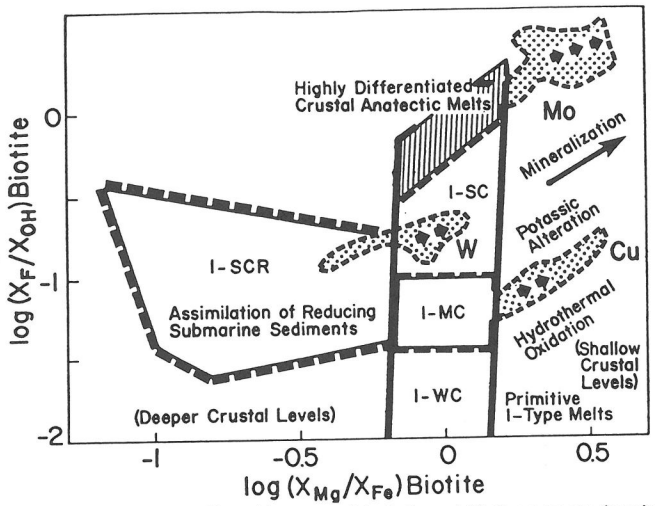

Figure 14. Summary of the relationships of igneous and hydrothermal biotites near ore deposits. From Brimhall and Ague (1988).

Assumption of ideal site mixing in biotite gives a useful simplification. For example:

$$a^{biotite}_{KFe_3AlSi_3O_{10}(F)_2} = X^3_{Fe} * X^2_F \quad , \qquad (3)$$

$$a^{biotite}_{KMg_3AlSi_3O_{10}(OH)_2} = X^3_{Mg} * X^2_{OH} \quad . \qquad (4)$$

The dependence of F and OH on Mg and Fe may be then derived after substituting the assumed ideal mixing activity-composition relations in (3) and (4), taking logarithms, and rearranging:

$$\log (X_F/X_{OH})^{biotite} = 1.5 \log (X_{Mg}/X_{Fe})^{biotite} + \log (a_{F^-}/a_{OH^-}) - 1.5 \log (a_{Mg^{2+}}/a_{Fe^{2+}})^{fluid} + 0.5 \log K \quad . \qquad (5)$$

Therefore, at constant pressure and temperature and F^-/OH^- and Mg^{2+}/Fe^{2+} ion activity ratios, log (X_F/X_{OH}) in biotite should increase linearly with log (X_{Mg}/X_{Fe}) at a rate of 1.5. Written more formally:

$$\left(\frac{\partial \log (X_F/X_{OH})^{biotite}}{\partial \log (X_{Mg}/X_{Fe})^{biotite}} \right)_{fluid\ composition,p,t} = 1.5 \quad . \qquad (6)$$

The alternative set of exchange components gives an analogous expression to (5) but with a slope (6) of negative 3/2. Since the data on natural biotites clearly indicate a positive correlation, the alternative set can be disregarded. Given that the observed slope is about 3/2, it is likely that hydrothermal biotite precipitates essentially under these constraints: essentially constant pressure, temperature, and the aqueous activity ratios indicated. What then causes the exchange reaction to proceed and cause the compositional variation which is characteristic of hydrothermal biotite in Cu, Mo, and W deposits?

Given the oxygen and halogen fugacities inferred from biotite and related mineral assemblages, the three magmatic-hydrothermal systems evolve from different starting points but apparently undergo processes held in common. In all three cases, the biotites formed are more magnesian than their igneous counterparts, and therefore it is likely that oxidation

accompanied the hydrothermal process. This conclusion is supported by the granite oxygen fugacity buffer of Wones and Eugster (1965):

$$\text{annite} + 0.5\,O_2 = \text{magnetite} + \text{alkali feldspar} + \text{water} \quad . \tag{7}$$

Using ideal site mixing in biotites again gives an expression for oxygen fugacity:

$$\log f_{O_2} = -6\log(1 - X_{Mg}) - 4\log X_{OH} + 2\log f_{H_2O} - 2\log K \quad . \tag{8}$$

Oxygen fugacity is expected to increase with X_{Mg} as with the activity of water. Consequently, oxidation could be the result of water saturation in the parent magma, although this explanation seems unlikely since the effect may be limited to melts containing only low iron contents (Candela, 1986).

Early high temperature hydrothermal oxidation. A more likely possibility is that oxidation is driven by changes in the solutes contained in magmatic aqueous fluids. Of these, perhaps the most likely to affect oxidation are the acidic components such as HCl, which at high temperatures are quite associated but ionize rapidly with decreasing temperature. With the quantitative partitioning of such acid constituents into aqueous fluids, their collective ionization could dramatically lower the fluid pH. Writing the granite oxygen fugacity buffer again in terms of H^+ and OH^- instead of water provides a way to relate oxidation to ionization.

$$\text{annite} + 0.5O_2 = \text{magnetite} + \text{alkali feldspar} + H^+ + OH^- \quad . \tag{9}$$

With the H^+ activity increasing by acid ionization and charge balance being maintained by increased chloride ion activity, the granite buffer reaction could be driven to the left, and in so doing, increase oxygen fugacity and modify biotite compositions producing the magnesium enrichment arrays present in all three types of base metal deposits. The simultaneous enrichment of fluorine may be due to maintenance of the biotite exchange component equilibrium (1) and the proportionality required (5) and (6).

Hydrothermal biotites and the compositional exchange path, probably due to late-stage magmatic and early-stage hydrothermal oxidation, are rare in major batholiths such as the Sierra Nevada, and so far have only been recognized in and near major ore deposits, the Pine Creek and Strawberry Mine tungsten skarn deposits (Brimhall and Ague, 1988). The technique of using biotite as a sensor for detecting mineralizing aqueous fluids is therefore specific to the oxidative events responsible for major deposition of ore metals (tungsten, copper and molybdenum), and therefore offers a means to differentiate between mineralized and unmineralized plutons.

Relative importance of magmatic and meteoric waters

Much of the above discussion supports the century-old theory that cooling plutons can exsolve hydrothermal brines which carry sufficient dissolved metal and sulfur to produce economically attractive deposits. The high acid potential and alkali chloride content of these solutions is also consistent with observed alteration of neighboring wall rocks and the high-salt fluid inclusions commonly associated with pluton-related ores. This is sufficient evidence to terminate the old debate on the importance of magmatic waters in ore deposition: exsolved magmatic waters have the full potential to produce ores given the appropriate physical environment for deposition and preservation.

At the same time, high-temperature aqueous solutions, no matter what their origin, are capable of leaching metals and other components from wall rocks as well as magmas. Thus, meteoric groundwaters entrained in a hydrothermal convection system also become potential ore-forming fluids; in some cases, such as the Mississippi Valley-type Pb-Zn deposits, they appear to be the sole aqueous component since no igneous intrusions occur anywhere nearby. In other cases, heated and recirculated seawater seems to be the ore– forming fluid (Kuroko, oceanic spreading centers), although here a small magmatic component cannot be entirely dismissed. Many ore bodies appear to have formed from multiple sources, perhaps starting with predominantly magmatic waters, and finishing with predominantly meteoric input (as apparent in Fig. 11). Quite clearly, there are many possible

sources of ore-forming solutions, all important to varying degrees in different environments.

The historic confusion and long-standing debate over the relative ore- forming potential of hydrothermal fluids from different sources is based more on geological than chemical arguments. In the field it is obvious that different ores were produced by different geological processes: porphyry coppers quite clearly formed by a different process and from a different source than Mississippi Valley-type Pb-Zn ores; these are different again from the Cyprus-type umbers or stratiform sulfides. Nevertheless, the chemical properties of water are the same, no matter what the origin. Aqueous solutions of different composition are governed by the same chemical principles. From the chemist's point of view, ore-forming aqueous solutions appear much less diverse. In the following sections we discuss some of these underlying chemical controls.

PART II. PHYSICAL CHEMISTRY OF HYDROTHERMAL ORE FLUIDS

SOLVENT-SOLUTE CONTROLS ON ORE SOLUTIONS

Water is, of course, the most abundant liquid in the Earth's crust and governs many chemical processes from surface to upper mantle. It seems ironic that water is also a very anomalous solvent, unlike most other liquids in many respects. For example, it has been called "the universal solvent" and "one of the most corrosive substances known" (Franks, 1972, p. 20). These peculiarities arise from the structure of the water molecule itself. The following discussion is taken largely from the series on the chemistry of water edited by Franks (1982, and preceding volumes). For further references, see Eisenberg and Kauzmann (1969), Horne (1969, 1972) and Neilson and Enderby (1986).

The water molecule

Figure 15 illustrates (very schematically) the electron structure of a gaseous water molecule. This has a distorted tetrahedral shape (the perfect tetrahedral angle being 109°28') with two sp^3 hybrid sigma bonds between O and H. Recall that the electron configuration of O is $1s^2\ 2s^2\ 2p^4$ (Fig. 15A). In the H_2O molecule the H-H repulsion increases the H-O-H angle from 90° to 92°. Shrinking of the two orbitals opposite the H atoms ($+p_y$, $-p_x$) and other interactions further increases this angle to 104°40' (nearly tetrahedral). The $2s^2$ and $2p_z^2$ electrons are not bonded to hydrogen and are left behind as two "lone-pairs" in approximate tetrahedral positions (Fig. 15B).

Water structure, hydrogen bonding and polarity

These lone-pair electrons cause much of the anomalous behavior of water. For example, they interact with electron-deficient species (such as cations). Perhaps the most important interaction is electrostatic bonding with hydrogen atoms in other water molecules. In the structure of ice, for example, all lone-pairs are bound to hydrogens in neighboring water molecules, and the lattice consists of a puckered, rigid network of $O\text{-}H_4^-$ tetrahedra analogous to silicate structures (Fig. 15C). In liquid water, hydrogen bonds are formed and broken, with a strength as high as 1/10 that of the sigma H-O molecular bond in the individual water molecules themselves. This imparts a structure to water consisting of random "flickering clusters" of hydrogen-bonded molecules (the Frank model), bending hydrogen bonds (Pople's model) and/or "iceberg" structures where individual molecules fill the interstices of broken-down ice structures (the Bernal and Fowler model). These models and their variations are reviewed by Horne (1969). In other words, liquid water retains some of the tetrahedral structure characteristic of ice through lone-pair interaction and hydrogen bonding. Hydrogen bonding accounts for many of the anomalous properties of water, many of which have tremendous geological implications: high heats of fusion and vaporization and high heat capacity (regulating effect on climate); high surface tension (capillary movement in soils, sediments and living organisms); high melting and boiling points (without

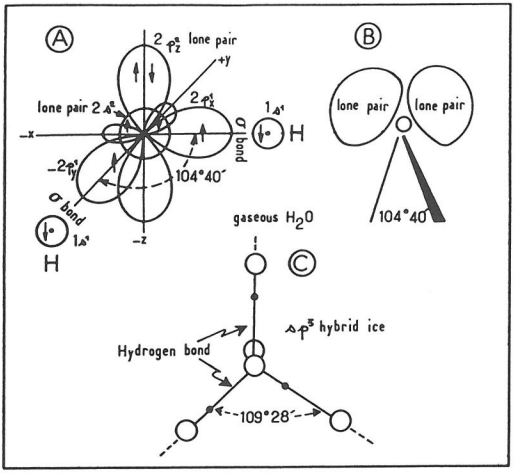

Figure 15. Schematic structure of the water molecule. (A) Electron orbitals just prior to formation of gaseous water showing 2s and 2p lone pairs and distortion of the 2p orbitals. (B) Gaseous water molecule showing near-tetrahedral H-O-H angle and two lone-pair distributions. (C) Tetrahedral structure of water in ice showing H-bonds. The hydrogens are constantly moving and, in general, no two hydrogens are at the same distance from any oxygen at one instant.

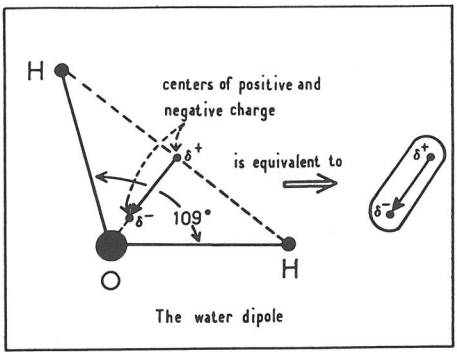

Figure 16. The dipole moment of water. The water molecule may be considered a simple electrical dipole because of the charge distribution shown here and in Figure 15B.

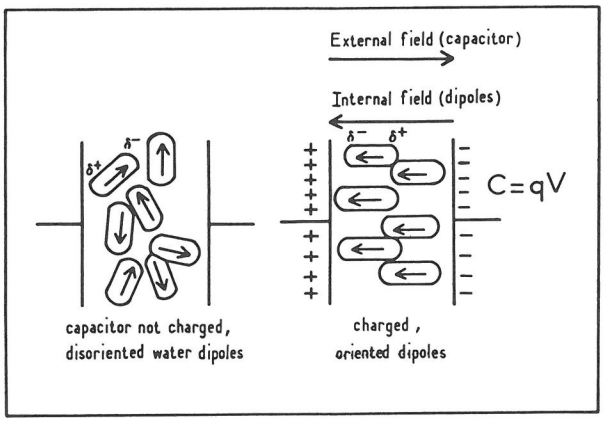

Figure 17. The dielectric constant of water, illustrated by the orientation of water molecules in an electrical field imposed between two capacitor plates. Oriented water dipoles create an internal field which opposes the external field of the capacitor and reduces net voltage across the plates. The dielectric constant of water is defined as the voltage across the plates when separated by a vacuum divided by the voltage when separated by water.

hydrogen bonding, water would be a gas at ambient temperature like NH_3, and Earth would have a hot, aqueous atmosphere); a local density maximum at 4°C (ice floats and insulates underlying water, but if it sank like solid NH_3, most regions of the Earth's oceans would freeze solid). An equally important property attributable to the same lone-pair structure is that water is quite polar. By this we mean that free water molecules (in liquid or gas) have negative and positive directions, or behave like electrical dipoles, as illustrated in Figure 16. The dipole moment of free gaseous water is 1.83×10^{-18} e.s.u., and this increases when associated with other molecules as in liquid water. By comparison, the dipole moments of other molecules, in units of 10^{-18} e.s.u. are: $CO_2 = 0$ (linear O-C-O molecule); $CCl_4 = 0$ (perfectly tetrahedral, sp^3 covalent molecule, no lone-pairs); $NH_3 = 1.3$ (distorted tetrahedron, sp^3, one lone-pair); $H_2S = 1.10$ (similar to water, two lone-pairs, but $3s^2\ 3p^4$ configuration); HCl = 1.08 (ionic); CsCl = 10.42 (extremely ionic).

Dielectric constant of water

Because of this high dipole moment, water molecules align themselves in an electrical field, as illustrated in Figure 17. Think of these as the two plates of a capacitor at voltage V with stored charge q. As shown, the alignment of water dipoles sets up an opposing field, so that the net potential across the plates decreases. In fact, the individual water molecules become even more polar in an electrical field, and their effect is accentuated by hydrogen bonding. For the same stored charge on the capacitor plates, you would find that if you started with a vacuum between the plates and then added water, the voltage across the plates would drop by a factor of 78.47 at 25°C. Recalling that capacitance is $C = q/V$, we define the dielectric constant of the medium between the plates relative to a vacuum as $C_{diel}/C_{vac} = V_{vac}/V_{diel}$. At 25°C and 1 bar, the dielectric constant of water (78.47) is extremely high, exceeded by only a few geologically unlikely liquids (such as pure hydrocyanic acid). For comparison, the dielectric constant of CCl_4 is 2.2, pure HCl is 4.6, H_2S is 9.1 (at −78°C) and pure NH_3 is 16.9.

Solvating power of water

Coulomb's law. There are several main reasons why water is an unusually good solvent for ionic (electrolytic) compounds such as NaCl. These all relate to the two lone-pair electrons and polarity of the water molecule itself; one of the most important effects stems from the dielectric constant of water. First, recall that Coulomb's law for the electric force between two charges in a medium of dielectric constant D is

$$F = \frac{q_1 q_2}{D r^2} \quad , \tag{10}$$

where r is the separation between the charges. The higher the dielectric constant, the lower the force of attraction between anions and cations. Thus, tightly bonded ionic crystals, such as NaCl break apart and ionize to Na^+ and Cl^- in water. By contrast, they remain associated in non-polar solvents such as CCl_4 and have much lower solubilities.

Hydration. A second, related effect, is that water dipoles align themselves around charged ions as shown in Figure 18, forming hydration shells. The physical picture here is called Gurney's co-sphere model of ionic hydration (see Gurney, 1962; Franks, 1973). In the primary, innermost hydration layer, called zone I, water molecules are relatively fixed (not free to rotate), are more compact than in normal water, and therefore have lower specific volume and entropy. In the next shell, zone II, water molecules are disoriented, pulled one way by the field of zone I and another by the flickering field of outside bulk water; thus zone II water has higher volume and entropy (disorder) than pure water. We should emphasize that the hydrated species itself is dynamic and that all water molecules are constantly moving and exchanging with a half-life as low as pure water structures (10^{-10}–10^{-11} sec.). In general, cations tend to be more highly hydrated than anions of similar charge and size, because the positive region of the water dipole is more dispersed than the negative (as you can see in Figure 16). Small, highly charged (Z) cations such as Li^+,

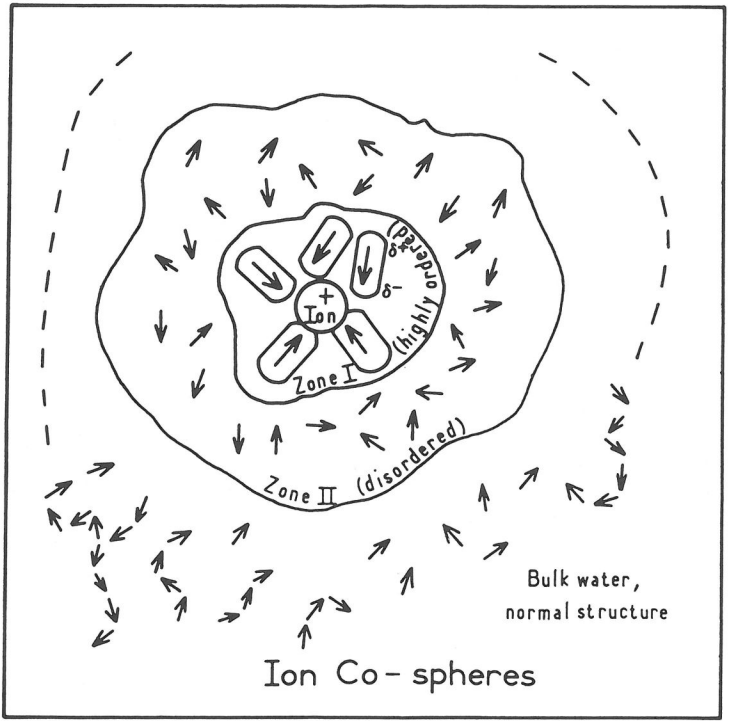

Figure 18. Gurney's co-sphere model of ion hydration. Zone I is an inner region of water dipoles relatively fixed about the ion. Zone II is intermediate and more disordered than bulk water. Water outside this zone is shown with a flickering cluster structure caused by H-bonding.

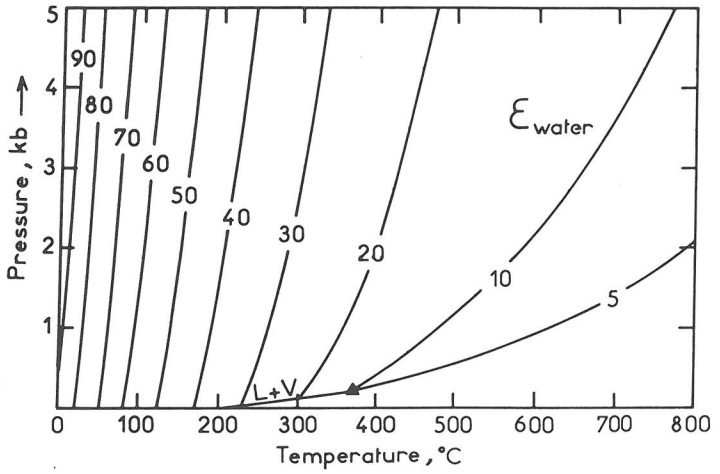

Figure 19. The dielectric constant of water as a function of temperature and pressure. The triangular spot marks the critical point of water. Data sources are cited by Seward (1981) and Eugster (1986).

Na^+, H_3O^+, Ca^{2+}, Ba^{2+}, Mg^{2+} (high Z/r) tend to be most highly hydrated, have a predominant zone I, and are called electrostrictive structure-making ions. These tend to decrease net solution entropy (increase order), to lower total density and to increase viscosity. In contrast, larger cations with low charge and some anions tend to have the opposite effect and are called structure breakers (K^+, NH^{3+}, Rb^+, Cs^+, Cl^-, Br^-, NO_3^-, BrO_3^-, IO_3^-, ClO_4^-).

These kinds of qualitative models need to be applied with care, but do account for observations such as the low viscosity of K^+, Rb^+ and Cs^+ salt solutions (lower than pure water) and the low electrophoretic mobility (movement in electrical fields) of Li^+. With the transition metals, spectroscopic studies mentioned below indicate that the primary hydration shell is bound in specific geometries, forming true molecular entities or complex ions.

The two combined properties of hydration and dielectric constant help explain the extraordinary solvating power water has for ionic compounds, at least at ambient T and P. Dissolved ions are effectively shielded or insulated from each other by their hydration shells and by the high dielectric constant of the solvent between each hydrated complex.

Solvation energies. As might be expected, there have been a great many attempts to quantify these effects, many summarized again in the volumes edited by Francks (1982 and preceding), and by Helgeson et al. (1981). Two of the oldest and more successful approaches have also received much use in geochemistry. The first is the Debye-Hückel equation for activity coefficients, which predicts the non-ideal (electrostatic) free energy of interaction based on Coulomb's law. The second approach is the Born Equation (1920) for the free energy change associated with removing an ion of radius r_i and charge $Z_i e$ from a vacuum and placing it in a solvent of dielectric constant D:

$$G = -N_A \frac{(Z_i e)^2}{2r_i}\left(1 - \frac{1}{D}\right) . \qquad (11)$$

Here N_A is Avogadro's number, so the equation applies per mole of ions. This comes directly from Coulomb's law (10), and despite its overly simplistic picture, is in reasonable agreement with experimental observation at 25°C (Bockris and Reddy, 1970, p. 69); growing evidence indicates it works even better at higher temperatures (e.g., Tremaine et al., 1986, and references therein). It is an important component of the model used by Helgeson et al. (1981) for electrolytic solutes in hydrothermal solutions. Note that since the dielectric constant of any medium is always greater than that of a vacuum, D>1 and the Born free energy (11) will always be negative; this also predicts that the free energy of ionic solvation should become more negative for smaller, more highly charged ions in solvents of higher dielectric constant. For singly charged ions of radius 1.5 Angstroms, Equation (11) predicts a free energy of solvation of roughly -100 kcal mole^{-1} at 25°C. These large negative free energies help explain the stability of ions in aqueous solutions even without taking into account the additional stabilizing effect of hydration shells.

Effects of temperature and pressure on the dielectric constant

The chemical behavior and solvating ability of water changes enormously with temperature and pressure. This is perhaps best illustrated by the changes in a fundamental property such as the dielectric constant shown in Figure 19. Notice that at liquid-vapor equilibrium the dielectric constant falls by almost an order of magnitude from 0°C to 374°C, the critical point of pure water. Under supercritical conditions the dielectric constant is 25 or less; at low temperatures it is high and almost independent of P, and at high temperatures, it increases with P.

Temperature. The effect of temperature can be explained, to a good approximation, by the Kirkwood equation, derived and discussed in detail by Bockris and Reddy (1970, p. 152):

$$\frac{(D-1)(2D+1)}{9D} = \frac{4\pi n}{3}\left[\alpha + \frac{\mu^2(1 + g\cos\gamma)^2}{3kT}\right] \qquad (12)$$

This includes the effects of molecular clusters (bound by hydrogen bonds) orienting in an electric field. Here α is a measure of the degree to which an electric field induces a dipole in any one molecule; g is the number of nearest-neighbor water molecules linked with a central water molecule as a cluster; cos γ is the average of the cosines between the dipole moment of the central molecule and those of its neighbors in the same cluster. This illustrates several important effects. First, the dielectric constant should decrease at higher temperatures simply from the inverse relationship in (12). Increasing temperature at constant P will also lower the quantities g and cos γ by breaking hydrogen bonds and disorienting individual molecules, causing a further decrease in D. This is expected intuitively because at higher temperatures molecular vibrations (including rotations and translations) increase, and the molecule is less capable of aligning itself in an applied electric field. Equation (12) also illustrates the importance of hydrogen bonding which increases the size of orientable clusters, g, and of cos γ. As an example, the dipole moments of liquid H_2O and SO_2 are similar, at 1.83 and 1.67 $\times$ 10^{-18} e.s.u., respectively. However, because water is hydrogen bonded and SO_2 is not, their dielectric constants at 25°C are 78.5 and 12.35.

Pressure. The effect of pressure on the dielectric constant of water may be predicted by analogy with Equation (12). At higher pressures individual molecules squeeze closer together, increasing interactions such as hydrogen bonding; this increases the dielectric constant. The detailed effects of pressure have been summarized by Millero (1971), Helgeson and Kirkham (1974, 1976), Seward (1981) and Eugster (1986). Of primary importance is the electrostrictive volume decrease due to ion hydration and collapse of water structure in the hydration shell (zone I). Again, this can be modeled very simplistically by Coulomb's law (10) for electrostatic interaction of water dipoles and charged ions. Differentiating the Born Equation (11) with respect to pressure leads to the expression

$$\bar{V}_{ion(electrostriction)} = \frac{Z^2e^2}{2Dr}\left(\frac{\partial \ln D}{\partial P}\right)_T . \qquad (13)$$

Rather surprisingly, this was derived before the Born equation by Drude and Nernst (1894). This gives the theoretical contraction of solvent of dielectric constant D, around a sphere of radius r with total charge Ze. This is a conservative estimate because it does not include specific solvent collapse and structuring in the primary hydration shell. For a simple ion of unit charge, Equation (13) predicts a volume decrease of roughly 10 cm^3 $mole^{-1}$ due simply to the electrostatic constriction of water around the ion (Seward, 1981, p. 119). For further details, see Hamann (1981).

The effect of this electrostrictive volume decrease around ions is to increase the tendency toward ionization at higher pressures. We guessed a similar result above by analogy with Equation (12); higher pressure should raise the solvent dielectric constant, thereby increasing ionization.

We have purposely chosen a very simple picture of electrostatic interactions in the above discussion, with Equations (11) through (13) following directly from Coulomb's law (10). Given what we have also said about water structure and solute hydration along with some of the effects to be considered below, the Coulombic view of hydrothermal solutions seems almost absurdly unrealistic. However, this simple electrostatic picture works to a first approximation for salt solutions that are not too concentrated, and it is an essential part of other more rigorous models. For example, the Debye-Hückel equation for activity coefficients of dissolved ionic species assumes Coulombic interactions. The more detailed expressions for activity coefficients derived by Pitzer and his colleagues (e.g., Pitzer, 1979; Pitzer and Weare, this volume) add a virial equation for non-ideal interaction to the basic Debye-Hückel equation. The Born Equation (11) and Debye-Hückel equation are the two primary components of the model proposed by Helgeson et al. (1981) for activity and osmotic coefficients of hydrothermal solutions (see also Sverjensky, this volume). The fact that Coulombic models work at all attests to the importance of electrostatic interactions between ions and water dipoles. For present purposes these models provide a simple and intuitively satisfying way of thinking about systems that in reality must be extraordinarily

complicated.

Effects of temperature and pressure on ionization

With this kind of reasoning we can predict that electrostatic interactions should increase at lower pressures and higher temperatures where the dielectric constant of water is reduced. This means that we should expect considerably increased ion-association for such conditions along with a tendency towards formation of electrically neutral or low-charge ion pairs and complex ions. Highly charged species such as $CuCl_4^{3-}$ are unstable at these lower dielectric constants, and electrically neutral complexes such as $CuCl°$ and $PbCl°_2$ predominate.

Similarly, association reactions such as

$$Na^+ + Cl^- \rightarrow NaCl° \qquad (14)$$

will increase, and compounds that we think of as strongly ionized at room temperature may become almost entirely associated at high T and low P. Compounds such as HCl which are strong acids (highly ionized) at ambient P and T, become weak to moderate acids at high T and low P. As an example, the dissociation constants of NaCl° and HCl° are plotted in Figure 20 as a function of P and T. At constant P, these decrease exponentially with T; at constant T, they increase with P, just as predicted above. Similarly, Figure 21 shows the temperature variation of dissociation constants for several geologically important acids at vapor-saturated pressure; all become more associated at higher T (including H_2O, which rises above 11.5 above 350°C). At the lower pressures of these vapor-saturated conditions, the effect of temperature predominates the change in dielectric constant and ionization, and pressure effects are negligible (see Fig. 19). By contrast, at very high pressures ionization may become extreme: it has been estimated, for example that water itself almost completely ionizes to OH^- and H_3O^+ at pressures in excess of 200 kbar and 800°-1000°C (Franck, 1981; Hamann, 1981). Under these conditions water would resemble a fused salt or ionic fluid, with interesting implications for behavior in the mantle.

Other effects of pressure and temperature on water-solute interactions

While changes in the solvent dielectric constant are extremely important, other factors also control changes in the chemical behavior of hydrothermal solutions with temperature and pressure.

Molecular vibration. At higher temperatures, molecular vibrations increase, making molecules such as the NaCl° species more likely to dissociate, and reversing the trend of Reaction (14). The two competing effects at higher T of decreasing dielectric constant (lowers ionization) and increasing vibration (increases ionization) account for the maxima commonly observed in the dissociation constants of ionic compounds as you can observe in Figure 21 (this was discussed at length 20 years ago by Helgeson, 1967).

Ligand field stabilization. With transition metals dissolved as aqueous complex ions, an additional stabilizing energy is produced by splitting of electronic d-orbitals, as illustrated in Figure 22. This is termed ligand-field stabilization energy (LFSE) and is proportional to $1/r^5$, the average separation between anions and cation in a complex ion (Dunn et al., 1965, p. 12). As we shall see below, this is a significant control on the behavior of transition metal ions in hydrothermal solutions, affecting the relative stabilities of the different metal complexes across each transition row. However, as predicted by the r^{-5} proportionality, the effect becomes less important at higher T and lower P. This is the P-T region where ion association is most intense because the dielectric constant is lower; the effect of LFSE might therefore be partly masked by important electrostatic, ionic interactions under the high-T, lower-P conditions typical of shallow ore-fluids at or near magmatic temperatures. While some preliminary work has been done on this problem for ore-forming conditions, much remains to be learned in this potentially quite important area (see discussions by Buback, 1981; Susak and Crerar, 1985; and Buback et al., 1987).

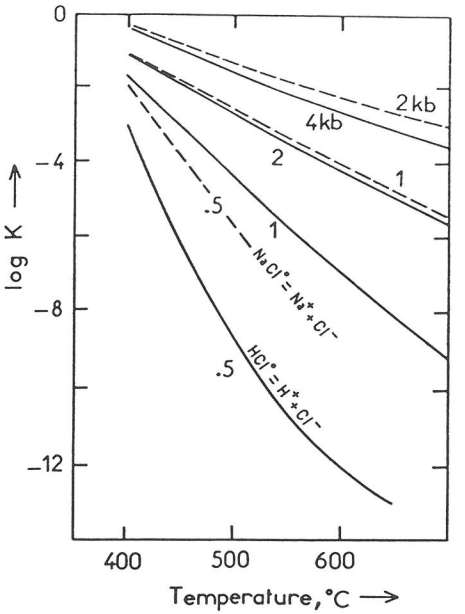

Figure 20. Dissociation constants of HCl and NaCl as a function of temperature and pressure. From Eugster (1986) after measurements by Quist and Marshall (1968) for NaCl, and Frantz and Marshall (1984) for HCl.

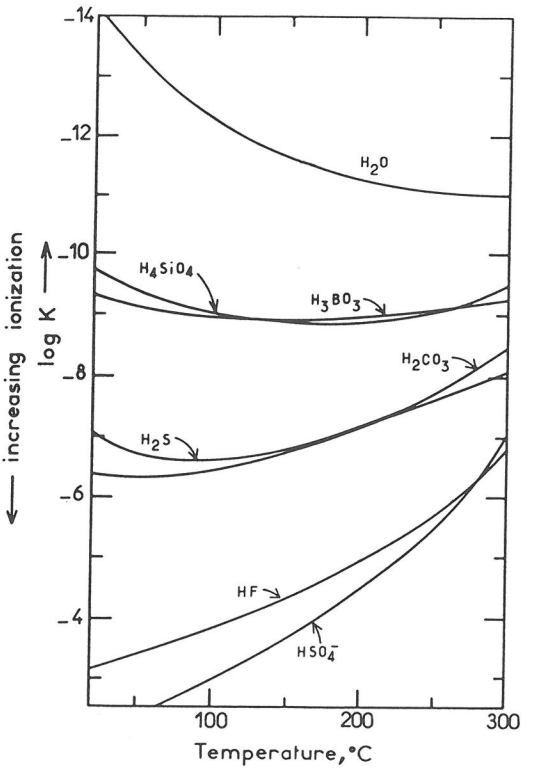

Figure 21. Variation of selected acid ionization constants with temperature at saturated water vapor pressures. Note tendency towards a maximum at intermediate temperatures. From Ellis and Mahon (1977).

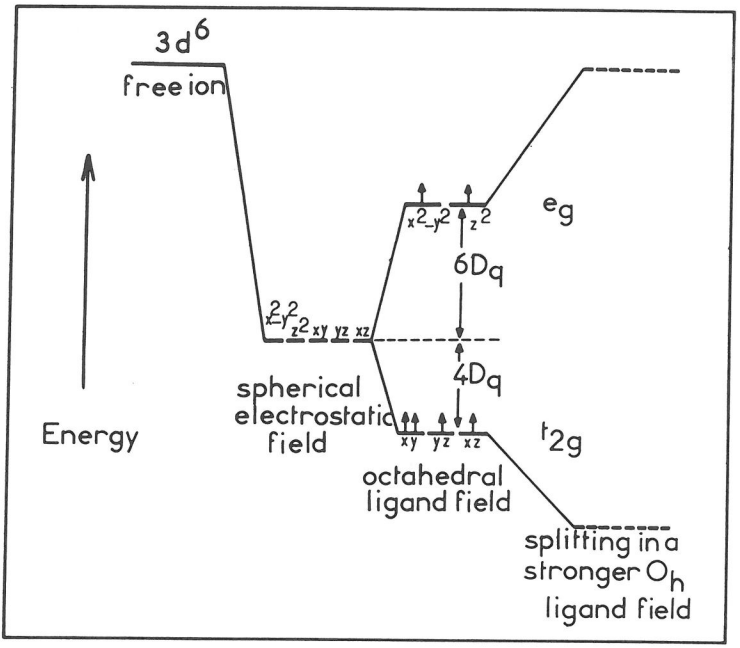

Figure 22. Splitting of 3d orbitals into two separate energies (e_g and t_{2g}) in an applied ligand field (such as occurs in transition metal complex ions). Note that 10Dq (the difference between the two new energy levels) depends strongly on the strength of the ligand field (hence on ligand type and metal-ligand bond length), and can change dramatically as shown to the right. Illustrated here with a high-spin d_6 ion such as Fe^{2+}. From Crerar et al. (1985).

Pressure-induced electron spin-pairing. Another related phenomenon is the possibility of an electronic transition from high- to low-spin state at elevated pressures (and with ligands which impose strong electrical fields). Figure 22 is drawn for the normal, high-spin case in which all electrons fill orbitals in accordance with Hund's rules. Under high pressures (or field strengths) it is possible to raise the upper e_g energy level illustrated here so far that electrons spin-pair and fill the lower level first, giving a low-spin configuration. The LFSE of high-spin Fe^{2+} shown here is $(2 \times 6Dq) - (4 \times (4Dq)) = -4Dq$; for the low-spin case, all six electrons would occupy the lower t_{2g} orbital with a total LFSE of $-6 \times 4Dq = -24Dq$. The quantity Dq is a measure of the field strength and is on the order of 5 kcal $mole^{-1}$ (or higher at higher pressures, Crerar et al., 1985). Hence low-spin LFSE could be -120 kcal $mole^{-1}$ or higher as opposed to high-spin which is only about -20 kcal $mole^{-1}$ for this ion. Therefore, transition to the low-spin state at higher pressures is potentially very important, capable of stabilizing complexes and increasing total solubility of complex-forming minerals. The low- to high-spin transition is also accompanied by a significant decrease in partial molal volume (Seward, 1981). Unfortunately, once again, there have been no experimental studies of geologically interesting systems under appropriate conditions. Several geochemical laboratories have the experimental capability at the present time, so we may hope for direct measurement of this effect in the near future.

TRANSITION METAL COMPLEX IONS

It is now recognized that complex ions are responsible for transport of transition metals in hydrothermal solutions. Aqueous transition-metal complex ions can be regarded as well-defined molecular entities having a specific geometry and coordination number and co-ordinate bonding described by ligand-field/molecular-orbital theory (Figgis , 1966; Huheey, 1978; Crerar et al., 1985). The chemical controls on metal complex behavior in

natural systems have been summarized in several recent reviews (Barnes, 1979; Seward, 1981; Crerar et al., 1985; Eugster, 1986), and we will only touch the more important points here.

Geologically important ligands

The metal in a complex ion is bound to, or coordinated by, ligands which serve as electron donors to the molecule. The potential ligands of most importance geologically have been discussed at length by Barnes (1979). These include: Cl^-, OH^-, HS^- and, of course, H_2O (probably the four most important); other probable ligands include organic acids, NH_3, F^-, S_x^{2-}, $S_2O_3^{2-}$ and HCO_3^-. Spectroscopic studies show that the transition metals are usually coordinated to water so that the formula for an octahedral one-chloro Cu(I) complex, for example, should really be written as $Cu(H_2O)_5Cl^\circ$. Available ligands are always competing with water for coordination sites about transition metal ions in aqueous solutions, and as we have seen above, water is a strong complexer, forming stable hydration shells.

Recent studies show that the speciation of natural hydrothermal systems may be much more diverse and complicated than was generally believed a decade or more ago. Based on a comprehensive solubility study of ten ore-forming minerals in hydrothermal solutions, for example, Scott Wood has recently concluded,

> "Our data underscore the highly complicated nature of ore-forming solutions. No single complex or species can be expected to predominate for any metal over reasonable ranges of solution composition and temperature, many different ligands may be significant in any given solution, different metals are likely to be transported by quite different mechanisms..., and mixed-ligand and perhaps also polynuclear species can be expected. In the mid-temperature range (approximately 200°-400°C) the most complicated solution chemistry and speciation is to be expected. At lower temperatures

Table 1. Classification of geological metals and ligands‡

Hard Acids	*Borderline Acids*
H^+, Li^+, Na^+, K^+, Rb^+, Cs^+	Fe^{2+}, Co^{2+}, Ni^{2+}, Cu^{2+}, Zn^{2+}
Ca^{2+}, Mg^{2+}, Ba^{2+}, Ti^{4+}, Sn^{4+}	Sn^{2+}, Pb^{2+}, Sb^{3+}, Bi^{3+}, SO_2
MoO^{3+}, WO^{4+}, Fe^{3+}, Al^{3+}, CO_2	
Soft Acids	
Cu^+, Ag^+, Au^+, Cd^{2+}, Hg^+, Hg^{2+}, M° (metal atoms and bulk metals)	
Hard Bases	
NH_3, H_2O, OH^-, CO_3^{2-}, NO_3^-, PO_4^{3-}, SO_4^{2-}, F^-, Cl^-	
Borderline Bases	*Soft Bases*
Br^-	CN^-, CO, H_2S, HS^-, I^-

‡According to relative hardness. Condensed from Huheey (1978).

Relative hardness of common metal ions and ligands*

$F^- > Cl^- > Br^- > I^-$	$Zn^{2+} > Pb^{2+}$
$Cu^+ > Ag^+ > Au^+$	$H^+ > Li^+ > Na^+ > K^+ > Rb^+ > Cs^+$
$Zn^{2+} > Cd^{2+} > Hg^{2+}$	$As^{3+} > Sb^{3+} = Bi^{3+}$

*Hardness decreases toward the right.

major electrolyte components are generally more dissociated and ion-pairing is less important. However, true inner sphere complexes remain important for some metals. At higher temperatures, there appears to be a simplification of metal complexes and a preponderance of species with neutral charge; the major electrolyte components (NaCl, KCl, $CaCl_2$) become essentially fully associated as ion pairs." (Wood et al., 1987).

Chemical controls

The ionic behavior of all transition metals is governed by d-orbital chemistry. There are four main chemical controls (Crerar et al., 1985): (1) Bonding changes from predominantly ionic to more covalent across each transition row from d^0 to d^{10} ions. (2) There is a general increase in electrostatic interactions with anions across each row (because ionic potential Z/r increases and ionic radius r decreases from Ti^{2+} to Cu^{2+} somewhat like the lanthanide contraction). Hence, complexes formed with a common ligand increase in stability from left to right across each row. (3) The splitting of d-orbitals mentioned above (Fig. 22) adds an additional LFSE (stabilization energy) to complexes formed by cations with configurations other than d^0, d^5 and d^{10}. (4) A relativistic effect dramatically increases covalency down each column of the heavier transition metals. Combined with rule #1, this means that the heavier d^{10} cations such as Au^+ and Hg^{2+} should form the strongest covalent complexes.

Hard-soft behavior

The interaction between specific metal ions and ligands (coordinating species, such as Cl^- or H_2O) can be regarded as acid-base reactions, with metal and ligand acting as electron acceptor and donor, respectively. In predicting which metals form complexes with which ligands, it is very helpful to use the hard-soft classification of Pearson (1963) and others (Ahrland, 1968, 1973; summary by Huheey, 1978). Class-A (or hard), metals and ligands are generally small, highly charged, and are only slightly polarizable. Class-B (or soft) species are large, relatively low in charge and highly polarizable. Hard species behave ionically, and soft species more covalently. The important point for present purposes is that, given competition between several ligands and metals, soft metals bind preferentially to soft ligands and hard metals bind with hard ligands. Table 1, from Crerar et al. (1985), classifies geologically important metals and ligands as hard, soft or borderline. Using this table we might guess, for example, that soft ligands such as HS^- might form relatively strong, predominantly covalent complexes with Hg, Au, Ag, Cu and Sb (all soft), weaker complexes with Pb and Zn (borderline), extremely weak complexes with Fe and Sn, and probably do not complex at all with W and Mo (hard). Borderline ligands such as Cl^- fall between the cracks and should form relatively stable complexes with most transition metals (except for the d^0 ions Sc^{3+}, Ti^{4+}, etc., which tend to form very weak chloride ion pairs). Finally, we should not expect stable complexes with mixed ligands if the ligands differ considerably in hardness; as an example, HS^- is much softer than Cl^- or OH^- and we should not expect mixed metal-Cl^--HS^- or M-OH^--HS^- species to be geologically important.

All transition metals should display increased type-A (hard acid) behavior at higher temperatures (and lower pressures) where electrostatic interactions increase as noted above. Thus complexes with intermediate or hard ligands such as Cl^- and OH^- should become more stable at higher T. This prediction is borne out by the observed increase in hydroxy complexing (Khodakovskiy and Yelkin, 1975; Baes and Mesmer, 1981), and the increased stability of chloro complexes, with temperature (Crerar et al., 1978; Barnes, 1979; Seward, 1981, 1984; Ruaya and Seward, 1986).

Electronegativity, LFSE and ionic potential. The effect of these three important variables on transition metal behavior is summarized in Figures 23 and 24. Try to picture these two diagrams as a single three-dimensional plot with axes Z/r, electronegativity and LFSE, since all three variables apply simultaneously. Ionic potential, Z/r, is a measure of the relative strength of electrostatic interaction and increases from left to right in each transition

row (as in rule #2, above). Electronegativity gives the relative degree of ionic or covalent bonding. LFSE is determined by the degree of splitting of metal d-orbitals in the presence of ligands (Fig. 22) and stabilizes complexes with configurations other than d^0, d^5 or d^{10}.

It is possible to outline four general regions on Figure 23 where different types of complex ions predominate. As we have mentioned above, bisulfide (HS^-) will preferentially complex the most electronegative, lower Z/r metals. We would expect this to be particularly important for Au^+ which, as you can see from this figure, is anomalously covalent; it is thought that Au and its neighbors Pt, Ag, Pb, Bi and Sb are so electronegative because of an interesting relativistic property summarized by Crerar et al. (1985) (the velocities of the inner s and p electrons of these metals approach the speed of light, their orbitals contract and more effectively shield the outer d and f orbitals). In fact, strong $Au(HS)_2^-$ complexes are known to exist in hydrothermal systems (Seward, 1973). Based on limited available data for gold chloride systems, Seward (1983) estimated that $Au(HS)_2^-$ complexes should be four orders of magnitude more concentrated than $AuCl_2^-$ complexes at near-neutral pH, total Cl = 1.0m and total S (reduced) = 0.05 m. Somewhat less dramatic differences might be expected with Ag+ and Hg^{2+} based on Figure 23. However, we should emphasize that at higher temperatures, strong bisulfide complexing is expected only with these most covalent metals. In general, bisulfide complexing should be less important for all other metals of intermediate or lower electronegativity; aside from its soft base behavior, the HS^- species predominates relative to $H_2S°$ (a weak ligand) only at basic pH at temperatures above 25°C (e.g., Crerar and Barnes, 1976). Instead, for most transition metals, Figure 23 shows that chloride and/or hydroxy complexes predominate. These borderline to hard bases preferentially bond to metal cations of intermediate ionic potential and electronegativity. Hence the most important transition metal species in many geological environments are probably OH^- and Cl^- complexes. For the extreme case of metals with very high ionic potentials, strong oxyanions such as molybdic and tungstic acids (H_2MoO_4, H_2WO_4) are expected instead of chloro or even aquo complexes; here metal-oxygen bond strengths exceed that of the H-O bond in water, and oxygen is effectively stripped from the water molecule itself.

Figure 24 is the parallel diagram for LFSE versus ionic potential, and we can broadly delineate two fields for ions that either commonly or rarely form hydrothermal ore deposits. This diagram seems paradoxical at first sight because it indicates that metals with the highest LSFE's (which should form the most stable aqueous complexes) are least likely to form hydrothermal ores. In fact, as noted by Crerar et al. (1985) only four of the ten metals in the first transition row (from Sc to Zn) typically form large hydrothermal deposits: Mn, Fe, Cu and Zn. These four metals have the lowest (or zero) LFSE's of the first transition row. The probable explanation is that the remaining six metals have even greater LFSE's in minerals or magmas and are not as easily leached by hydrothermal solutions in the first place.

Of the 30 transition metals only 9 or 10 commonly form sizable hydrothermal deposits (Mn, Fe, Cu, Zn, Mo, Ag, W, Au, Hg and occasionally Co), and this in no way correlates with average crustal abundance. This interesting problem needs further research. Much can probably be learned about the metals that do form ores from the chemistry of those that do not. Figure 24 suggests that LFSE is one of the more promising chemical properties on which to focus initial attention. A possible relationship between LFSE and porphyry copper mineralization has already been recognized by Feiss (1978); he showed that economic mineralization correlates with the $Al_2O_3/(K_2O + Na_2O + CaO)$ ratio of plutons in the American southwest. High Al/alkali magmas have more liquid octahedral structures (with high LFSE's); crystallizing plutons comprising such magmas might be able to retain metals longer, perhaps to the point of water saturation. Susak and Crerar (1982,1985) have suggested that the coordination and structure of metal ion complexes might help control deposition; there is some preliminary evidence that large deposits correlate with conditions that produce complexes of tetrahedral (or lower) coordination—see Figure 25 and discussion

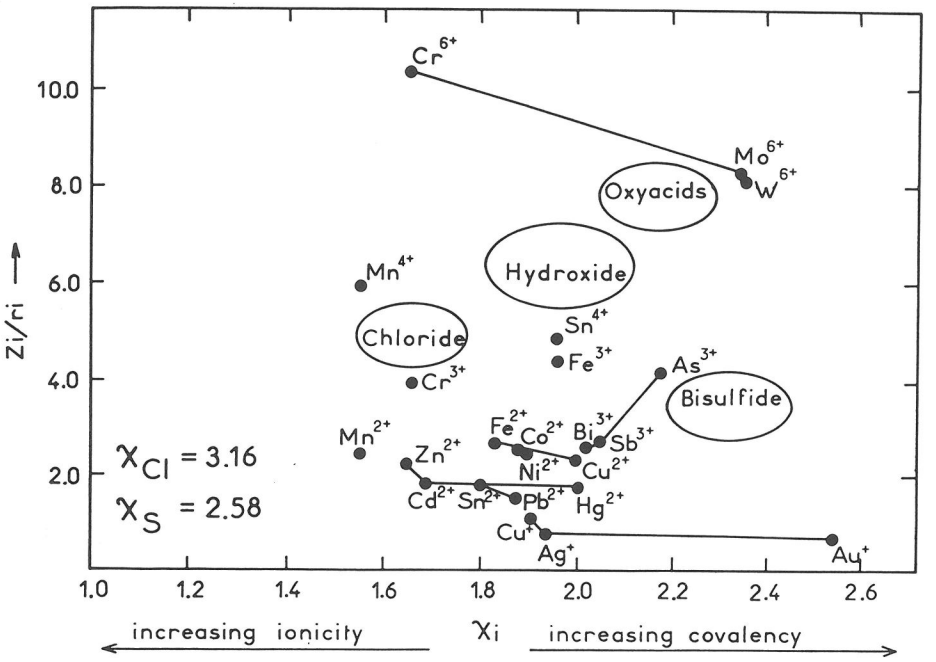

Figure 23. Plot of ionic potential (Z/r) versus Pauling electronegativity for selected ions. Crystal radii and electronegativities from Huheey (1978). Ions in selected columns of the periodic table are connected by solid lines, as are ions of the first transition series. Note that the ions group into four overlapping, general fields forming oxyacids, hydroxide, chloride and bisulfide complexes. From Crerar et al. (1985).

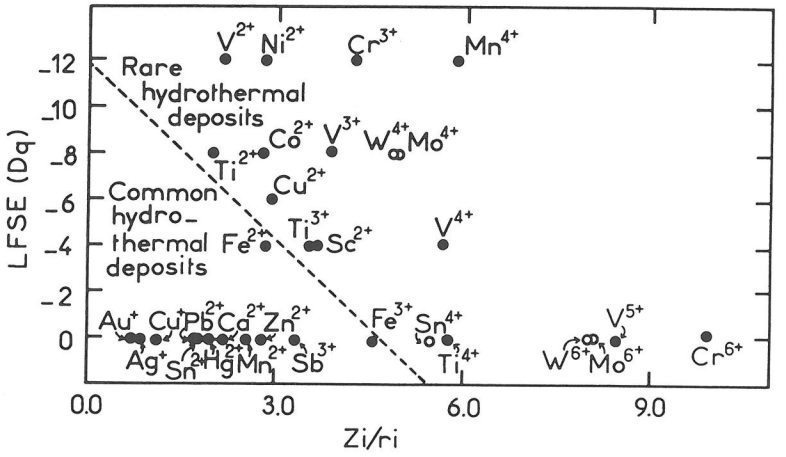

Figure 24. Ligand field stabilization energy (LFSE) versus ionic potential (Z/r) for selected metals. The valences shown are common in geological systems. A rough discrimination is drawn between metals that either commonly or rarely form large hydrothermal ore deposits. The tetravalent Sn, Mo and W ions are exceptions since they are heavy and more electronegative; on a three-dimensional plot including electronegativity, LFSE and Z/r, these three metals fall in the field of hydrothermal ores. From Crerar et al. (1985).

below. Since metals with higher LFSE tend to form complexes of octahedral (and possibly higher) coordination, this is another potential clue to the inverse relation between LFSE and ore deposition indicated on Figure 24.

Why solubilities increase with temperature

There is a general tendency for the solubilities of most substances in water to increase at higher temperature. This is a matter of everyday experience, dissolving sugar or salt in hot water for example. It is true that there are some minerals that show an anomalous retrograde solubility (become less soluble in hot water), at least up to certain limiting temperatures; this includes carbonates (calcite, dolomite, strontianite, witherite) and some sulfates (anhydrite, celestite) (see Holland and Malinin, 1979). However, these minerals are exceptions. Magma-water element partitioning experiments summarized above suggest that some metals might reach concentrations on the order of 1 wt % in exsolving water, and high-temperature fluid inclusion data from mineral deposits occasionally indicates similar high metal content (Roedder, 1979; Kwak et al., 1986). In most ore mineral solubility studies, solubility increases at higher temperatures. For example, experiments by Whitney et al. (1985) and Hemley et al. (1986) with magnetite, and sulfides in NaCl-H_2O-quartz monzonite systems above 500°C gave metal concentrations (Fe, Mn and Zn) on the order of 1 wt %.

This is really a very complicated question, with different explanations for different minerals. Many variables such as pH, oxygen and sulfur fugacity and even solution density change with T, and these all influence solubility. However, we will single out a few general effects which are directly related to temperature from our preceding discussion.

First, molecular vibration increases at higher T, increasing the probability for molecular dissociation; this partly explained the maxima in ionization constants observed in Figure 21. For most metal oxides, sulfides and silicates, this effect should increase the solubility product (see for example, mineral solubility products tabulated as a function of temperature by Helgeson, 1969).

We have also observed that at higher T there is a general increase in electrostatic interactions because of the decreased dielectric constant of water. We noted that transition metals all show increased type-A (hard acid) behavior at higher T. Now the relative stability of any species is determined by its Gibbs free energy (more stable compounds have more negative free energies). This, in turn, is a balance between enthalpy and entropy

$$\Delta G = \Delta H - T\Delta S \quad , \tag{15}$$

with entropy becoming increasingly important at higher T because of the $T\Delta S$ term. As summarized by Ahrland (1968) and Seward (1981), soft-soft interactions are characterized by exothermic (negative) enthalpies and low entropies (possibly even negative, which indicates increased molecular order). Thus the free energy of these species is dominated by the large negative enthalpy of predominantly covalent bonds. The low to negative entropy is less significant, and arises from the decrease in the total number of particles (through complex formation) and ordering of ligands around metal ions. Disruption of water structure (which would cause an increase in entropy) is minimal because these type-B complexes do not display strong electrostatic interactions and are not heavily solvated by water dipoles. The energy required to displace water dipoles from the hydration shell by a coordinating ligand such as Cl^- must be less than that gained by the metal-ligand bond (with the end result being an exothermic process).

At higher T where the dielectric constant falls, the situation reverses and ion-solvent interactions become increasingly electrostatic. Type A (hard) interactions are characterized by large positive enthalpies and entropies of complex formation (Ahrland, 1968). Recall that from the Born Equation (11) and the related Drude-Nernst Equation (13) we now expect a major effect from the electrostatic attraction between metal cations and water dipoles as well as other coordinating ligands. This would occur largely in zone I of the co-sphere model in Figure 18, with concomitant disorder in zone II. The electrostriction of water around the metal ion and its displacement by coordinating ligands causes a large,

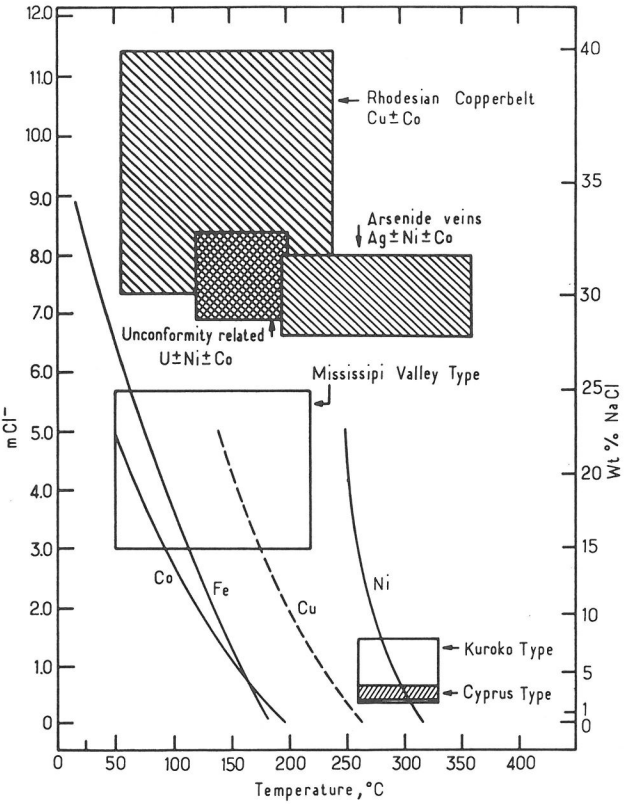

Figure 25. First appearance of tetrahedral complex ions for aqueous chloro complexes of four metals. Octahedral complexes predominate to the left, and tetrahedral complexes begin to the right of each line, with tetrahedral coordination eventually predominating at high T and/or Cl concentration. Data for Co(II) and Fe(II) from Susak and Crerar (1985) and Vogel et al. (1987), respectively. Lines for Cu(II) and Ni(II) are estimated by Susak and Crerar (1985). Environments of deposition for various types of ore deposits tend to occur in the tetrahedral region for each metal. Data on depositional fields are summarized by Susak and Crerar (1985).

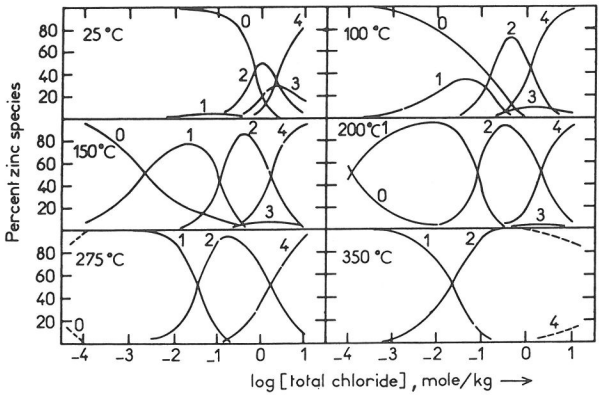

Figure 26. Distribution of aqueous chloro-zinc(II) complexes at different temperatures and total chloride concentrations, calculated from measured stability constants. The number of chloride ligands attached to each Zn nucleus is indicated on each curve (e.g., "1" refers to the $ZnCl^+$ complex). Notice that the one- and two-chloro species predominate at high T, and that speciation is much more diverse at lower T. From Ruaya and Seward (1986).

positive (endothermic) enthalpy. In other words, energy has to be put into the system to create this kind of inner sphere ordering and volume constriction (Nancollas, 1970). According to (15) the free energy would be positive and the complex unstable unless the entropy term overwhelms this positive enthalpy. In fact, the entropy term usually is sufficiently large, and dominates the free energy expression. Thus ligation by an anion such as Cl^- displaces waters in co-sphere I, causing increased disruption in co-sphere II (Fig. 18) and perhaps also in bulk solvent (which is already more disordered because of the higher temperature and decreased hydrogen bonding). This requires more energy than is gained by the metal-ligand bond (hence is endothermic) and increases disorder (positive entropy change). These changes in speciation with temperature are apparent in Figure 26 for aqueous chloro-Zn(II) complexes—see also discussion of complex stoichiometries below.

Of course, covalent molecular bonding is also possible at higher T (this is indicated by the Raman peaks of Figure 27, for example, which represent strong, predominantly covalent vibrations). The complex itself is a polar entity though, and at high T (and low dielectric constant), electrostatic interactions also occur. The net result is a complex doubly stabilized by both true molecular bonding and electrostatic attraction at high T.

These effects are summarized in Table 2. This shows the free energy, enthalpy and entropy of formation of the three neutral complexes $AgCl^\circ$, $PbCl^\circ_2$ and $ZnCl^\circ_2$, all of which predominate at 300°C-350°C at vapor-saturated pressures, from data of Seward (1981, 1984) and Ruaya and Seward (1986). These properties were derived from the observed variation of complex stability constants with T, and are not as reliable as quantities obtained directly by calorimetry, but the trends are significant. In all cases, the enthalpies and entropies of reaction increase at higher T; the free energy decreases, signifying greater stability; and the overall formation constants increase with temperature. This, coupled with increased mineral solubility products, results in higher solubility at higher temperature.

At high temperatures, water dissolves most minerals, whereas at low T it is a better solvent of ionic salts. As pointed out by Eugster (1986), low-T water tends to dissolve more covalent structures such as silicates only at low or high pH, whereas at high T most silicates dissolve readily and at roughly the same rate (Wood and Walther, 1983; Walther and Wood, 1986).

Note that large positive enthalpies are required for increased stability at higher T as predicted by the van't Hoff equation:

$$\left(\frac{\partial \ln K}{\partial T}\right)_P = \frac{\Delta H^\circ_r}{RT^2} \quad . \tag{16}$$

Species such as the $ZnCl_3^-$ which die out at higher T have exothermic (negative) enthalpies of formation. This illustrates the importance of electrostatic interactions at elevated T, since they produce large positive enthalpies.

RECENT EXAMPLES AND APPLICATIONS

It is no longer possible in a single article to adequately review all research involving metal-bearing hydrothermal solutions. Instead we will illustrate some of the chemical controls described above with recent experimental results. The examples are chosen to display some of the enormous diversity of the field as well as the many different experimental approaches now being used.

Molecular structures of complex ions

Aqueous transition metal complexes have clearly defined structures that can be determined by spectroscopic techniques. The two most successful approaches to date have been laser Raman spectroscopy and UV/Visible/Near-IR optical absorption spectroscopy. Raman

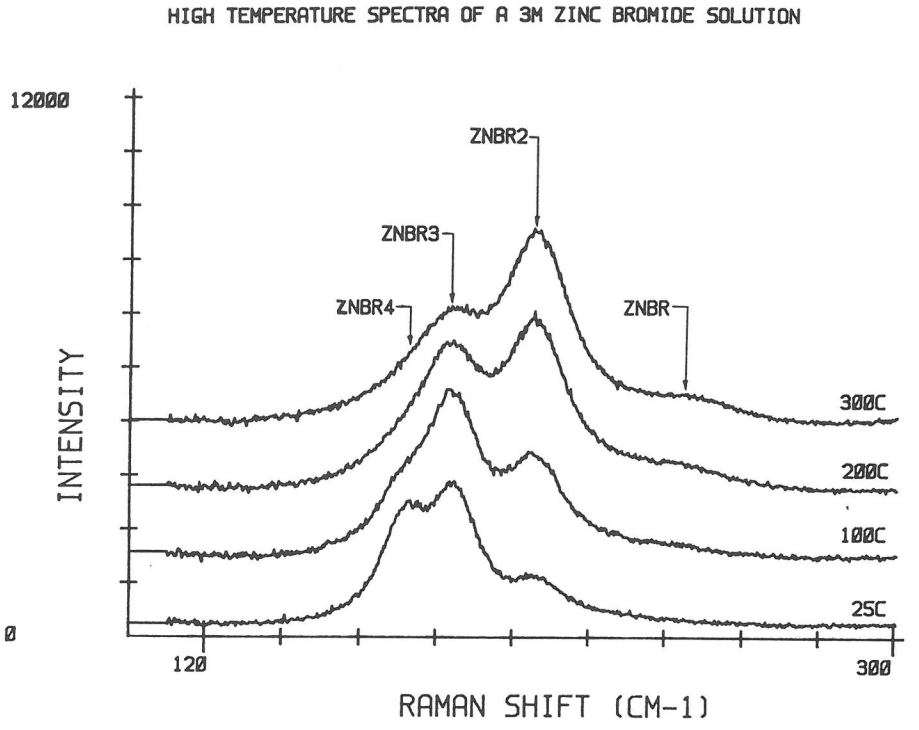

Figure 27. Raman spectra of aqueous zinc(II) bromide complex ions as a function of temperature. Peaks represent the totally symmetric vibration of each species. Notice that the dibromo complex predominates at high T, while speciation is more diverse at lower T. Spectra by Mary Yang, Princeton University.

Table 2. Enthalpy, entropy, Gibbs free energy and overall formation constants for the $AgCl^{\circ}$, $PbCl_2^{\circ}$ and $ZnCl_2^{\circ}$ aqueous complex ions from 25° to 350° C. Data from Seward (1976, 1984, 1986).

	$Ag^+ + Cl^- = AgCl^{\circ}$				$Pb^{2+} + 2Cl^- = PbCl_2^{\circ}$				$Zn^{2+} + 2Cl^- = ZnCl_2^{\circ}$			
T° C	log K	ΔG_r° kJ mole^{-1}	ΔH_r° kJ mole^{-1}	ΔS_r° J K^{-1}mole^{-1}	log K	ΔG_r° kJ mole^{-1}	ΔH_r° kJ mole^{-1}	ΔS_r° J K^{-1}mole^{-1}	log K	ΔG_r° kJ mole^{-1}	ΔH_r° kJ mole^{-1}	ΔS_r° J K^{-1}mole
25	3.27	−18.66	−12.5	20	1.95	−11.14	14.76	87	0.620	−3.54	30.3	112
50	3.10	−19.17	−12.5	20	2.16	−13.37	16.72	93	1.04	−6.46	33.0	121
100	2.88	−20.57	−5.9	39	2.61	−18.65	26.5	121	1.89	−13.5	48.5	170
150	2.88	−23.33	0	55	3.18	−25.75	47.4	168	2.90	−23.5	77.4	240
200	2.87	−26.00	2.0	59	3.95	−35.8	75.7	236	4.12	−37.7	119	334
250	3.07	−30.74	36.6	130	4.96	−49.7	119.2	320	5.70	−57.1	176	449
300	3.52	−38.62	73.6	200	6.23	−68.4	178.1	430	7.52	−82.5	245	570
350	4.21	−50.22	121	280	—	—	—	—	9.59	−114.4	328	710

spectroscopy measures molecular vibrations and optical absorption spectra result from electronic transitions between molecular orbitals. The peak energies and shapes of both kinds of spectra are controlled by the geometry, bond strengths, and ligation numbers of the complex ion, so these techniques probe the molecule itself. The method requires sealing windows (quartz, sapphire or diamond) into high-pressure-temperature autoclaves, which is not entirely straightforward; some of the ingenious methods devised by different laboratories to do this have been summarized by Buback (1981) and Buback et al. (1987).

Experimental measurements to date indicate that most transition metal complexes are distorted tetrahedral or octahedral molecules, with the metal at the center surrounded by four or six coordinating ligands (e.g., Susak and Crerar, 1984). The higher coordination numbers are favored by higher LFSE's. Recent Raman studies by Mary Yang at Princeton University indicate that Zn(II)-chloro complexes are probably linear, as predicted by Crerar et al. (1985) for this and other d^{10} ions (see discussion of Figure 27, below). Coordination numbers as high as 8 or even 12 might be possible at high pressures, although there is no experimental evidence for this as yet. The octahedral $\rightarrow$ tetrahedral transition occurs at higher T and chloride activity as indicated in Figure 25 (which includes recent data for Fe(II)-chloro complexes by Vogel et al., 1987).

As noted above, Susak and Crerar (1982, 1985) have suggested that large ore deposits might correlate with conditions that promote tetrahedral (or even lower) coordination; this is evident on Figure 25. Recall that Figure 24 shows an apparent inverse relation between LFSE and ore deposition. Electronic spectroscopy gives both the LFSE and geometry of metal complexes directly, and is therefore ideally suited for work on such questions.

Stoichiometries

The formulas or stoichiometries of complex ions can be determined in many different ways. Many of these methods give the stability constants for the predominant complexes at the same time. The most common approach is statistical analysis of mineral solubility data as a function of ligand concentration (for different techniques, see Crerar et al., 1978; Barnes, 1981; Wood and Crerar, 1985; Eugster, 1986; Ruaya and Seward, 1986). Spectroscopic techniques have also been used successfully for both purposes at hydrothermal conditions (references above, and Irish and Brooker, 1976; Seward, 1984).

An example of the changing speciation of Zn-chloro complexes with temperature at saturated vapor pressures is given in Figure 26. This comes from recent solubility studies by Ruaya and Seward (1986) which determined complex stoichiometries and stability constants simultaneously. The most important point to notice here is the relative simplification of species at higher temperatures. At 25°C all species from Zn^{2+} to $ZnCl_4^{2-}$ occur together at significant concentrations; at higher temperatures only the $ZnCl^+$ and $ZnCl^\circ_2$ complexes are important, and $ZnCl^\circ_2$ predominates at moderate chloride concentrations. This trend toward neutral-charge at higher T was predicted above from the decrease in dielectric constant of water with temperature.

A similar trend is evident in the Raman spectra of Zn-bromo complexes shown in Figure 27, measured recently by Mary Yang. This is a spectroscopist's view of the totally symmetric vibration of these tetrahedral complexes at different temperatures and the same total bromide concentration. Once again, the neutral $ZnBr_2$ species predominates at the highest temperature while higher ligation numbers are significant at and below 200°C. The $ZnBr^+$ complex is apparently linear because there is no evidence for associated waters elsewhere in the spectrum as there is with $ZnBr_2(H_2O)^\circ_2$ and $ZnBr_3(H_2O)^-$.

Stability constants

Stability constants of metal complexes in hydrothermal systems can be determined by many techniques, as outlined in the references cited in the previous section. Compilations and references to complex stability constants at elevated temperatures are given by Baes

and Mesmer (1976, 1981), Barnes (1979, 1981), Frantz et al. (1981), Seward (1981, 1984), Eugster (1986), and Wood et al. (1987).

There are two fundamentally different ways of measuring stability constants for metal-complexing reactions, each with its pros and cons. We will illustrate these using Fe(II) and the mineral pyrite as an example.

First, you can consider the aqueous species alone, and determine overall formation constants for ionic reactions such as:

$$Fe^{2+} + nCl^- = FeCl_n^{2-n} \; ; \; K_n = \frac{(FeCl_n^{2-n})}{(Fe^{2+})(Cl^-)^n} \quad (n = 1,2,...,6) \; . \tag{17}$$

In this and the following equations, parentheses denote activities (and thus implicitly include activity coefficient corrections). There is one Expression (17) for each different complex, depending on the value of n. The measurement is usually accomplished by spectrophotometric or electrochemical techniques which are sensitive to the concentrations of individual aqueous species. There are innumerable examples at 25°C (see Smith and Martell, 1976), and one outstanding study at hydrothermal conditions by Seward (1984) who determined Pb(II)-chloro stability constants from UV charge-transfer spectra. These methods should give the most accurate and precise measurements of stability constants for ionic reactions.

However, if stability constants such as (17) are to be used to calculate mineral solubilities, additional information is required. To calculate the solubility of pyrite at given temperature, Cl^- activity, pH, and oxygen and sulfur fugacities, for example, we would also need equilibrium constants for the following reactions:

$$FeS_2 + 2H^+ + H_2O = Fe^{2+} + 2H_2S + 1/2O_2 \; ; \; K = \frac{f_{O_2}^{1/2}(H_2S)^2(Fe^{2+})}{(H^+)^2} \; , \tag{18}$$

and

$$H_2S + 1/2O_2 = H_2O + 1/2S_2 \; ; \; K = \frac{f_{S_2}^{1/2}}{f_{O_2}^{1/2}(H_2S)} \; . \tag{19}$$

Finally, Reactions (17) + 2 × (19) + (18) give

$$FeS_2 + 2H^+ + nCl^- + 1/2O_2 = FeCl_n^{2-n} + S_2 + H_2O \; ; \; K_n = \frac{f_{S_2}(FeCl_n^{2-n})}{f_{O_2}^{1/2}(H^+)^2(Cl^-)^n} \; . \tag{20}$$

This is the kind of reaction geologists need: the solubility of a mineral is expressed in terms of accessible variables such as pH, Cl^- activity, and oxygen and sulfur fugacities. Unfortunately, it is two steps removed (Reactions 18 and 19) from the stability constant (17). There are two alternatives. We could devise some means of measuring or estimating equilibrium constants for Reactions (18) and (19), which would then allow us to calculate the constant for Reaction (20) from $K_{20} = K_{17} \times 2K_{19} \times K_{18}$; the cumulative errors here could be daunting. A more direct approach would be to measure the equilibrium constant for Reaction (20) by determining the solubility of pyrite as a function of T, P, pH, Cl^- activity, and sulfur and oxygen fugacities.

Such experiments are difficult but possible, and this is the second common approach (see Barnes, 1981, for an overview). Here the most difficult problem is controlling or measuring all necessary variables required to evaluate the equilibrium constant: for reactions such as (20) these variables are pH, oxygen and sulfur fugacity, chloride ion activity, and metal ion activities. Since one equilibrium constant K_n applies to each complex $FeCl_n^{2-n}$, the individual stability constants can be found by rewriting (20) as the sum of all

metal ion concentrations:

$$\sum Fe = \frac{f_{O_2}^{1/2}}{f_{S_2}}(H^+)^2 \sum_{i=1}^{n} \frac{K_i(Cl^-)^i}{\gamma_i} \qquad (21)$$

The right side is divided here by the activity coefficient γ_i of each metal complex to convert from metal activities to concentrations. Expression (21) is fitted as a regression equation to total Fe versus Cl^- activity data, which gives the stability constants K_n for each complex as regression parameters (Crerar et al., 1978; Wood and Crerar, 1985). This same expression may also be used to calculate solubilities for given T, P, Cl^- activity, pH, and oxygen and sulfur fugacities, once the equilibrium constants are evaluated. Note that once again, this requires knowledge of activity coefficients for all species in Expression (21); this is a serious problem and is discussed below.

We mentioned that there are pros and cons for both general methods of obtaining stability constants for reactions such as (20) or (17). The positive aspect of this second method is obvious—a mineral solubility is obtained directly in terms of geologically useful or reasonable variables. On the negative side, the experiments require control or measurement of many variables and thus cumulative errors can be large. In theory, it should be possible to use such experiments to obtain equilibrium constants for the purely ionic reactions such as (17); for example, if the stability constants K_3 and K_2 are measured for the 3– and 2-chloro forms of Reaction (20) then the constant for the reaction

$$FeCl^\circ_2 + Cl^- = FeCl_3^-$$

is obtained from K_3/K_2 (equivalent to subtracting reaction 20 with n = 2 from the same reaction for n = 3). This is equivalent to (17) as determined by spectroscopic or electrochemical methods. However, the equilibrium constant obtained by the solubility approach is likely to be less accurate for the reasons just given. In other words, solubility experiments are better suited to measuring full mineral dissolution reactions such as (20); the other approaches are best for determining stepwise stability constants such as (17).

Ore zoning

It has been recognized for over a century that there is a rough zoning of metals within many hydrothermal ore deposits, particularly those associated with large igneous intrusions. This is a subject of great controversy with absolutely no common agreement, but a very general, simplified sequence of metals from source to periphery might be Mo→Fe→Ni→Sn→Au→Cu→Zn-Pb→Sb-Hg (e.g., Barnes, 1975). You should not expect to find this exact sequence in any one deposit since it is an average drawn from many different places and types of ores. Ore zoning is much more than a simple effect of temperature. Susak and Crerar (1982), for example, have recently emphasized that it depends on many variables such as degree of saturation, T, P, pH, sulfur and oxygen fugacities, mineral stoichiometries, crystal structures and the molecular and thermodynamic properties of aqueous metal complexes.

This is a wonderful chemical problem, of obvious interest to the mining community as well. However, it is not likely to be answered definitively until much more is known about mineral solubility and deposition reactions. At present it is difficult to compare data for different minerals because of possible systematic errors involved in the various experimental approaches; there are even some differences in what the various experimental methods actually measure. One possible approach is to run solubility experiments containing many compatible minerals. Here, most systematic errors should apply to all minerals simultaneously, and the dissolution behavior of different minerals can be compared more easily. In a recent experiment of this type, Wood et al. (1987) measured simultaneous solubilities of the minerals pyrite, pyrrhotite, magnetite, sphalerite, galena, gold, stibnite, bismuthinite, argentite and molybdenite in hydrothermal NaCl solutions to 350°C at controlled oxygen and sulfur fugacities and fixed CO_2 partial pressure. Relative solubilities followed the order

Sb>Fe>Zn>Pb>Ag,Mo>Au in chloride-free solutions, and Fe>Sb, Zn>Pb>Au>Ag, Mo, Bi in concentrated chloride solutions. This is in rough agreement with the zoning sequence suggested by Barnes, above. Major differences in chemical behavior were apparent in this data set. Fe, Zn , Pb, Au and Ag formed chloride or hydroxy-chloride complexes in 0.5 to 5.0 m NaCl solutions; in contrast, Mo formed an oxyacid (tentatively, molybdic acid), and Sb appeared to dissolve as an neutral hydroxy complex. In chloride-free solutions, Au and Ag apparently formed bisulfide complexes; Fe formed the simple aquo complex; Zn, Sb and Bi formed hydroxy species; and Pb formed a carbonate. Much of this behavior could be predicted from the chemical controls outlined above. This diversity suggests that natural ore-forming solutions may be extremely complicated, with no single type of complex predominating over a wide range of conditions. The application to questions such as ore zoning will require much more work, methodically defining these species and their dissolution-precipitation reactions.

Metal-organic complexing

The importance of natural compounds in dissolving and transporting metals has been clearly demonstrated for surface- and ground-waters (see, for example, Reuter and Perdue, 1977; Jackson et al., 1978). Many natural humic and fulvic acids can chelate (form multiple bonds) metals and have stability constants on the order of 10^6 for metal complex formation at 25°C (Sohn and Hughes, 1981). By contrast, monochloro complex stability constants for many transition metals at 25°C are on the order of 1 to 100 (Smith and Martell, 1976). Organic matter is commonly associated with sedimentary and lower-temperature hydrothermal ore deposits (e.g., Nissenbaum and Swaine, 1976; Macqueen and Powell, 1983). Coupled with the strong metal-complexing ability, this has led to suggestions that the acids may participate in metal transport in hydrothermal systems (Barnes, 1979; Giordano and Barnes, 1981; Giordano, 1985). There are three interrelated problems here: what is the concentration of organic ligands in hydrothermal solutions? To what temperature do these ligands persist without degrading? What is their chelating capability at higher temperatures?

None of these questions can be answered very satisfactorily at the present time, but each is the topic of considerable current research in several laboratories. Data from Willey et al., (1975) and Carothers and Kharaka (1980) summarized by Giordano (1985) suggests that concentrations of potential organic ligands in sedimentary basin brines may range from < 1 ppm to several thousand ppm. Experimental work on organic degradation kinetics in aqueous systems shows that aliphatic and aromatic compounds with metal-binding carboxy and phenolic –OH functional groups can persist to temperatures between 100° and 200°C (Kharaka et al., 1983; Drummond and Palmer, 1986; Boles et al., 1987). Electrochemical measurements in progress at Princeton by Remy Hennet (1987) show Pb-organic stability constants ranging from log K = 2.3 (acetate, 85°C) to 7.8 (dipicolinate, 90°C). Given sufficient concentrations, such ligands could be significant metal transporting agents. However, this requires that the concentrations of other competing cations are not too high. Preliminary calculations by Giordano (1985) and Hennet (1987), for example, show that Na, Ca and Mg may bind organic ligands in solutions believed typical of the Mississippi Valley-type Pb-Zn ore-forming environment; if so, there would not be sufficient free organic ligands left to complex significant concentrations of Pb or Zn. At present, the question is not resolved. It appears likely that metal-organic interactions will be important in organic-rich environments, contributing to diagenetic processes, but that very unusual conditions will be required for organic deposition of metallic ores (high organic concentrations, low reduced sulfide and low alkali and akaline earth concentrations).

Activity coefficients

Now we come to one of the most perplexing barriers to understanding ore-forming solutions. Activity coefficients are essential in deriving thermodynamic data from experimental measurements (as with Eqns. (17) and (21), above). They are also necessary in calculating solution behavior from known stability constants and thermodynamic data. All species, whether ionic or neutral require this correction. Unfortunately, it is not certain

what the correction should actually be in many cases.

Major salts. Experimental information is most complete for the major salt components of hydrothermal solutions, NaCl, KCl and $CaCl_2$. Much of this is reviewed by Wood et al. (1984). There are considerable data on mixed salts so that it is now possible to describe some multi-component salt solutions of geological interest to temperatures of 300° to 350°C. For this purpose, you should use the Pitzer (1979) formalism which is also described in this book (Pitzer and Weare, this volume). With this approach data on two salt systems can be used to predict activity coefficients in much more complex mixtures containing the same salt components.

Activity coefficients of several common salts at 350°C are compared in Figure 28.

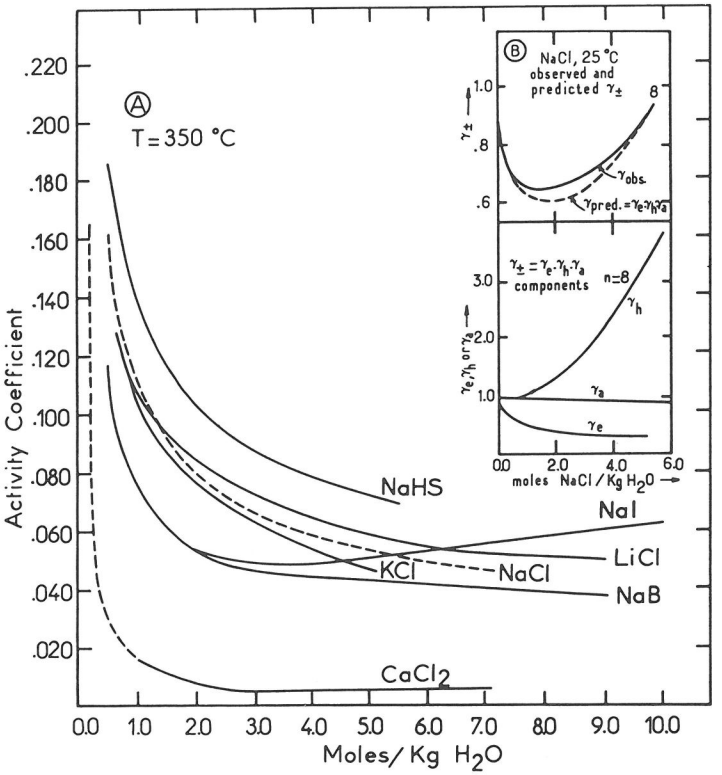

Figure 28. Mean molal stoichiometric activity coefficients for selected salts at 350°C versus salt concentration. Note that coefficients of all 1:1 salts are similar but that $CaCl_2$ is much lower. Activity coefficients of all salts at this temperature are roughly independent of concentration for concentrations above 2 m. Data from Wood et al. (1984) and Crerar et al. (1985).

At this higher temperature, the correction is considerable; the activity coefficient remains roughly the same at total salt concentrations exceeding 1 molal; and the activity coefficients of many of the 1:1 salts are similar. Lindsay (1980) suggested that at 300° to 350°C the structure of water becomes so thermally disrupted that all ions begin to act as structure-makers and will have similar activity coefficients. This approximation appears to work reasonably well for the alkali halides, but Wood et al. (1984) showed that it fails with other halides such as LiI. As should be expected from the charge difference alone, 2:1 electrolytes such as $CaCl_2$ show quite different behavior, and the activity coefficient for $CaCl_2$ at these elevated temperatures is on the order of 10^{-3}. These low values can be attributed in part to formation of the $CaCl^+$ ion pair; there have now been several problems fitting the Pitzer equations to data for NaCl-$CaCl_2$ mixtures both at 25°C (Ananthaswamy and Atkinson,

1982) and at elevated temperatures (Brantley, 1986) which could be attributed to such species. This is a problem for people working with hydrothermal solutions since NaCl and $CaCl_2$ are often predominant components. Resolution of this difficulty could require inclusion of Ca-Cl speciation in the fitting procedure.

Three main non-ideal effects. The non-ideal effects which contribute to activity coefficients can be divided into three broad categories based on a simple model described by Crerar (1973) and summarized by Wood et al. (1984). These include ion association (γ_a, short-range solute interactions), ion hydration (γ_h, short-range ion-solvent interactions) and electrostatic effects (γ_e, long-range solute interactions). As shown in the insert, Part B, of Figure 28, each effect can be represented by an activity coefficient γ_e, γ_h, and γ_a; the multiple $\gamma_e \cdot \gamma_h \cdot \gamma_a$ of these three coefficients gives the overall stoichiometric activity coefficient $\gamma_\pm$. Agreement between predicted and measured activity coefficients is surprisingly good using hydration numbers derived by Marshall (see Marshall, 1972, and references therein).

Because the physical model involved in our approach is too simplistic, we do not recommend it for predicting activity coefficients; however, it is a very helpful way of visualizing non-ideal processes in electrolyte solutions. Ion association and electrostatic interaction both contribute activity coefficients less than unity, while hydration causes large positive deviations, particularly at higher ionic strengths. At lower temperatures activity coefficients for many salts reach values as high as 10-30, reflecting low electrostatic interaction and ion-association, and high hydration. At temperatures above 300°C, activities fall below 0.1-0.001 because electrostatic interactions and association have increased significantly.

Minor components in concentrated solutions. The behavior of minor components in concentrated salt solutions is a major, unresolved problem. All components, whether dilute or concentrated, can have significant activity coefficients; this includes minor species such as dissolved metal complexes as well as the major dissolved salts like NaCl. At present there is no really adequate model for these minor species under the full range of ore-forming conditions.

For highly dilute solutions (less than 0.01m ionic strength), the Debye-Hückel (D-H) equation can be used. This gives γ_e, and the effects of association and hydration are assumed insignificant by comparison. This might be appropriate with a low temperature, relatively pure ground- or surface-water, for example. At high T and relatively low P where the dielectric constant is minimized, ion association becomes most important and neutral species such as $NaCl^\circ$ or $CuCl^\circ$ predominate. Here the ionic strength ($1/2\ \Sigma\ m_i Z_i^2$) may become sufficiently low that the D-H equation can be used again, provided that your calculation includes all relevant association reactions (i.e., calculate ionic strength and activity coefficients, use them to calculate association again and iterate to convergence). The D-H equation has been recommended by Eugster (1986), for example, for high-T, supercritical ore fluids. This might work to a first approximation, but does not take into account the effect of hydration (which may be significant at low P and low dielectric constant). It is also not clear how to treat neutral species under these (or any other) conditions, since the D-H equation applies only to charged ions. Common recommendations are to treat neutral species such as $NaCl^\circ$ as ideal and to assign them unit activity coefficients (e.g., Helgeson and Kirkham, 1981, p. 1478), or to treat them the same as CO_2 dissolved in a solution of the same ionic strength (Helgeson, 1969). Neither approach seems satisfactory, since intermolecular interactions, hydration and even electrostatic effects (with polar molecules) can be expected to vary with different species. At high ionic strengths, activity coefficients of neutral species might rise above unity simply because the other ionic species in solution are hydrated.

One point of related interest comes from a study of brucite dehydration by Barnes and Ernst (1963). They showed that NaOH exists predominantly as a neutral ion pair above 400°C in hydrothermal solutions, and that it mixes approximately ideally with water above 500°C. This means that both water and $NaOH^\circ$ obey the Lewis fugacity rule, $f_i = X_i f^\circ_i$

(where f_i is fugacity of i in solution, $f°_i$ is the fugacity of pure i at the same P and T, and X_i is its mole fraction; see Nordstrum and Munoz, 1985, p. 148) This is convenient for calculating activities of volatile components (like water), but does not help particularly with NaOH° unless you know its fugacity at T and P. Also, components may mix ideally and obey the Lewis fugacity rule without being ideal themselves: in the Barnes and Ernst experiments, water fugacity differed from water pressure, hence neither H_2O nor NaOH were ideal (which would require $f_i = P_i$).

At any rate it appears that the simplest activity corrections may apply at the two temperature extremes: dilute low-T solutions, and supercritical, high-T, lower-P fluids. The truly difficult problem lies between these two limits; unfortunately these are precisely the conditions expected for most ore fluids. Here, as we have already seen, speciation is most complicated, and ionic strengths may still be quite high.

The approach most frequently used by geochemists over the past several decades for calculating activities of minor components in concentrated salt solutions was suggested by Helgeson (1969); this in turn was an outgrowth of earlier work by chemists such as Scatchard and Harned summarized by Pitzer and Brewer (in Lewis and Randall, 1961, pp. 326, 578 and Appendix 4). A deviation function "B-dot" was defined as the difference between observed and predicted activity coefficients for an electrolyte such as NaCl:

$$B^{\bullet}(\bar{I}) = \frac{\log \gamma_{m_\pm}^{obs} + A\,|\,Z_+Z_-\,|\,\sqrt{\bar{I}}/(1 + \mathring{a}\,B\sqrt{\bar{I}})}{\bar{I}} = \log \gamma_{m_\pm}^{obs.} - \log \gamma_{m_\pm}^{D-H} \quad . \qquad (22)$$

Here the second term in the numerator is the D-H equation, A and B are D-H constants at any T and P and å is an adjustable parameter specific to each solute (representing the "distance of closest approach of two ions"). In Helgeson's treatment, the true (association-corrected) ionic strength $\bar{I}$ is used. According to our simple model above, association is therefore accounted for in (22) and electrostatic interactions are partly included by the D-H equation. $B^{\bullet}$ should therefore mostly represent hydration corrections and other left-over non-ideal interactions not included in our model (solvent electrostriction and structural changes, etc.).

Now (22) can be rearranged to give a guess at the activity coefficient of a minor species (such as several ppm $FeCl^{2+}$) in a strong salt solution (perhaps 2m NaCl):

$$\log \gamma_i^{\text{minor species}} = \frac{-A\,|\,Z_i\,|^2\sqrt{\bar{I}}}{1 + \mathring{a}_i B\sqrt{\bar{I}}} + B^{\bullet}(\bar{I})\cdot\bar{I} \quad . \qquad (23)$$

Here, γ_i is the activity coefficient for the minor component, Z_i and å are for the minor component (not NaCl), $\bar{I}$ is calculated from the total salt concentration (and known association constants and activity coefficients), and $B^{\bullet}(\bar{I})$ for NaCl over a range of P and T is tabulated by Helgeson (1969, and 1981, pp. 1345 and 1457). This presumes that the deviations from the D-H equation are the same for minor species as for NaCl, and to a rough approximation this might be so (for example, if removal of free water from the system by hydration of NaCl is predominant, it would have roughly the same effect on the activity coefficients of minor species as on NaCl). The problem is that $FeCl^+$ is a very different entity from Na^+ and Cl^- ions and will undergo different interactions, each capable of changing its activity coefficient.

More recently, Helgeson et al. (1981) have revised Equation (23) by splitting the $B^{\bullet}$ term into two parts:

$$\log \gamma_i = \frac{-AZ_i^2\sqrt{\bar{I}}}{1 + r_{e,i}B\sqrt{\bar{I}}} + \Gamma + \left[\omega_i b_{NaCl} + b_{Na^+Cl^-} - 0.19(\,|\,Z_i\,|\,-1)\right]\bar{I} \quad . \qquad (24)$$

The first term here is the D-H equation again; Γ is a small correction to change from mole fraction to molar concentration (Helgeson et al., 1981, p. 1322); $\omega_i b_{NaCl}$ is a hydration parameter derived from the Born Equation (11); and all the rest accounts for remaining non-ideal short-range interactions (and any other effects). The Born parameter $\omega_j = 1.66027 \times 10^5 \, Z_j^2/r_{e,j}$, and values of the Born ionic radius $r_{e,j}$ are tabulated by Helgeson et al. (1981, p. 1304). Values of b_{NaCl} and $b_{Na^+Cl^-}$ for NaCl to 500°C and 5 kbar are tabulated on p. 1477 of the same article. The D-H parameters A and B are given by Helgeson and Kirkham (1974, pp. 1202 and 1256).

This equation is more flexible than (23) but similar concerns still apply. As before, the only parameter specific to a minor component (one other than NaCl) in (24) is the radius $r_{e,j}$. Equation (24) is a major contribution and the best method available for estimating activities of minor components in the absence of direct experimental data. Unfortunately, until such data appear we are left with considerable uncertainty in modeling multicomponent hydrothermal solutions.

Mineral solubility calculations from thermodynamic data

Geologists interested in the formation of a specific ore deposit commonly need to calculate the mineral solubilities for the presumed conditions at the time of ore deposition. This gives the saturation compositions of ore components in the solution and often provides insight into deposition processes. This is also important for engineers working with geothermal reservoirs. There are many examples of such calculations in the literature, and the following list is selected to cover some of the variations and complications that can arise: see for example, Crerar and Barnes, (1976), Barton et al. (1977), Crerar et al. (1978), Barnes (1979), Frantz et al. (1981), Henley et al. (1984), Seward (1976, 1983, 1984), Henley (1985) and Ruaya and Seward (1986).

There are two fundamentally different ways of working through a solubility calculation based on the available thermodynamic data. First, if you are lucky, you will find an accurate equilibrium constant for a mineral dissolution reaction such as (20) above. In this case you will need estimates for T, P, and for pertinent variables which appear in the equilibrium constant (in this case, pH, oxygen and sulfur fugacity and total chloride). Finally, you will have to estimate activity coefficients for each species. Using an equation such as (21), which sums all the Reactions (20) for each of the different complexes (or values of n), you then have an estimate of total metal solubility. NaCl activity has been measured to 350°C, and if concentrations of other components are insignificant by comparison, then you know the chloride activity coefficients (tabulated by Wood et al., 1984).

The second approach is more difficult, and we will illustrate it with calculations being completed currently by G. M. Anderson (Barrett and Anderson, 1987, and personal communication). In this case data for a mineral solubility reaction such as (20) are not available. However, there do exist stepwise formation constants for aqueous complexes such as (17), and data for the "solubility product" or equilibrium constant for the solubility Reaction (18) forming the simple ion.

Anderson wanted to know the solubility of galena and sphalerite to 300°C. We start with Seward's (1984) overall formation constants for PbS and Ruaya and Seward's (1986) analogous constants for ZnS to 300°C:

$$M^{2+} + nCl^- = MCl_n^{2-n} \; ; \; \beta_n = \frac{\left(MCl_n^{2-n}\right)}{(M^{2+})(Cl^-)^n} \quad . \tag{25}$$

Here parentheses denote activities (so activity coefficients are included), and M stands for either Pb or Zn. There is a separate formation constant (25) for each value of n (e.g., $ZnCl^+$, $ZnCl^\circ_2$,...,$ZnCl_n^{2-n}$). Next, we obtain equilibrium constants from the compilation of Bowers et al. (1984) for the hydrolysis reactions

$$MS + 2H^+ = M^{2+} + H_2S_{(aq)} \; ; \; K_{MS} = \frac{(M^{2+})(H_2S)}{(H^+)^2} \quad . \tag{26}$$

Adding Reactions (26) and (25) gives an expression for the total metal concentration:

$$\sum M = M^{2+} + \sum_n MCl_n^{2-n} = a_{M^{2+}}/\gamma_{M^{2+}} + \sum_n a_{MCl_n}/\gamma_{MCl_n} \quad , \tag{27}$$

where we have divided the activities on the right hand side by the appropriate activity coefficients to obtain concentrations. Substituting (25) and (26) for (M^{2+}) and (MCl_n^{2-n}) into (27) gives

$$\sum M = \frac{K_{MS}(H^+)^2}{\gamma_{M^{2+}}(H_2S)} \left[1 + \sum_n \frac{\beta_n (Cl^-)^n \gamma_{M^{2+}}}{\gamma_{MCl_n}} \right] \quad . \tag{28}$$

This is our desired expression for total concentration of Pb and Zn as a function of dissolved H_2S, Cl^- activity and pH. This is also where the real problems start, since we now need activity coefficients for all the quantities in parentheses and for all the metal species. We outline the calculation here since it is so crucial.

The first problem is to calculate the true ionic strength. If we choose a total 3m NaCl concentration, then true (association-corrected) ionic strength can be calculated from the known dissociation constant of NaCl° (Helgeson et al., 1981, pp. 1427 and 1428) and the measured activity coefficients of NaCl (Wood et al., 1984). The true ionic strength is required by Equation (24) and sums the true concentrations of all ions, corrected for association:

$$\bar{I} = 1/2 \sum m_i Z_i^2 \quad (= m_{Na} \text{ for NaCl}) \tag{29}$$

This is different from the stoichiometric ionic strength which presumes complete dissociation of all NaCl:

$$I = m_{NaCl}^{tot} \tag{30}$$

There are both rigorous (and more tedious) and approximate (simpler) ways to calculate true ionic strength, and we will illustrate the tedious way first.

The equilibrium constant for the association Reaction (14) of NaCl° is

$$K = \frac{m_{NaCl^\circ}}{m_{Na^+} m_{Cl^-}} \frac{\gamma_o}{\gamma_+ \gamma_-} = \frac{[m_{NaCl}^{tot} - m_{Na^+}]}{m_{Na^+}^2} \frac{\gamma_o}{\gamma_+ \gamma_-} \quad . \tag{31}$$

Solving this for m_{Na} gives

$$m_{Na} = \bar{I} = \frac{-1 + \sqrt{1 + 4 K m_{NaCl}^{tot} \dfrac{\gamma_o}{\gamma_+ \gamma_-}}}{2K \dfrac{\gamma_o}{\gamma_+ \gamma_-}} \tag{32}$$

This can be solved initially by setting all activity coefficients equal to 1.0 (or by using the measured stoichiometric coefficients at T, P and total NaCl concentration). With the new value for $\bar{I}$ calculate new activity coefficients from Equation (24). Start the procedure over again, using the new activity coefficients to calculate a better true ionic strength from (32), and iterate to convergence. The difference between true and stoichiometric ionic strength is considerable at higher T; such calculations show, for example, that at 300° a 1m NaCl solution is 41% associated and a 3m solution is 57% associated.

There are two, simpler but approximate ways to calculate true ionic strength. The first was suggested by Helgeson (1981, p. 162): approximate the true ionic strength by calculating stoichiometric ionic strength up to 300°C and 3m NaCl, since there is little effect on calculated activity coefficients below this limit. The second assumes the ratio of the true to

stoichiometric ionic strength stays fairly constant over small ranges of concentration and uses the following equation (Helgeson, 1981, p. 162):

$$I = \bar{I} + \frac{\gamma_{\pm}^2 \bar{I}^2}{K_n \gamma_n} \quad . \tag{33}$$

If you want to calculate the true ionic strength of a 3m NaCl solution, substitute 3 for $\bar{I}$ to give I. Then the desired true ionic strength is given by scaling total molality according to the ratio $\bar{I}/I \times 3$ = desired true ionic strength. This can also be solved by iterative interval-halving on $\bar{I}$ for an exact solution.

With the true ionic strength estimated, Equation (24) can now be used to calculate activity coefficients of individual species for use in Equation (28). For this you will need the ionic radii $r_{e,j}$. These are available for everything but the $PbCl_n^{2-n}$ complexes for this particular example. However, these too can be estimated from correlation plots between $r_{e,j}$ and ionic entropy given by Helgeson et al. (1981, pp. 1302 and 1303). In this case, the necessary entropies of Pb and Zn chloro complexes can be taken from Seward's (1984) and Ruaya and Seward's (1986) data, respectively.

How accurate are calculated solubilities?

At this point the solubilities of galena and sphalerite can be calculated from Equation (28). Calculated results are shown in Figure 29 where they are compared with actual measured solubilities by Barrett and Anderson. There is good agreement between observed and predicted solubilities at 25°C, but calculated solubilities are roughly an order of magnitude higher than observed values at 80°C. Both the theoretical calculations and the experimental measurements are arguably state-of-the-art. Hence this probably represents the minimum difference or error we can expect between observed and calculated properties at the present time. There are many sources of potential error, including any of the equilibrium constants used in the calculation as well as errors involved in using Equation (24) for the activity coefficients of minor species in concentrated NaCl solutions.

Estimating chemical conditions in mineral deposits

As we have seen, solubility expressions such as (21) and (28) require knowledge of variables such as pH, oxygen and sulfur fugacities, T, P, chloride concentration and so on. With mineral deposits the original solution has long since disappeared (with the important exception of fluid inclusions), but many of the chemical properties at the time of deposition can be estimated from the minerals themselves. Fluid inclusions can provide important information on many of these parameters, and are the most commonly used method of estimating temperature and chloride concentration (see reviews by Roedder, 1979; Hollister and Crawford, 1981; and references therein).

Another common approach is to use coexisting minerals to provide estimates of chemical conditions at the time they were formed. Here you must be careful to show that equilibrium was attained for each assemblage used. Of course, different minerals may have appeared at different times so textures must be studied quite carefully. We will use Figure 30, a phase diagram by Crerar and Barnes (1976), to illustrate the method. Referring to the stability fields in this figure you might argue that many porphyry type deposits contain bornite, pyrite, chalcopyrite, but no graphite or native sulfur. Often calcite, barite and/or anhydrite appear to have been mobile (depositing and dissolving), and the ores frequently form where K-feldspar has altered to muscovite (sericite zone). This is a simplification because these minerals probably did not deposit simultaneously. However, it does suggest some reasonable chemical limits for an ore-forming fluid: This would be somewhere near the stippled center of the diagram, constraining pH (slightly acid), oxygen fugacity (about 10^{-37}), sulfur fugacity (average 10^{-11}) and so on. We have contoured pyrite solubilities as ppm Fe in this region of the diagram; according to Reaction (18) if we decreased total dissolved sulfur to 10^{-2} m, iron concentrations would increase 100 times, which gives quite

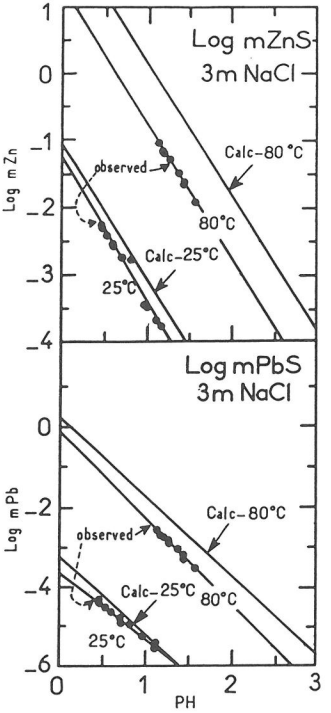

Figure 29. Comparison of calculated and measured ZnS and PbS solubilities in 3 m NaCl solutions at H_2S-saturated pressures as a function of pH and temperature. From T.J. Barrett and G.M. Anderson (personal communication).

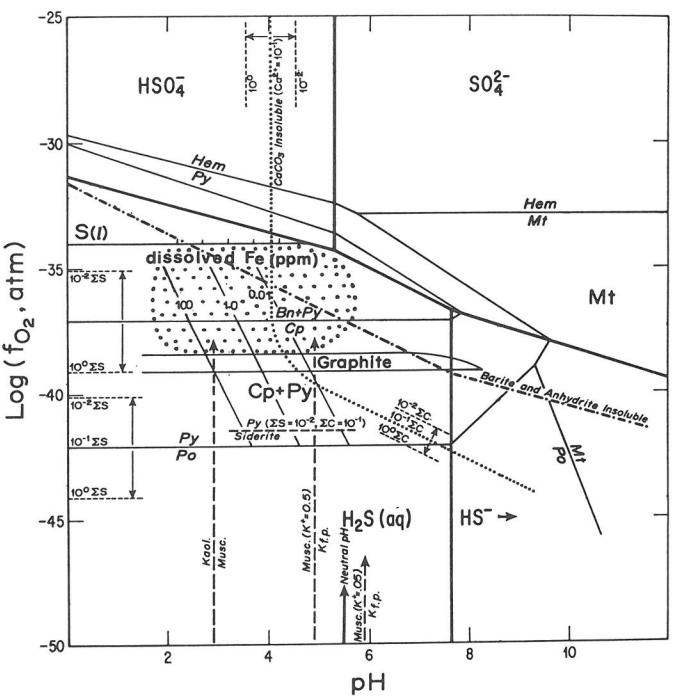

Figure 30. Oxygen fugacity versus pH stability fields of Cu-Fe-S-O minerals, plus calcite, barite, anhydrite, graphite, sericite (muscovite), and aqueous sulfur species at 250°C. Drawn for total S = 0.1 m; $Ba^{2+} = 10^{-3}$ m; total carbon = 0.1 m; $K^+ = 0.5$ m; $Ca^{2+} = 0.1$ m. The stippled region is the "most probable ore fluid" for porphyry deposits discussed in the text. Pyrite solubility is contoured as ppm Fe within this region based on data in Crerar et al. (1978). Pyrite solubility increases 100-fold for a 10-fold decrease in total dissolved sulfur. Revised from Crerar and Barnes (1976).

respectable solubilities of 1 to 1000 ppm Fe in the stippled field. One of the best examples of this kind of reasoning is the study by Barton et al. (1977) of the Creede ore deposit. A similar approach is often used with active geothermal reservoirs where deep hydrothermal waters can often be sampled directly; in such cases solution chemistry can sometimes be described in considerable detail (see Ellis and Mahon, 1977, p. 101, and Ellis, 1979, for examples).

The variables chosen as axes for these diagrams should depend on what you know about the system or wish to describe. For example, if the deposit contains many sulfide and oxide minerals, oxygen and sulfur fugacity would be useful coordinates. If some information is available on dissolved components, activity ratios of cations can be very helpful. Details on the calculation of such diagrams are given by Holland (1959), Barnes and Kullerud (1961), Garrels and Christ (1965, Ch. 10), Barton and Skinner (1979) and Stumm and Morgan (1981, Ch. 9). An extensive compilation of activity diagrams to 5 kbar and 600°C, together with thermodynamic data used in their calculation, has been provided by Bowers et al. (1984).

A third, important class of techniques for estimating the physical and chemical parameters of ore deposition requires isotopic analyses. Since this could be (and is) the subject of several books, we will only recommend several comprehensive reviews for the details. First, isotope ratios between coexisting minerals can be used to estimate deposition temperatures (provided the minerals equilibrated). The most useful isotope geothermometers have proven to be $^{18}O/^{16}O$, summarized by Taylor (1979), and $^{34}S/^{32}S$ (Ohmoto and Rye, 1979). With sulfur and $^{13}C/^{12}C$ isotopes it is often also possible to trace the evolution of pH and oxygen fugacity of ore-forming fluids throughout the period of active ore deposition; this was discovered by Hiroshi Ohmoto (1972). In conjunction with the other methods outlined in this section and information on mineral solubilities, the isotope record often provides remarkably detailed information on the chemical history of ore deposits (for some examples, see Rye and Ohmoto, 1974).

PART III. FORMATION OF PRIMARY AND SECONDARY ORE DEPOSITS

PRIMARY ORE DEPOSITION

Up to this point, we have been primarily concerned with generation and transport of ore components in hydrothermal solutions. We now consider the reverse problem, that of precipitating ore minerals from solution. There are many possible precipitation processes, many of them interrelated. The list includes: decreasing solubility by decreasing temperature; decreasing solubility by raising pH; decreasing ligand concentration (by dilution with groundwater); boiling; reaction with reduced sulfur; and changing oxygen fugacity.

Initial acidity

Starting with a high-T vapor phase which has just exsolved from a magma, we have seen that it is likely to be charged with ore components, as well as acidic components such as HCl°. Most species should be electrically neutral and associated at these temperatures. The exsolving solution will also contain dissolved sulfur, which you will recall partitions about as strongly as Cl from magma into vapor. The initial oxidation state of this exsolved sulfur depends on the oxygen fugacity at magmatic temperatures; for all natural mineral buffers (such as hematite-magnetite, $2Fe_3O_4 + 1/2\ O_2 = 3Fe_2O_3$) oxygen fugacity increases exponentially with temperature (see tabulation by Huebner, 1971). The oxygen fugacity of rhyolitic and dacitic lavas summarized by Carmichael et al. (1974, p. 330) fall between the QFM and HM buffers with values on the order of 10^{-11}-10^{-15} bars. For a similar argument, see Henley et al. (1984, p. 156). Figure 30 provides a dramatic contrast with the oxygen fugacity of roughly 10^{-34}-10^{-37} bars estimated for a porphyry-type ore environment at 250°C. Under these magmatic conditions, much of the exsolved sulfur may be oxidized to SO_2. Burnham (1979), for example, estimates that about 50-90% of the exsolving sulfur

will be oxidized by reactions such as

$$SH^-_{melt} + 5\,OH^-_{melt} = 3\,O^{2-}_{melt} + SO_{2,vapor} + 3\,H_{2,vapor} \quad . \tag{34}$$

This SO_2 has considerable acid potential too (like undissociated HCl°), and as temperature falls it should hydrolyze, producing H_2S and H_2SO_4 in a 1:3 ratio by the Reaction (Holland and Malinin, 1979):

$$4\,SO_2 + 4\,H_2O \rightarrow H_2S + 3\,H_2SO_4 \quad . \tag{35}$$

The ionization constant of HCl° also increases exponentially at lower temperatures (Fig. 20) so considerable acidity can be generated by both sulfur and chlorine as our exsolving solution cools.

Sulfur

Reaction (35) has immediate implications for ore deposition: Reduced sulfur will precipitate metal sulfides. The sulfate is the probable source of barite and particularly anhydrite which can be quite abundant in higher-T alteration zones (notice that the stability lines for both minerals pass through the center of our "most probable" porphyry ore fluid zone on Fig. 30). Eugster (1985, p. 20) summarizes isotopic evidence that "most or at least some of the sulfur in Sn-W deposits" associated with granites came from the original magma. The country rock itself is the only other possible source of sulfur. This could be derived in part from evaporitic sulfates (e.g., the carbonate-hosted Sn-W Dachang ores of SE China, Eugster, 1985; sulfide deposits in the Red Sea brines, Shanks and Bischoff, 1977), or from disseminated sulfide and sulfate minerals in adjacent wall rocks. Thermal or bacterial degradation of organic components is often invoked as the source of reduced sulfur for lower temperature sediment-hosted deposits such as the Mississippi Valley-type Pb-Zn ores (see review by Anderson, 1975). H_2S-charged brines and gas pockets are relatively common in deep sedimentary basins; mixing with metalliferous chloride brines could produce the sulfide deposits characteristic of the rims of large sedimentary basins (Jackson and Beales, 1967). There is no doubt about the sulfide-rich rims, but whether or not this mixing process really happens has been a topic of great debate and considerable interest for many years (for a critical review read Sverjensky, 1986).

pH and alteration reactions

Almost all ore mineral precipitation reactions such as

$$FeCl_n^{2-n} + 2\,H_2S + 1/2\,O_2 \rightarrow FeS_2 + 2\,H^+ + H_2O + nCl^- \tag{36}$$

not only generate acidity (H^+), but are actually driven to the left by acidity. (Notice on Fig. 30 that pyrite solubility increases by two orders of magnitude for each unit decrease in pH). This is certainly a complicating factor since we have just observed that ore solutions should become increasingly acidic as they cool. Reaction (35) generates three times as much sulfuric acid as H_2S (and even H_2S is a weak acid), and the ionization of HCl° with decreasing T compounds the problem. We clearly need some means of titrating out the acidity of cooling hydrothermal solutions if ore minerals are to precipitate at all.

This problem was resolved with the work of Julian Hemley (1959; Montoya and Hemley, 1975) and many others since (summary by Rose and Burt, 1979). The minerals of the host rocks themselves react with these corrosive ore fluids. Many of these wall-rock alteration reactions consume acidity with the minerals acting as proton sinks or Brønsted-Lowry bases. This can produce an enormously complex assemblage of changing alteration zones around and within large pluton-related deposits. For example, in the typical porphyry copper deposit, a central potassic zone of biotite-orthoclase alteration grades outward through quartz-sericite to sericite-kaolinite and finally to propylitic chlorite-epidote-calcite zones; primary copper sulfides are commonly most abundant in the sericitic zone near the potassic core (Lowell and Guilbert, 1970; Crerar and Barnes, 1976). Silicate alteration is typified by the orthoclase-sericite-kaolinite reactions:

$$3\,\underset{\text{orthoclase}}{KAlSi_3O_8} + 2\,H^+ = \underset{\text{sericite}}{KAl_2AlSi_3O_{10}(OH)_2} + 2K^+ + 6SiO_2 \;;\; K' + \frac{(K^+)^2}{(H^+)^2} \quad , \qquad (37)$$

$$2\,\underset{\text{sericite}}{KAl_2AlSi_3O_{10}(OH)_2} + 2\,H^+ + 3\,H_2O = 3\,\underset{\text{kaolinite}}{Al_2Si_2O_5(OH)_4} + 2K^+ \;;\; K'' + \frac{(K^+)^2}{(H^+)^2} \quad . (38)$$

Equilibrium constants for these two reactions have been measured by Montoya and Hemley (1975) both in terms of total m_{KCl}/m_{HCl} and the activity ratios (37) and (38) (both are necessary since the degree of ionization of KCl° and HCl° increases at lower temperatures). Given an estimate for K concentration and temperature, the pH of the ore fluid can be calculated from these constants. The vertical arrows on Figure 30 delimiting the fields of orthoclase, sericite and kaolinite alteration were derived this way. Equilibrium constants for many alteration reactions have been tabulated by Frantz et al. (1981) and Bowers et al. (1984).

Alteration processes such as (37) and (38) continue down to the lowest ore-forming temperatures and play an important role in supergene, freshwater, and marine environments. At lower temperatures these are usually thought of as weathering reactions, and are discussed in detail in the low-temperature aqueous literature (e.g., Stumm and Morgan, 1981, Ch. 9; Morel, 1983, Ch. 5).

Ore mineral deposition in an alteration environment probably proceeds by two mechanisms, both of which can produce replacement textures. First, the wall rock minerals themselves might react with ore fluids, raising pH and thereby driving precipitation reactions such as (36). The second possibility is that the mineral precipitates in response to some other stimulus; with Reaction (36) this might be decreasing T or chloride activity, or increasing oxygen fugacity or H_2S. Sulfide precipitation releases protons (2 moles of H^+ for every mole of pyrite deposited), which then react with host rock minerals. For a precipitation reaction such as

$$ZnCl^\circ_2 + H_2S \rightarrow ZnS + 2\,HCl^\circ \;; \qquad (39)$$

the total reaction in carbonate host rocks might be:

$$ZnCl^\circ_2 + \underset{\text{calcite}}{CaCO_3} + H_2S \rightarrow \underset{\text{sphalerite}}{ZnS} + CaCl^\circ_2 + H_2CO^\circ_3 \quad , \qquad (40)$$

or, in silicates:

$$ZnCl^\circ_2 + \underset{\text{orthoclase}}{3KAlSi_3O_8} + H_2S \rightarrow \underset{\text{sphalerite}}{ZnS} + \underset{\text{muscovite}}{KAl_3Si_3O_{10}(OH)_2} + 6\,SiO_2 + 2\,KCl^\circ \quad . (41)$$

The field record indicates that these are very important, common causes of ore mineral deposition. Sulfide/silicate or sulfide/carbonate replacement textures are very common; large hydrothermal deposits related to igneous plutons are almost invariably associated with extensive wall rock alteration.

pH buffer capacity. This is an important control on the potential for corrosion or mineral deposition which has not received much attention to date. pH buffer capacity is defined as the increment of acid or base that causes unit change in pH. A hydrothermal solution with a high buffer capacity will resist change in pH during wall rock alteration and mineral precipitation reactions; it will be highly corrosive and will show less tendency to precipitate metallic minerals. Crerar et al. (1985) have calculated the pH buffer capacities of some idealized ore fluids: these vary by 5 orders of magnitude, from simple quartz-saturated NaCl solutions (low buffering) to high-T seawater and basic NaCl-NaHS solution (highest). Many calculated buffer capacities also increase exponentially with temperature.

The geological ramifications are considerable. Weakly buffered systems which react with wall rocks will become basic more quickly and will rapidly deposit metals via reactions such as (39). If the same solutions do not react with wall rocks, the precipitation of a trace of metal (same reaction) will lower pH and metals will stay in solution, so the alteration reactions are necessary for ore deposition. Our calculations suggest that the NaCl-rich

ore fluids associated with felsic plutons are weakly buffered and that they rapidly precipitate copper, molybdenum and other sulfide ores in response to extensive wall rock alteration reactions at moderate to high temperatures. As temperature falls, the buffer capacity of these same solutions becomes even less and most metals are probably dumped before the solutions become too cool to react quickly with wall rocks. In contrast, fluids in carbonate terranes are highly buffered by the H2CO3-HCO3-conjugate pair; this helps explain how Mississippi Valley-type ore fluids can travel great distances without precipitating much metal; it also suggests that in this case metals may be precipitated by something other than a pH change (for example, meeting H_2S brines). Finally, seawater heated above 200°C has a very high buffer capacity, and also becomes acidic at elevated temperatures (Bischoff and Seyfried, 1978), both of which make it very corrosive; this is why circulating hydrothermal systems at oceanic spreading centers are so effective at leaching metals up and out of the oceanic crust. This is now recognized as a major control on the chemistry of the world ocean and a likely cause of many massive sulfide deposits (see Von Damm et al., 1985a,b; Bowers et al., 1985 and references therein).

Boiling

Extremely high salt concentrations (roughly 40 wt %) and variable liquid/vapor ratios are not uncommon in fluid inclusions (e.g., Roedder, 1979) and suggest the solution was boiling at the time of entrapment. There are many known geothermal reservoirs which discharge steam and boil at depth (Larderello, The Geysers, Matsukawa, and others described by Ellis and Mahon, 1977, p. 52). Hydrothermal fluids appear to have boiled in specific deposits ranging from porphyry copper-molybdenum and tin-tungsten ores to silver-gold and polymetallic vein deposits (summarized by Drummond and Ohmoto, 1985).

Physical models for convective flow around plutons, such as Figure 10 indicate boiling regions (see Cathles, 1977; Henley and McNabb, 1978). The "vapor" region shown in Figure 10 above the pluton is actually generated under supercritical conditions for pure water (so is not true boiling). However, addition of only 10 wt % salinity extends the boiling region (critical curve) so that boiling occurs for the same conditions. The computed lifetime of these vapor-dominated regions is less than 5,000-10,000 years, so if the computations are physically realistic, boiling is geologically short-lived.

The qualitative model for ore deposition in boiling systems is clearly outlined by Barton et al. (1977) for the Creede polymetallic vein deposits (see also Slack, 1980):

> "The ores were deposited from a freely convecting hydrothermal system that probably was initially charged by meteoric solutions, although the salts, metals, and sulfur may well have been derived from deeper sources. The circulating solutions deposited gangue and ore minerals near the top of the convecting cell in a hypogene enrichment process that extracted metals and sulfur from whatever sources were available at depth and swept them toward the surface. Boiling, with the loss of acid components (H_2S and CO_2) which recondensed in the cooler overlying rocks, led to the formation of an intensely altered sericitic capping above the ore. Precipitation of the ore is attributed to cooling and perhaps to a slight pH rise complementary to the loss of acid constituents through boiling."

The possible relation between boiling and ore deposition has now been modeled quantitatively by Drummond and Ohmoto (1985). In their work the essential features of the Creede model remain unchanged, except that the effect of boiling on pH is even greater than previously envisioned. Because natural hydrothermal solutions are complicated, multicomponent systems, the detailed behavior is highly dependent on solution composition. The effects are most pronounced for open, saline systems at lower temperatures with initially high CO_2/H^+ and CO_2/SO_4 ratios. The predominant volatile components partition from the liquid into a boiling vapor phase in the order $H_2>CH_4>CO_2>H_2S>SO_2$. While the computed results vary considerably with initial composition, the computation shown in Figure 31 is not atypical. Here you can see that the first 5% boiling (5% liquid converted to

vapor) raises pH roughly 1 unit, which in turn precipitates most dissolved metals. The effect is highly temperature-dependent, and all changes are maximized at about 300°C. Drummond's model shows that typical boiling hydrothermal solutions should lose most of their volatile components to the steam phase and precipitate most of their metals by the time the volumes of vapor and liquid are equal; this occurs at 1, 2, 5 and 10% boiling at 200°, 250°, 300° and 350°C, respectively. Obviously, boiling can be a powerful deposition mechanism, for those circumstances where it occurs. It remains to be demonstrated how common this is geologically, since not all systems are sufficiently hot and shallow, and/or sufficiently saline, to boil, and when this does occur, hydrodynamic models indicate boiling is relatively short-lived.

Remaining deposition controls

The remaining controls seem rather obvious at first sight, but even here there are potential complications, suggesting enough interesting research directions to keep us all occupied for years. It is unreasonable to think that any one deposition mechanism predominates, and in fact, it is likely that some or all are important to varying degrees in different environments.

Temperature. This seems the most obvious control since the solubilities of most ore minerals decrease at lower temperatures. Based on measured solubilities of chalcopyrite, pyrite and bornite, the concentration of $CuCl^{\circ}$ should drop two orders of magnitude from 350° to 250°C in the center of the "average" ore fluid zone of Figure 30, and Fe concentrations should fall roughly an order of magnitude. For this reason, Crerar and Barnes (1976) suggested that the general, large-scale deposition of porphyry coppers might be attributable to decreasing temperature, with wall rock alteration and increasing pH being a secondary cause of local, highly disseminated precipitation. That idea lasted one year, until Larry Cathles (1977) argued that porphyry copper ore shells are not very thick (averaging about 200 m thickness by 1 km depth) and that the temperature gradients across such zones are probably too small (or too short-lived) in circulating systems to be the major cause of deposition. His preferred mechanism was boiling, but we have just pointed out some possible objections to that theory, too.

Dilution. The argument here is that dilution by relatively pure groundwaters entrained in a more saline, convecting hydrothermal system decreases ligand concentrations, driving precipitation reactions such as (36) to the right. A pronounced decrease in the chloride concentrations of fluid inclusions at greater distances from intrusive source rocks is commonly observed (see references in Crerar and Barnes, 1976), but this does not necessarily imply a cause-and-effect relation with ore deposition. If the pluton was the source of chloride then such gradients are expected. Dilution also reduces metal concentration (and degree of saturation) as well as that of other species such as H_2S; if a 1:1 complex such as $FeCl^{\circ}$ predominates there should be no net result. If complexes with higher ligation numbers predominate, then precipitation might be possible, and becomes more probable if the entrained solutions also decrease temperature or raise pH.

Oxygen fugacity. The oxygen and sulfur fugacities of typical mineral buffers increase exponentially with temperature (Eugster and Wones, 1962; Huebner, 1971; Barton and Skinner, 1979). In our discussion of initial acidity above, we observed that oxygen fugacity drops by about 20 orders of magnitude from magmatic temperatures to 250°C in porphyry systems. Many mineral dissolution reactions such as (36) are dependent on oxygen (or hydrogen) fugacity, so it seems reasonable to expect a profound effect on solubilities. Oxygen fugacity has opposing effects on different minerals as illustrated by magnetite and pyrite dissolution:

$$\underset{\text{pyrite}}{FeS_2} + 2H^+ + 1/2\,O_2 = Fe^{2+} + S_2 + H_2O \quad ; \tag{42}$$

$$1/3\ \underset{\text{magnetite}}{Fe_3O_4} + 2H^+ = Fe^{2+} + H_2O + 1/6\,O_2 \quad . \tag{43}$$

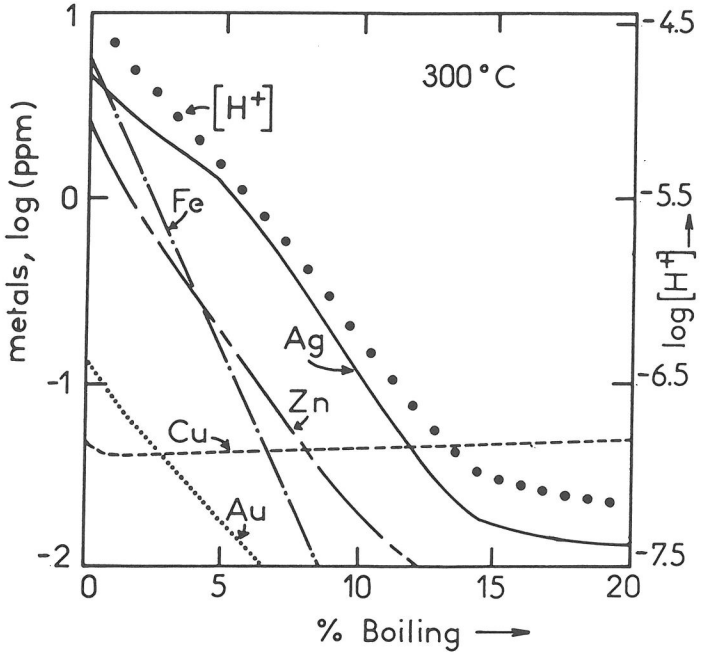

Figure 31. Change in metal and proton concentrations as a function of boiling for an open hydrothermal system at 300°C. The % boiling axis represents the wt % liquid converted to steam. Drawn for total carbonate = 3 m, and total sulfate = 3×10^{-9} m. Solubility data are summarized by Drummond and Ohmoto (1985). Diagram from Drummond and Ohmoto (1985).

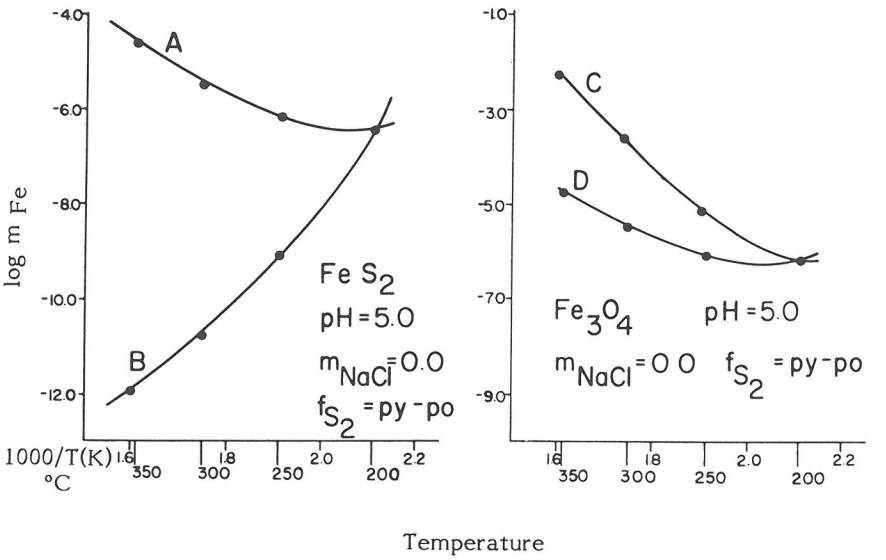

Figure 32. Solubilities of pyrite and magnetite versus 1/T for different oxygen fugacities in pure water. (A) Pyrite solubility when oxygen fugacity is buffered by pyrite + pyrrhotite + magnetite. (B) Pyrite solubility at constant log $f(O_2) = -43.9$. (C) Magnetite solubility at constant log $f(O_2) = -43.9$. (D) Magnetite solubility when oxygen fugacity is buffered by pyrite + pyrrhotite + magnetite. Solubility data from Crerar et al. (1978) and original diagram from Crerar et al. (1985).

The combined effects of oxygen fugacity and temperature on solubilities of both minerals are illustrated in Figure 32 (from solubility studies by Crerar et al., 1978). Curves B and C are for constant oxygen fugacity while A and D represent the fugacity change of the pyrite + pyrrhotite + magnetite buffer with temperature. The oxygen fugacity of this buffer increases roughly 13 orders of magnitude between from 200° to 350°C. Despite the reverse sense of oxygen in Reaction (43), magnetite solubility increases with temperature for both cases (the equilibrium constant for this reaction increases sufficiently with temperature to outweigh the opposing effect of higher oxygen fugacities). However, the solubilities for curve D (increasing oxygen fugacity) fall to 1% of that for C (constant oxygen) by 350°C. For pyrite, the effects are reversed and more pronounced, with concentration increasing 100-fold to 350°C for A (increasing oxygen) and decreasing enormously at constant oxygen fugacity. In general, the solubility of minerals such as gold, pyrite and molybdenite (for which solubility increases with oxygen fugacity) should increase dramatically with temperature. This helps explain the sharp rise in solubility of minerals such as gold with temperature (Fyfe and Hemley, 1973; Seward, 1983) and is consistent with the common occurrence of metals such as Au, Mo and Cu in higher-T deposits. Minerals such as cassiterite (SnO_2) and magnetite which show the reverse trend (since dissolved species are more reduced than the minerals) pose a different problem; here solubilities can decrease at higher oxygen fugacities (hence at higher T if the same mineral assemblage controls oxygen fugacity at all temperatures). See, for example, the data for cassiterite (SnO_2) solubility summarized by Eugster (1986), and the study of magnetite solubility under supercritical conditions by Chou and Eugster (1977).

Natural processes responsible for sulfide precipitation are complex, and depending upon specific circumstances, an array of mechanisms such as boiling or variation of sulfide solubilities with temperature may operate. However, in the absence of fluid inclusion data indicating boiling or strong temperature gradients, it is likely that alteration reactions are necessary to explain the observed metal concentrations within ore zones. Genetic and spatial associations of hydrothermally altered wall rocks and fracture- controlled sulfides are common (Meyer et al.,1968; Brimhall, 1977) indicating the importance of irreversible reactions between ore-forming solutions and surrounding wall rocks to the final deposition of sulfides. Circulation of hydrothermal fluids through previously-mineralized wall rocks occurs frequently in nature and is the norm not the exception.

Multi-stage mineralization and ore metal remobilization

Field studies of hydrothermal mineralization in porphyry systems have shown that primary mineralization, that is ore which is unoxidized by chemical weathering, is generally composed of superimposed networks of veins and veinlets which control alteration patterns, either in halos around individual veins or pervasive zones in regions of high fracture density. The fracture networks and corresponding alteration is formed during single or multiple hydrothermal events, each of which can be attributed to the intrusion, convective fluid circulation, and cooling of a specific parent pluton (Meyer et al., 1968; Lowell and Guilbert, 1970; Gustafson and Hunt, 1975; Brimhall, 1977 and 1979).

Ore metal remobilization versus introduction. Certain systems, particularly porphyry molybdenum deposits often have multiple intrusions, each having localized ore grade mineralization (Wallace et al., 1968) near the apex of each successive intrusion as at Climax, Colorado. Field and petrographic evidence strongly suggest that each intrusive released its own ore-forming fluid. In contrast, copper rich porphyry systems seldom have as many mineralized plutons as in the molybdenum systems. In fact in copper systems driven by only a single thermal event, the nature of mineralization and alteration may change drastically during the cooling history with the incursion of meteoric water. The superposition of phyllic (sericite-bearing, biotite destructive) alteration on earlier, higher temperature potassic alteration assemblage (biotite, muscovite, and alkali feldspar) is due to this late-stage modification of the ore– forming hydrothermal fluid (Taylor 1979).

Ore metals are clearly first emplaced locally in a district from saline magmatic aqueous fluids through circulation in the highest temperature vein networks and biotitic igneous

breccias which control potassic alteration. With cooling and dilution by meteoric water, the ore-forming aqueous fluids become highly acid and circulate more extensively than before. Intense hydrolysis reactions pervade the wall rocks as well as the earlier, sulfide- bearing potassium silicate altered proto– ore (protore). At this stage, the source or sources of metals is difficult to ascertain. The basic question is whether or not ore metals in veins within phyllic alteration halos were derived by dissolution of earlier sulfides related to potassic alteration mineral assemblages, or whether they were simply scavenged by circulation of late hydrothermal fluids through ordinary unmineralized wall rock. The former mechanism is referred to as ore metal remobilization, the latter as scavenging. Both processes actually involve remobilization, but the former mechanism refers to extraction of metals from a previously mineralized state, rather than from ordinary wall rocks. In actuality, both mechanisms may occur, and given the enormous size of hydrothermal convection cells, the possible source regions for metals is not only gigantic but potentially quite varied as well. Resolution of this question is important as it relates to two of the most fundamental aspects of understanding ore fluids: the source of metals and their behavior during superposition of hydrothermal circulation systems.

Relationships of wall rock alteration to mineralization. Assessment of the effects of superposition of young hydrothermal events upon pre-existing protores can only be addressed from a practical standpoint within available exposures in mines. The deep reaches of convective systems are therefore rarely accessible as they are low grade, and hence are of little interest to mine operators. This leaves only three possibilities for addressing the issue of remobilization: (1) petrologic and geochemical analysis of the few optimal mining exposures where source regions of metals have been recognized, (2) theoretical analysis using irreversible chemical thermodynamics to model multi-stage mineralization, and (3) experiment. In all cases, the essential question is the net effect that superimposed alteration reactions have on protore sulfide, silicate, and oxide mineral assemblages. There is much evidence to suggest that hydrothermal remobilization and redistribution is common, at least for copper. Molybdenum, tungsten, and tin have received much less attention is this respect. The varied array of copper sulfides (chalcopyrite, bornite, chalcocite, and digenite) which are known as hydrothermal products and the thermochemical conditions of their stability may contribute to the relative mobility and complex history of copper in contrast to molybdenum and tungsten.

Hypogene leaching. Lacy and Hosmer (1956) recognized evidence suggesting the leaching of metals during hypogene mineralization at Cerro de Pasco, Peru. This important discovery opened the way for pursuing the behavior of metals during multiple hydrothermal events and for improving understanding of the space-time patterns, relationships of mineralization to alteration, plutonism, and temporal evolution of fluid composition. Continued pursuit of this problem has been possible in the extensive exposures in the Butte Mining District of Montana where multi-stage mineralization was recognized (Meyer et al., 1968). Here a large fissure vein system with phyllic and argillic alteration, the Main Stage, was superimposed upon a pre-Main Stage ore, a fracture-controlled disseminated chalcopyrite-pyrite-magnetite porphyry copper deposit with potassic alteration containing secondary biotite. The late veins are particularly well-developed as mineralization was syntectonic with regional compressive stress during Laramide thrusting and folding (Woodward, 1986), producing high fracture permeability and intimate fluid/rock interaction. Using the concept of reaction progress (De Donder, 1928, 1936; Prigogine, 1955; Helgeson, 1968) for monitoring the net extent of Main Stage alteration and mineralization effects on the pre-Main Stage protore, Brimhall (1977) developed a lithologic method for evaluating the transfer of metals between an early type of mineralization and a later ore-forming fluid with subsequent precipitation of sulfides.

Chalcopyrite abundance, determined from quantitative modal analysis on heavy mineral separates, can be used to monitor the amount of Main Stage reaction progress. Figure 33 shows the progressive leaching of chalcopyrite, destruction of pre-Main Stage mineral assemblage (biotite, magnetite, hematite, orthoclase), and the precipitation of Main Stage ore minerals (enargite, covellite, digenite, chalcocite, quartz, and pyrite. From this lithologic analysis, it is clear that phyllic (sericitic) alteration can leach copper from

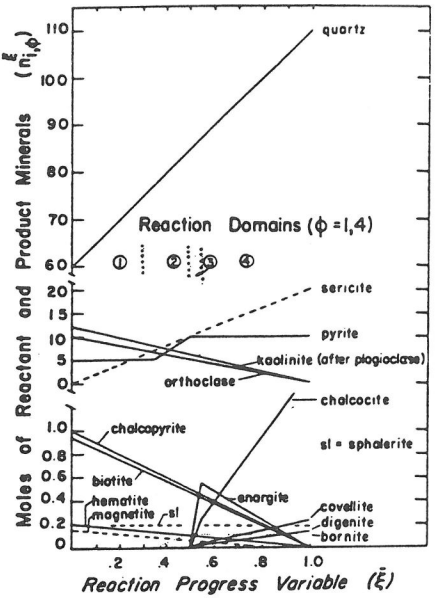

Figure 33. Generalized molar variation patterns based on lithological analysis. Four reaction domains are recognized as shown with abrupt changes in the slope of piecewise continuous molar curves. Slopes of molar variation curves with reaction progress (based on chalcopyrite abundance) are equal to stoichiometric reaction coefficients. From Brimhall (1979).

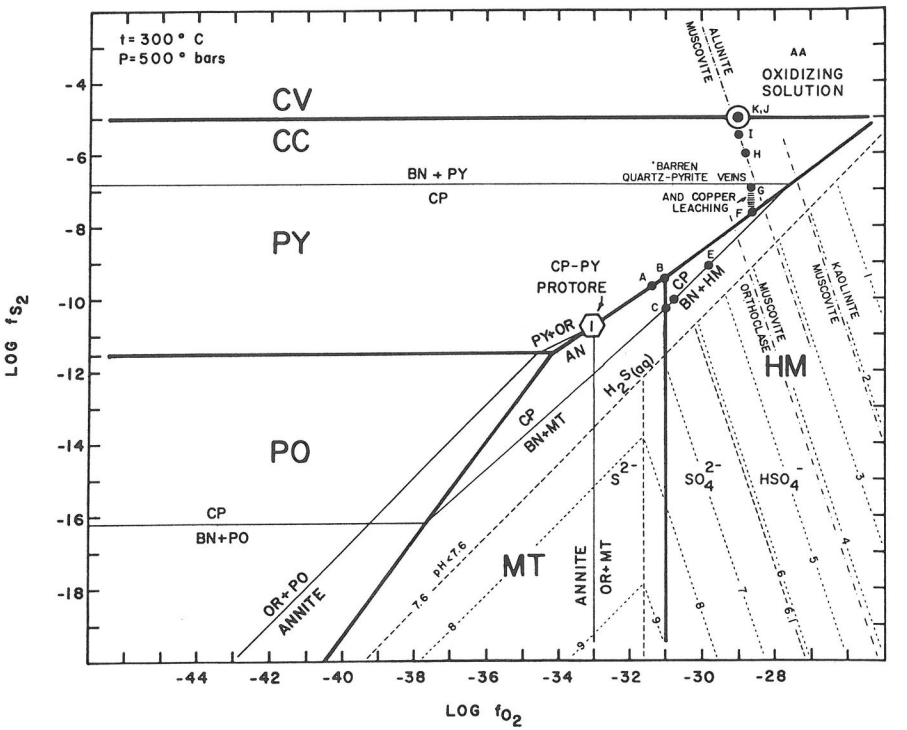

Figure 34. Isothermal isobaric fugacity diagram showing the stability fields of covellite (CV), chalcocite (CC), pyrite (PY), pyrrhotite (PO), magnetite (MT), and hematite (HM). Chalcopyrite field is surrounded by bornite plus an additional sulfide. Annite stability field is surrounded by orthoclase plus sulfides and oxides. Position of potassium-silicate protore at Butte, Montana is given at 1. Position of advanced argillic alteration assemblage and Main Stage oxidizing fluid is at the intersection of CV-CC phase boundary and that of alunite- muscovite. From Brimhall (1980) and Brimhall and Ghiorso (1983).

chalcopyrite-bearing potassic alteration assemblages. Hence, the pre-Main Stage mineralization serves as a protore for leaching copper which is remobilized and reprecipitated during Main Stage hydrothermal mineralization.

Thermodynamic modeling of hypogene oxidation and sulfidation: effects of magmatic volatiles on hydrothermal fluids and protores. Thermodynamic modeling of the copper mass transfer process described is possible using standard thermochemical data available in SUPCRIT (Helgeson et al., 1978) in conjunction with numerical modeling programs to simulate the irreversible reaction chemistry (Wolery, 1979). First, phase equilibria are examined which are relevant to the mineral assemblages present in the potassic alteration protore. Second, the end product Main Stage mineral assemblage is characterized in terms of its equilibrium fluid composition at conditions typical of vein formation (300°C and 1 kbar). The protore mineral assemblage chalcopyrite, pyrite, biotite magnetite is the starting point for the Main Stage reaction path which leads ultimately to the mineral assemblage chalcocite-covellite-muscovite-alunite as seen in Figure 33, an oxygen-sulfur fugacity diagram (Holland, 1959, 1965; Meyer and Hemley, 1967; Brimhall, 1979, 1980). While the pre-Main Stage assemblage formed at much higher temperatures, near 650 °C, Main Stage reactions proceeded at a lower temperatures, near 300°C, based on fluid inclusion homogenation temperatures. The Main Stage fluid, in the areas of most intense alteration, is in equilibrium with the advanced argillic assemblage (alunite, muscovite, kaolinite, quartz), often with covellite and chalcocite (Hemley and Jones, 1964; Meyer and Hemley, 1967; Hemley et al., 1969; 1980). It is clear in Figure 34, that this high f_{S_2} fluid composition is at considerable disequilibrium with respect to the chalcopyrite-pyrite-biotite-magnetite protore. The highly acid fluids of the Main Stage were probably generated by degassing of late volatile-rich magmas, volatile condensation, ionization, and subsequent hydrothermal metasomatic reactions between protore, magmatic gasses (SO_2 and H_2S), and ground water (Brimhall and Ghiorso, 1983; Head et al., 1987).

Destruction of wall rock buffer control: the role of biotite. The isothermal calculation of the reaction path is shown in Figure 34 extending from the protore containing chalcopyrite along the pyrite- magnetite phase boundary, along magnetite-hematite, then along chalcopyrite- hematite, finally leaving the chalcopyrite field and arriving ultimately at the covellite-chalcocite boundary in the presence of alunite-muscovite. Upon leaving the chalcocite field, an interval of the reaction path is attained over which the fluid is not in equilibrium with any copper-bearing sulfide. The copper released from the dissolution of chalcopyrite is all contained in the fluid phase. This is thermodynamic confirmation of copper leaching from the protore. To understand the phase equilibria involved it is useful to introduce the $a_{H_2S_{(aq)}}$ and $a_{Fe^{2+}}/a_{Cu^+}$ variables. Figure 35 presents phase diagrams at different a_{H_2S}, and shows how the biotite stability field is limited to log a_{H_2S} values less than −0.5. The composition of the protore is shown in Figure 35d which, given the sulfide-oxide-silicate assemblage present, buffers the log f_{O_2} at a value of −33. In contrast, the Main Stage fluid shown in Figure 35f, has a log f_{O_2} at a much higher value, −29. The role of biotite in buffering the oxygen fugacity, and tending to keep it at a low value in equilibrium with the protore is evident in Figure 35d. Figure 36 shows the dramatic effect of H_2S fugacity on the equilibria, especially the Fe to Cu activity ratio in the fluid. This figure is a plot of the triple points shown in Figure 35.

Combining Figures 35 and 36 in Figure 37 conveniently shows the region occupied by biotite, a domain characterized by a high $a_{Fe^{2+}}/a_{Cu^+}$ and low f_{H_2S} and f_{O_2}. The pyrite-chalcopyrite-orthoclase-biotite protore assemblage plots directly on the upper and outer phase boundary of biotite. At higher values of f_{O_2}, magnetite is stable instead of biotite. The computed Main Stage reaction path departs this protore composition only when biotite is destroyed by hydrolysis reactions in which muscovite (sericite) is produced. At this point, the buffering effect of the protore assemblage to maintain an equilibrium fluid composition is eliminated, and the fluid composition is free to evolve towards the Main Stage fluid, a composition rich in aqueous H_2S and Cu (AA for advanced argillic assemblage). Over this path leading up to the advanced argillic assemblage, the fluid becomes progressively more oxidized and sulfidized. This assemblage is attained in nature only in the

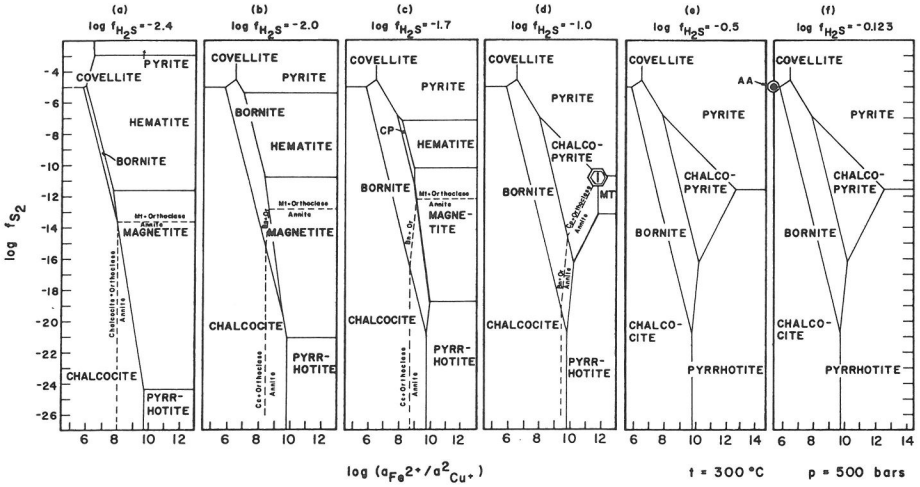

Figure 35. Oxygen fugacity-iron/copper activity diagrams at 300°C and 500 bars. Figures 35a through f are cross sections of Figure 36 at different H_2S fugacities where the triple points of Figure 35 are shown. The composition of the potassic-alteration protore assemblage is shown in relation to the composition of the Main Stage fluid. The annite (biotite) stability field occurs in the lower right of each figure except at highest H_2S fugacities where it is unstable. From Brimhall (1980).

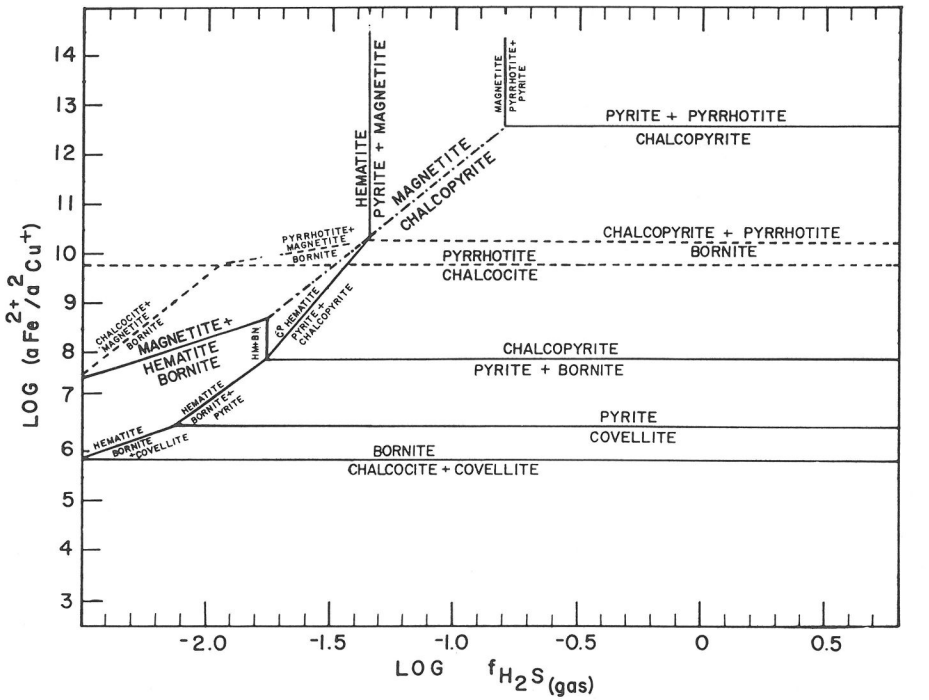

Figure 36. Activity-fugacity diagram at 300°C and 500 bars representing the locus of triple points shown in Figure 35.

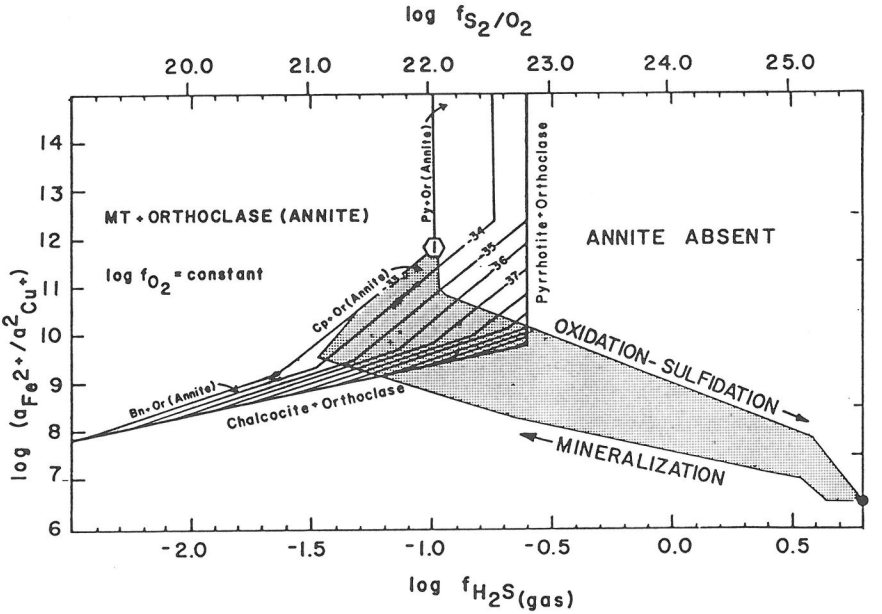

Figure 37. Calculated reaction loop for growth of Main Stage hydrothermal veins from Potassic alteration protore which plots at point 1 on the phase boundary of annite-chalcopyrite-orthoclase-pyrite. Biotite (annite component) is restricted to the upper left portion of the diagram at high aqueous Fe/Cu ratios and low activity of H_2S. Oxygen fugacity contours are shown. Above a log fugacity of oxygen of −33, annite is unstable, yielding to magnetite, orthoclase, and water. Biotite imposes strong buffering effects on reacting fluids, and until it is destroyed, fluid composition is largely fixed. Upon alteration of biotite by sericitization, the reaction path proceeds to the advanced argillic composition (alunite, muscovite, kaolinite) (AA), as magmatic volatiles are released and ionize reacting with the protore. With cessation of magmatic gas contamination of the hydrothermal fluid, reaction occurs between the advanced argillic fluid and the protore along the mineralization path. In contrast to the oxidation-sulfidation path leading the the AA fluid over which copper is leached, the mineralization path precipitates ore sulfides. These are the Main Stage Veins. Their copper has been remobilized from the older disseminated chalcopyrite protore. From Brimhall (1980).

regions of most intense fluid circulation, at the veinward edge of alteration halos, or in regions of highest fracture density within or near the parent pluton.

There are two parts to the calculated reaction path. The first is due to the development of the Main Stage fluid, the hypogene oxidation-sulfidation path leading to the advanced argillic assemblage (Brimhall and Ghiorso, 1983). This process has modeled the degassing of SO_2-H_2S-rich felsic magmas, with interaction with ground water in equilibrium with the protore. The magmatic volatiles disproportionate to yield sulfuric acid solutions. Over this leg, copper-bearing sulfides are only briefly thermodynamically stable as the fluid composition has such a high f_{O_2} that pyrite is the only stable sulfide see Figure 38 (and Fig. 35e). During this excursion, copper is leached from the protore and enriched in the Main Stage fluid. Finally, during reaction between this advanced argillic fluid and the protore, the stability of copper sulfides is once again attained (Brimhall, 1980). This is the Main Stage mineralization leg of the reaction path (Figs. 37 and 38) over which high grade copper sulfide veins have formed.

Feedback of chemical reaction and fluid flow: fluid dominated threshold states and the importance of the advanced argillic alteration mineral assemblage. The theoretical mass transport calculations modeling redistributive phenomena of vein formation help isolate some of the critical attributes necessary for ore metal remobilization to occur. What

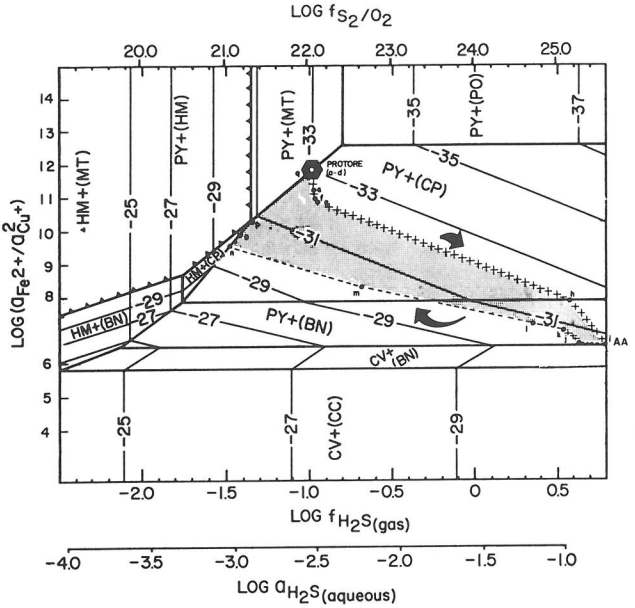

Figure 38. Same coordinate system as Figure 37, but this figure is contoured on log oxygen fugacity. Phase boundaries are shown as surfaces contoured on log oxygen fugacity with the mineral above the surface (high) fugacity phase shown without parentheses and the subjacent phase (low oxygen fugacity) phase in parentheses. For example, PY+ (CP) means pyrite exists at a higher oxygen fugacity than chalcopyrite as shown in Figure 35. The reaction loop of Figure 37 is shown. This path is shown with a plus sign when it is up in the pyrite (PY) field and as a minus sign when it occurs along a phase boundary with a copper-bearing sulfide. The oxidation-sulfidation path leaches copper, the mineralization path fixes copper. From Brimhall (1980). Points along reaction path labeled (a-q) are also shown in Figure 39 for comparison.

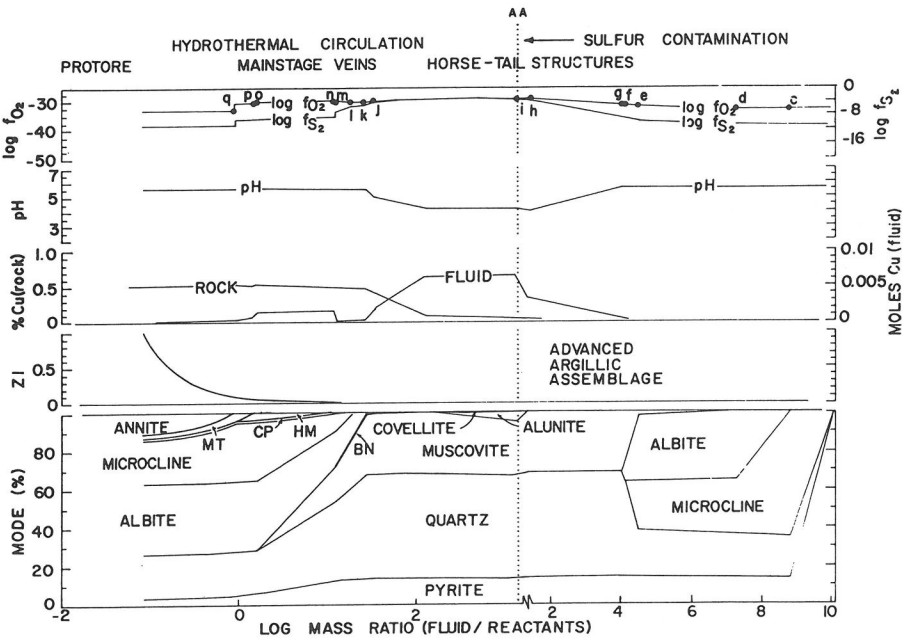

Figure 39. Complete reaction cycle at 300°C and 500 bars. Read from left to right the sulfur contamination path followed by the the hydrothermal mineralization phase with the advanced argillic (AA) zone in between. The AA represents extreme values in aqueous copper, pH, and molar volume change of reaction. Negative volume change may mean that porosity or permeability are enhanced at the AA stage. From Brimhall and Ghiorso (1983).

emerges from the simulation is the fact that the advanced argillic alteration mineral assemblage is a unique hydrochemical state in the chemical evolution of sulfur-rich hydrothermal systems. Not only are the oxidation and sulfidation states extremely high, so high in fact that copper-bearing protore host minerals become unstable releasing copper to the ore fluid, but a structural threshold is attained as well. Figure 39 shows that during the development of the advanced argillic alteration assemblage a negative calculated volume change (products minus reactants) of the alteration reaction occurs. This state corresponds also to maxima in f_{O_2}, f_{S_2}, and aqueous copper content and is accompanied by a minima in solution pH. With the indicated negative volume change, creation of void space or enhancement of fracture permeability is likely. Once this state is attained, then it is probable that continued reaction with wall rock mineral assemblages will tend to neutralize the advanced argillic fluid, and ultimately reprecipitate ore sulfides. The enhanced porosity or permeability increases the likelihood that such hydrothermal reactions can proceed to completion. The advanced argillic assemblage can be viewed then as a physiochemical threshold state, which if attained, can have major ore-forming consequences, particularly metal redistribution in the porphyry copper environment.

Consistent with these conclusions based on chemical thermodynamic modeling, are more recent calculations combining fluid flow with chemical reaction (Lichtner, 1985; Helgeson and Lichtner, 1987) which indicate that the decrease in fluid pressure accompanying upward flow of acid solutions favors dissolution of sulfides and precipitation of quartz.

Epithermal Systems: manifestations of deep porphyry mineralization? There is mounting evidence suggesting that the alteration- and ore mineral assemblages in acid-sulfate precious metal deposits and in some active geothermal systems within calc-alkaline stratovolcanoes may be the upper manifestations of deeper base metal mineralization (Wallace, 1979; Henley and Ellis, 1983; Brimhall and Ghiorso, 1983). However the question remains as to whether acid-sulfate epithermal precious metal deposits are typically located above porphyry copper deposits, whether they are near surface, low temperature equivalents, or whether they are shallow deposits formed from a reworked porphyry copper deposit at depth (Healds et al., 1987).

SECONDARY ORE DEPOSITION

Upon erosion of the overlying volcanic or plutonic edifice, base metal ores related to porphyritic intrusives are exposed to reactive surficial fluids, both ground water and air. All primary ores, of porphyry type or otherwise, are subject to intense chemical weathering in the near surface environment under conditions far different than at depth. Reaction products formed during imposition of surficial conditions are referred to as secondary ores, in contrast to all the older products of multi-stage processes which enriched ore metals at greater depths, generally under the influence of hydrothermal fluids. Not all ore-grade weathering products have hydrothermal ores as a precursor. In fact, under certain conditions, weathering produces minable ores from rather ordinary rocks containing ore metals at only crustal abundance levels, for example the formation of bauxites from granites. Analysis of these processes will be included here as they are part of a family of related secondary transport processes and help to illustrate the full range of possibilities of hydrochemical behavior.

Atmosphere-dominated states

To a large extent, given the uniquely oxygen-rich composition of the earth's atmosphere, surficial oxidation is a ubiquitous factor in hydrochemical modification of sulfide ores and exposed rocks in general. So intense are the oxidation and hydrolysis reactions which proceed to minimize the state of disequilibrium between the atmosphere and rocks formed in the subsurface, that weathered material may often retain little resemblance to its protolith. Ore-forming constituents such as sulfides, formed at depth, may contribute additionally to the intensity and extent of weathering reactions by producing natural sulfuric acid which destroys the capacity of rock mineral assemblages to buffer oxygen fugacity, and

hence resist modification by imposed fluids. Ultimately, atmospheric gasses dominate the pore spaces of weathered rocks, a condition which may be maintained to the depth of the ground water table. We will see that the transition from unsaturated to saturated conditions is an interface between geochemical systems dominated by the Earth's atmosphere, and a subsurface domain controlled by the primary mineral assemblages, protected from oxidation by the presence of water in pore spaces which precludes oxidizing atmospheric gasses.

Chemical weathering is responsible for the final enrichment of ore metals in large low-grade ore deposits which in many cases, for example copper, is necessary for the mineralization to be considered minable. Because of the diversity of primary ore types and the zoning within a single deposit, chemical effects due to weathering are varied and depend upon the level of exposure and position within a primary district zoning pattern.

Some enrichment mechanisms involve the dissolution of ore minerals with subsequent transport and ultimate redeposition of ore metals in an enriched state. Other processes enrich ore metals without their migration simply by virtue of removing other more mobile species. In all cases, weathering results in strong physical and chemical modification of primary ores. Consequently, in order to interpret elemental mobility patterns, it is necessary to consider both physical properties as well as chemical composition in addressing secondary enrichment. The relationships between rock density, chemical composition, porosity, and deformation are described by constitutive mass balance models given in Brimhall et al. (1985) and Brimhall and Dietrich (1987). Mass balance models describe the conservation of mass of an element of interest and provide a practical means of using chemical elements as geochemical tracers for interpreting mass transport mechanisms. Mass balances provide the ultimate limits on enrichment processes.

Constitutive mass balance models and simplified chemical controls

Four major classes of surficial transport behavior account for the secondary enrichment of ore deposits: (1) residual, (2) supergene, (3) hypogene, and (4) perfectly mobile or continuously leached. These differ primarily as to whether or not an ore metal of interest is a mobile chemical species, and if so, whether its migration is upwards or downward, and is reprecipitated or not. In the case of mobile elements, the concern for this sense of transport has to do with identification of the source region of the metal of interest, and hence the direction from which metals have come: "supergene" literally from above, "hypogene" from below. This directionality in transport of mobile metals is also of significance because of a need to understand the contrasting physiochemical conditions may which at first release metals from the source, mobilize them into ground water, and ultimately, reprecipitate them in an enriched state. Considering the broad range of metals in primary ores, all four types of transport behavior often occur within the same secondary hydrochemical system. The specific behavior taken by an element depends upon the mineralogy and pore structure of the protolith, mineral stability and kinetics of a particular system in relation to advective flow and gas diffusion rates of ground water and ground gasses respectively. The behavior of a given element can vary markedly from system to system, in one being immobile and residually enriched, to nearly complete removal as a mobile species.

Residual enrichment. If an ore metal of interest is present in a rock before weathering, and is geochemically immobile, it may become enriched simply by removal of perfectly mobile elements from the rock by migrating ground water. This passive enrichment is referred to as residual, and results for the most part by a rock becoming more porous, as unstable minerals are attacked and dissolved. The mass balance model describing conservation of mass of an immobile species during residual enrichment is simply that the total mass of an element contained within a representative elementary volume after weathering is equal to the mass of that element before weathering. The mass of such an element is given by the product of the volume of the system of interest, V, bulk rock density, ρ, and concentration, C, before weathering in the protolith state, p, and after weathering, w (44):

$$V_p \rho_p C_{i,p} = V_w \rho_w C_{i,w} \quad . \tag{44}$$

This may be reduced from a three dimensional volume to one dimension, B. The possible effects of compaction or expansion during weathering can be accounted for by defining strain, ε_i, as the change in length in the vertical direction divided by the initial length (45)

$$\varepsilon_{i,w} = \frac{B_{i,w} - B_{i,P}}{B_{i,P}} \quad . \tag{45}$$

With this definition of deformational strain, and reduction to one dimension where V terms reduce to one dimension, B, (44) may be solved in non-dimensional form for an enrichment factor (46), the ratio of the concentration of an immobile element in the weathered state of a rock to that of the protolith.

$$\frac{C_{i,w}}{C_{i,p}} = \frac{B_{i,p}}{B_{i,w}} \frac{\rho_p}{\rho_w} = \frac{1}{\varepsilon_{i,w} + 1} \frac{\rho_p}{\rho_w} \quad . \tag{46}$$

This expression offers a simple means of interpreting the enrichment factor of an element in terms of changes in physical properties of a rock after weathering. In Figure 40 the residual enrichment mass balance model is shown diagrammatically, and in Figure 41 a set of data is presented on nickel enrichment in weathered ultramafic protoliths (Brimhall and Dietrich, 1987). Closed system residual enrichment of nickel is evident as a harzburgite protore is converted into laterite saprolite and pisolitic reddish soil, all without demonstrable deformation, a slope of one for $\varepsilon = 0.0$. It is clear that from (46) simple residual enrichment is governed primarily by the magnitude of the change in rock density, and secondarily by collapse, that is negative strain.

Figure 42 explains the observed paragenesis in typical nickeliferous laterite profiles in terms of the equilibrium solubilities of minerals (Golightly, 1981) given as moles per liter of cationic species. In this figure ideal or stoichiometric solubility as a function of solution pH, is consistent with the vertical weathering profile with the least soluble mineral, goethite at the top, and the most soluble mineral, forsterite at the bottom. The most soluble mineral is followed upwards by pyroxenes, serpentines, chlorite, talc, nepouite (nickel serpentine), kerolite (nickel talc), kaolinite, gibbsite, and finally goethite on top. The pH of surface water in laterites has been measured at values near 5, while at depth the fluids are alkaline, with a pH of 8.5. The nickel originally contained in forsterite at a concentration of generally 0.20 wt.%, is ultimately retained in the weathering product, and enriched in accord with the reduction in density.

The chemical weathering path by which this dramatic density reduction occurs and causes residual enrichment is shown in Figure 43, extending from a non-porous protolith with an initial bulk density of 3 and an average grain density of 3.1 to saprolites with bulk densities of 0.6, grain densities of 2.5 and porosities of 0.75 (75%). Porosity is calculated from bulk and grain density from the relationship: porosity equals one minus bulk density divided by grain density.

Supergene enrichment. The second type of transport process which causes metal enrichment during weathering is supergene enrichment. This is the dominant type of secondary enrichment leading to ore-grade deposits as the supergene enrichment factors are typically several times those of maximum residual enrichment. The difference between the mobility of elements which are enriched by supergene and hypogene processes and perfectly mobile elements, is that in the former two cases, once mobilized, elements are at least partially reprecipitated. The efficiency of reprecipitation is addressed in (Brimhall et al., 1985). In supergene enrichment ore metals are introduced to a zone of enrichment from above where leaching has released them to migrating meteoric water.

Figure 44 shows that in copper systems, leaching of copper from primary sulfides (typically chalcopyrite and bornite) occurs, followed by reprecipitation of copper as secondary chalcocite and covellite. Mg, Ca, and Na are leached without reprecipitation, behaving as perfectly mobile elements. In deposits other than porphyry copper deposits, for example gold-rich laterites developed over primary mineralization in greenstone terranes, Au, Ce, Cr, Mo and Fe behave as supergene elements with Nb, Sn, Th, V, W, Zr, Al, and Ti being

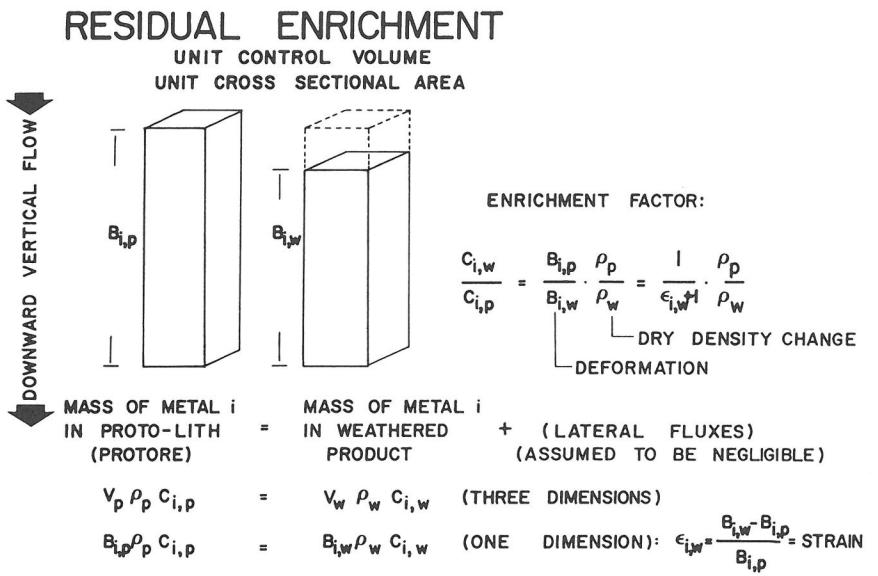

Figure 40. Mass conservation during residual enrichment, showing how three-dimensional volume changes may be represented in one dimension using strain. From Brimhall and Dietrich (1987).

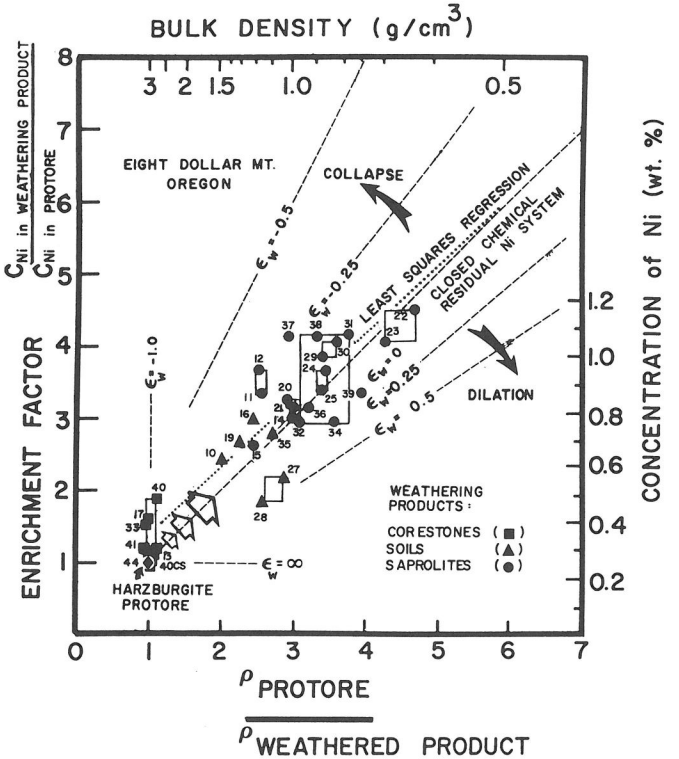

Figure 41. Data array for Eight Dollar Mountain Ni laterite in southwestern Oregon. The boxes represent data for two samples taken at the same depth in the weathering profile. Weathering path is shown with arrows extending away from the ultrmafic protore through saprolites and soils. Position of data array with respect to lines of constant strain (collapse or expansion indicate that there was no systematic deformation during weathering. From Brimhall and Dietrich (1987).

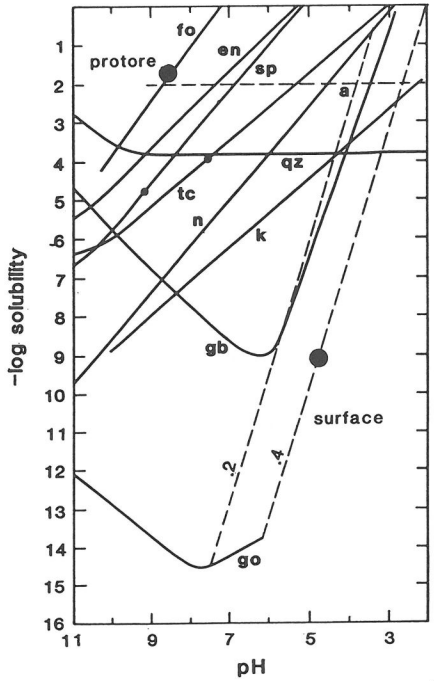

Figure 42. The pH dependence of the congruent solubility of minerals in laterite development. S is the calculated equilibrium concentration in moles per liter of Mg, Si, Fe, Al, or Ni as appropriate. Abbreviations are: fo=forsterite, en=enstatitie, sp=serpentine, tc=talc, n=nickel serpentine (nepouite), k=nickel talc (kerolite), qz=quartz, a=amorphous silica, gb=gibbsite, go=goethite. pH at the surface is about 4.5 and 8.5 at depth. From Golightly (1981).

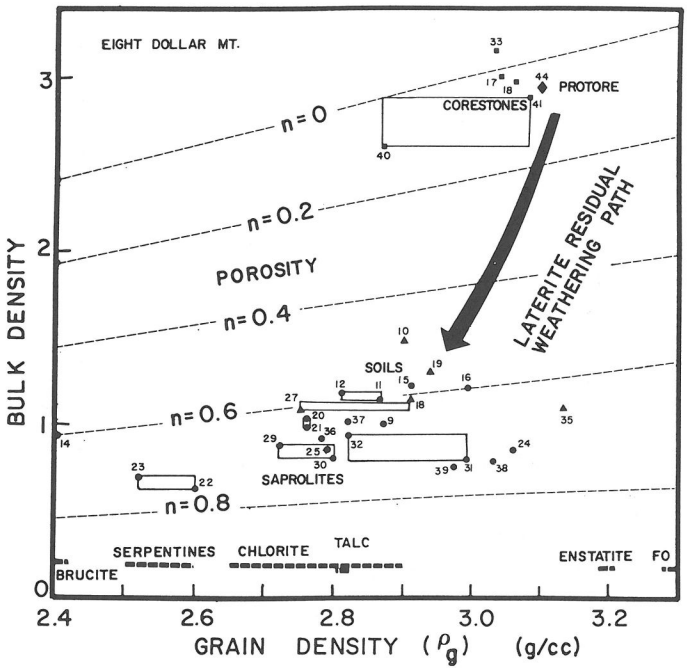

Figure 43. Variation in bulk density as a function of grain density showing the weathering path from the protore for the Eight Eight Dollar Mountain deposit, Oregon (Fig. 41). From Brimhall and Dietrich (1987).

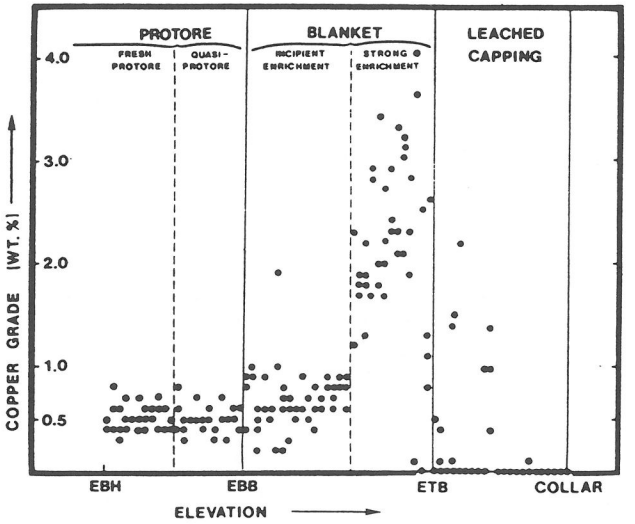

Figure 44. Supergene copper grade profile for the La Escondida porphyry copper deposit, northern Chile. From Brimhall et al. (1985).

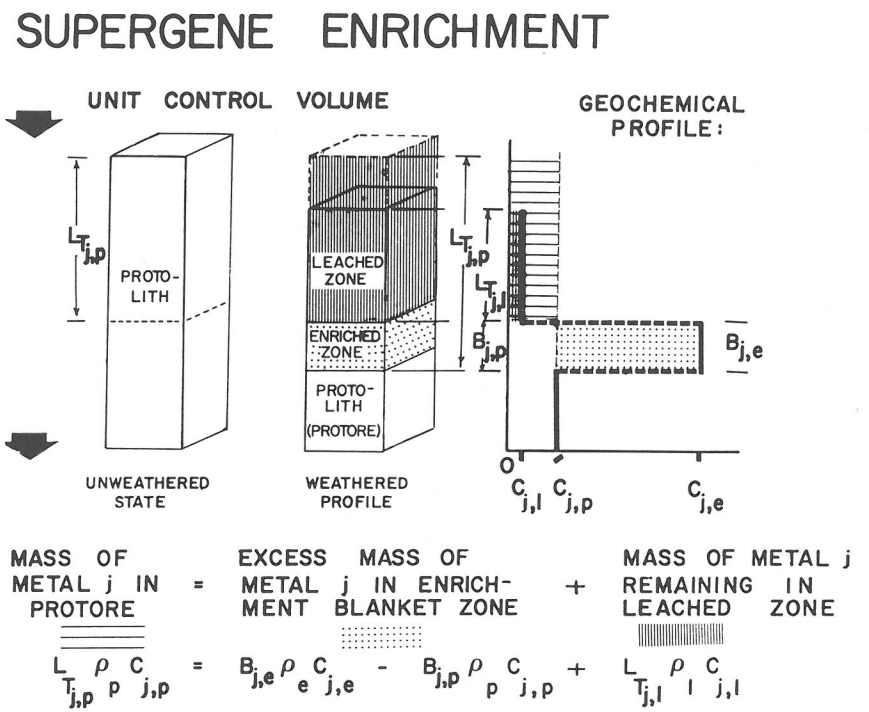

Figure 45. Mass balance model for supergene enrichment depicting the meaning of terms in the algebraic model. Mass of metal within a control volume is given by a product of column height, bulk density, and metal concentration. From Brimhall and Dietrich (1987).

immobile and enriched only residually (Davy and El-Ansary, 1986). Ba, Co, La, Mn, Rb, Sr, Ta, Y, Zn, Ca, K, Mg, and Na are all leached, behaving as perfectly mobile elements.

Local secondary gold enrichment, increase in gold fineness, and formation of gold nuggets are currently of major importance in mineral exploration, and have been ascribed to gold complexing by transient sulfur-bearing ligands such as thiosulfate and bisulfide complexes (Webster and Mann, 1984; Webster, 1986; Stoffregen, 1986) in regions where chloride-rich ground water is often lacking, or alternatively by chloride complexes where such fluids are known (Mann, 1984; Webster and Mann, 1984). Gold is clearly transported by supergene processes.

Supergene systems are therefore chemically differentiated into two related subsystems positioned sequentially along a fluid flow path, a source region and a sink, where reprecipitation occurs. Obviously, the two subsystems are related through rigid mass conservation constraints of a mobile element, j. Equation (47) gives the supergene enrichment factor in non-dimensional form equivalent to (46) for residual enrichment.

$$\frac{C_{j,e}}{C_{j,p}} = \frac{(L_{T_{j,p}} + B_{j,p})}{B_{j,p}} \frac{1}{(\varepsilon_{i,e} + 1)} \frac{\rho_p}{\rho_e} - \frac{L_{T_{j,p}}}{B_{j,p}} \frac{C_{j,l}}{C_{j,p}} \frac{(\varepsilon_{i,l} + 1)}{(\varepsilon_{i,e} + 1)} \frac{\rho_l}{\rho_e} \quad . \tag{47}$$

These terms are illustrated in Figure 45. In (47) $L_{T_{j,p}}$ is the total thickness of the zone of leaching of supergene element, j. $B_{j,p}$ is the thickness of the zone of enrichment of element,j. The strain terms for immobile element i undergoing simple residual enrichment, are $\varepsilon_{i,e}$ for the zone of enrichment and $\varepsilon_{i,l}$ for the leached zone. The density terms are rp, re, and rl for the protore, enriched and leached zones respectively. The concentration terms for supergene element, j, are $C_{j,e}$, $C_{j,p}$, and $C_{j,l}$ for the enriched zone, protolith and leached zone respectively. Note that (47) reduces down to simple residual enrichment in the limit when the thickness of the leached zone, $L_{T_{j,p}}$ approaches zero. Residual and supergene enrichment are therefore two extreme cases of related processes. The prime difference is the focussing effect of removing elements from a leached zone and concentrating them in a zone of enrichment. This volumetric effect is portrayed in the first term in (47) $(L_{T_{j,p}} + B_{j,p})/B_{j,p}$, which enhances the enrichment due to change in density (rp/re) as leached zones are typically several times as thick as enriched zones. Collapse, negative strain, tends to increase the enrichment factor as well, as does complete leaching in the leached zone as $C_{j,l}$ approaches zero.

In (47), the only unknown is $L_{T_{j,p}}$. This may be found by substituting in appropriate values of the other variables, concentration, density, and strain. Given the difference between the calculated total leached column height $L_{T,p}$ and the thickness of the present leached zone, the amount of erosion can be calculated, and with age dates of secondary minerals, the erosion rate determined (Alpers and Brimhall, 1988a,b). Also pre-weathering paleo-topography can be reconstructed from addition of $L_{T_{j,p}}$ terms for weathering columns to the elevation of the top of secondary enrichment. This provides a means to evaluate sub-surface horizontal fluid fluxes in terms of hydrological gradients and regional fracture patterns. This use of mobile supergene elements in appropriate mass balance models affords a means to relate near surface geochemistry to surficial processes and geomorphic evolution. Thus there is clearly a complex interplay between heterogeneous mineral-solution-gas reactions affecting chemical transport and weathering and the ground water table. These effects are amenable to thermodynamic modeling, and illustrate the necessity of treating fluid flow along with chemical transport in order to approach reality.

Thermodynamic and fluid flow modeling of supergene enrichment. The division between the leached and enriched zones is generally the top of the capillary fringe, a zone of saturation above the ground water table in which capillary forces between grains induce tension saturation. Above the capillary fringe the voids are filled with air making oxidation a dominant process. From the top of the capillary fringe downward, ground water fills the voids precluding air except as a relatively minor dissolved constituent. The top of the capillary fringe separates two quite distinct environments, and hence represents a dramatic gradient in chemical composition.

The oxidation of pyrite within the unsaturated zone is a process of great importance in supergene enrichment since hydrogen ion is generated by pyrite destruction. The rate at which acid generation occurs is largely controlled by the amount of oxygen available. The movement of O_2 gas then is of critical importance, especially its replenishment in the unsaturated zone. Diffusion of oxygen through air-filled pore spaces is considered to be the dominant process of oxygen interchange between the atmosphere and the porous rock undergoing weathering. Troeh et al. (1982) developed Fick's first law type equations for diffusive transport in porous materials (48).

$$Q = D_0 \frac{V_v(1 - S_{sat})}{V_T} A \frac{\Delta C}{\Delta L} \tag{48}$$

Here Q is mass per second of a gas diffusing across cross sectional area A. $\Delta C/\Delta L$ is the oxygen concentration gradient. V_v is the void volume, and S_{sat} is the saturation state, and D_0 is the maximum diffusional rate of oxygen through air. The saturation term reduces the oxygen flux. Therefore, above the capillary fringe, oxygen diffusion is much more rapid than below. This appears to be the rate limiting step in pyrite oxidation and supergene enrichment of copper. At 25°C, the computed logarithms of the oxygen fugacities in the leached, enriched, and protore portions of a porphyry copper deposit are −38, −63, and −71 showing that the effect of oxygen diffusion is dramatic. It is this change in redox state which causes elements to be leached under oxidizing conditions, transported, and finally reprecipitated in reducing environments.

By incorporating (48) describing oxygen diffusion, Cunningham (1984) has theoretically modeled the irreversible reaction chemistry of supergene copper enrichment of a pyrite-chalcopyrite-magnetite-biotite-alkali feldspar protore along with fluid flow in a simplified integrated finite difference model system consisting from top to bottom of a leached zone, enriched zone and protore—see Figure 46. The following preliminary results are offered as an illustration of a technique of approaching an important ore-forming porous media flow problem and the necessity of subdividing it into related unsaturated and saturated zones.

The computer programs used were EQ3/EQ6 (Wolery, 1979) for reaction chemistry and speciation of the aqueous fluid, and TRUST (Narasimhan et al., 1977) for fluid flow through the unsaturated zone into the capillary fringe, and into the saturated zone. EQ3/EQ6 solves a series of differential equations describing mass balance, mass action, and ionic strength. The algorithm is based on the work of Helgeson (1968). Kinetic data for minerals used are as follows: rates of silicates are from Wood and Walther (1983), dissolution rate of pyrite is from Wiersma and Rimstidt (1984), and chalcopyrite dissolution rate from Braithwaite (1976). Program TRUST uses the integrated finite differences method to solve for ground water flow conditions, specifically mass conservation of water, the hydraulic potential gradient, and fluid fluxes.

Computed chemical reaction paths, considering both fluid flow and chemical reaction are shown in Figures 47, 48, and 49. In this modeling an explicit coupling of fluid flow and chemical reaction has been accomplished by alternating between fluid flow calculations, fluid mixing, and chemical reaction over short time steps. No feedback between fluid flow and such chemical variables as volume change of net chemical reactions is considered here. The starting fluid composition is rain water, which reacts with the minerals contained in the potassium-silicate protore in which a steady, non- transient flow regime exists divided into unsaturated and saturated zones. The effluent fluid from the base of each system enters the subjacent system, and mixes with the contained fluids. Reaction progress in EQ3/EQ6 is related to real time necessary for kinetics and fluid flow through the total surface area of exposed mineral grains.

The equilibrium composition of the copper enrichment blanket and protore are distinct, the former along the chalcocite-covellite phase boundary in the alunite field, the latter in the pyrite-chalcopyrite field near equilibrium with biotite (Fig. 47), consistent with petrographic observation. The relatively reducing conditions prevailing in the enrichment blanket and protore are evident in Figure 47 in contrast to those in the leached zone. The low sulfur

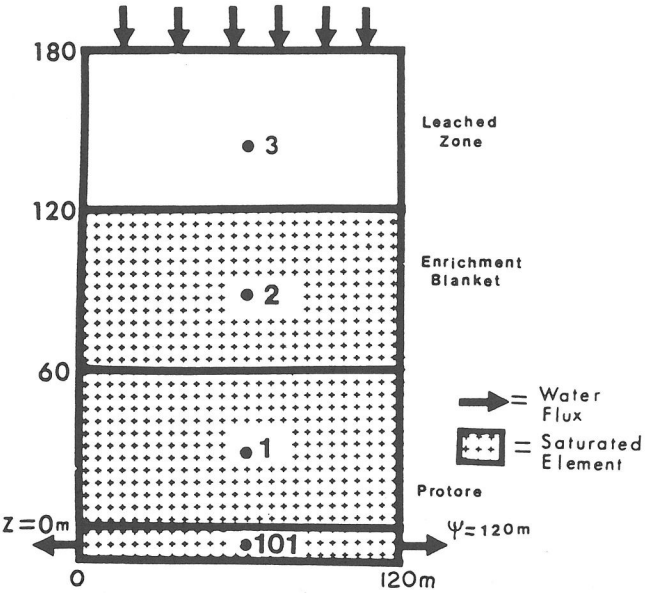

Figure 46. Idealized three-cell computation framework for steady state flow hydrological modeling of supergene enrichment. Cell 3 is unsaturated, and cells 1 and 2 are saturated. The top of the capillary fringe is taken to be the interface of cells 2 and 3. Depth below the surface is shown in meters. From Cunningham (1984).

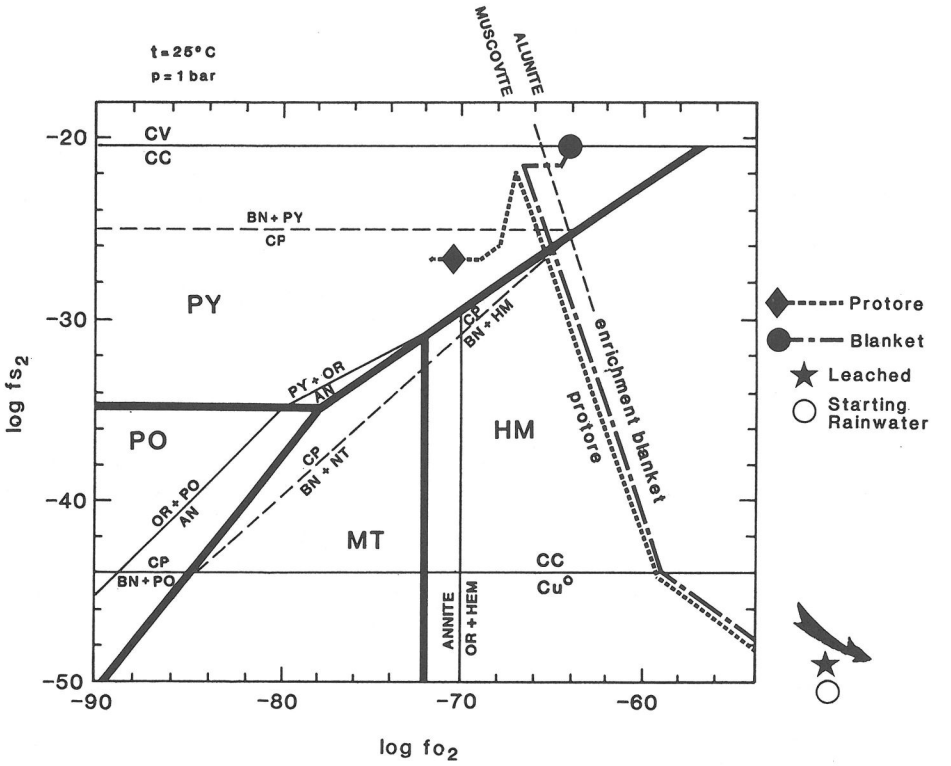

Figure 47. Computed chemical reaction paths at 25°C and 1 bar for supergene enrichment. Shown are the paths for the enrichment blanket and the protore. The starting rainwater and leached zone compositions are off-scale. Notice that the enrichment blanket reaches the chalcocite-covellite phase boundary. From Cunningham (1984).

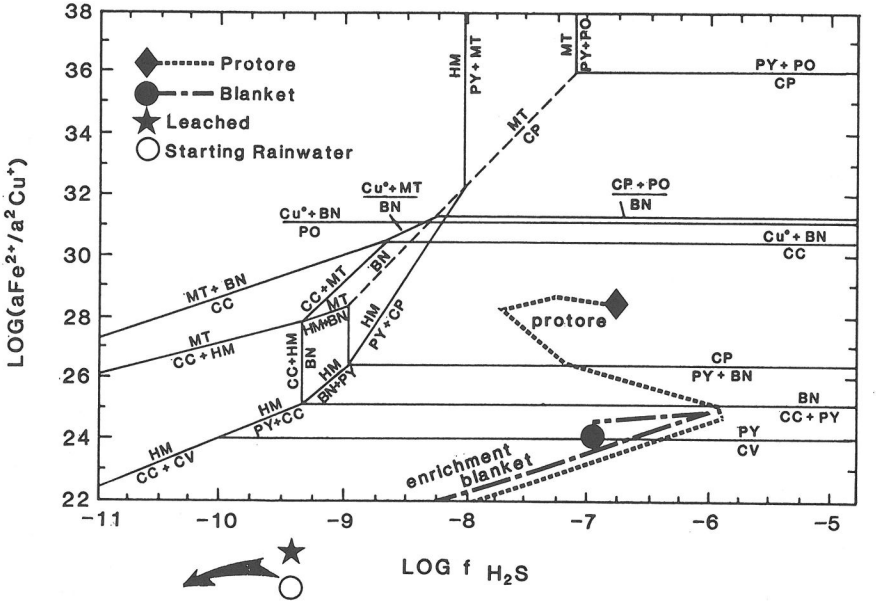

Figure 48. Computed chemical reaction paths at 25°C and 1 bar for supergene enrichment showing enrichment blanket and protore paths. Compare with the vein forming hydrothermal paths in Figures 37 and 38. From Cunningham (1984). Supergene and hydrothermal hypogene oxidation produce very distinct paths.

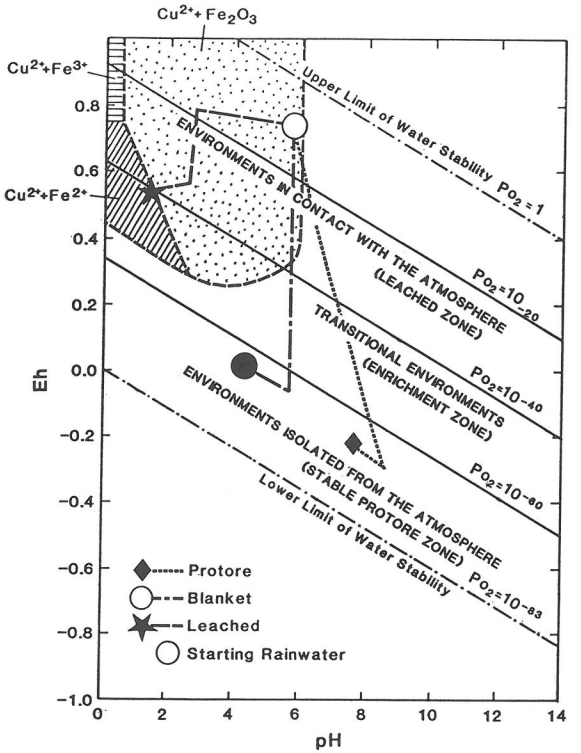

Figure 49. Computed Eh-pH diagram for supergene leaching and enrichment. The main reason for copper leaching is illustrated here as the leached zone path remains in the aqueous copper field at high Eh values. From Cunningham (1984).

fugacity in the leached zone is due to the quantitative oxidation of sulfide to sulfate which is flushed down into the enrichment blanket. The striking disequilibrium between the mineral assemblages contained in the leached zone and enrichment blanket is illustrated in Figure 48, as is the similarity of fluid composition between the enrichment blanket and the protore. The reaction paths are plotted finally on an Eh-pH diagram (Fig. 49) which confirms the similarity of enriched zone and protore in terms of relatively reducing conditions (similar oxygen partial pressures) in environments removed from the atmosphere, and the contrast with the leached zone and surficial fluid dominated by oxygen-rich gasses. This contrast is the fundamental reason for the release of copper and its reprecipitation after a short excursion by downward aqueous fluid advection.

Hypogene enrichment by ferrolysis. An analogous type of transport to supergene behavior is known for iron and perhaps manganese, differing only in that certain metals migrate upward instead of downward, and move not by advection but by chemical diffusion (Webster and Mann, 1984). The driving forces and metal concentration gradients are related to Eh and pH gradients created between the water table and ground surface during oxidation. This process has been called ferrolysis (Brinkman, 1977), a mechanism involving oxidation and hydrolysis of iron (Mann, 1984). It is not widely considered as an iron or manganese ore- forming processes in itself, but is mainly of interest because of its effects on gold solubility and supergene deposition (Mann, 1984, 1985; Webster and Mann, 1984; Mann and Ollier, 1985). Ferrolysis is however, widespread, and is likely to be important in the formation of ferruginous nodules and ferricretes in laterites and bauxites (Grubb, 1970, 1971; Sadleir and Gilkes, 1976; Valeton, 1972) in general involving an evolution from iron-rich mottles in a kaolinite matrix to Al-rich hematite, to Al-rich goethite nodules to pisolites following a cortification processes (Tardy and Nahon, 1985).

According to Mann (1984) in the case of a laterite profile iron oxidation probably occurs in two discrete steps, the first at the weathering bedrock front (49).

$$FeS_2 + 2\,H_2O + 7\,O_2 = 2\,Fe^{2+} + 4\,SO_4^{2-} + 4\,H^+ \quad . \tag{49}$$

The second step occurs at or near the water table at a higher oxygen fugacity (50).

$$2\,Fe^{2+} + 3\,H_2O + 0.5\,O_2 = 2\,FeOOH + 4\,H^+ \quad . \tag{50}$$

The applicability of (50) is observed by use of water samples of active weathering profiles in Western Australia (Mann, 1984). The path of oxidation and hydrolysis of iron is reconstructed on a pH-Eh diagram Figure 50 in comparison to a theoretically derived path (51) from this study assuming unit activity coefficients of dissolved species.

$$Fe^{2+} + 2\,H_2O = FeOOH + 3\,H^+ + e^- \quad . \tag{51}$$

The measured and calculated ferrolysis paths have precisely the same slope (one electron for each iron oxidized from ferrous to ferric), but are coincident for an aqueous iron concentration of 200 milligrams per liter, the highest measured concentration. The postulated conditions and direction of iron migration by diffusion after its release at the weathering front is shown in Figure 51. There is an increase in Eh and decrease in pH up towards the water table.

The hypothesis relating gold transport to ferrolysis is illustrated in Figure 51. Dissolution of gold and silver from a primary deposit exposed to weathering undergoes dissolution by (52) at or near the water table where Cl^-, H^+, and O_2 are abundant, and there is little or no ferrous iron.

$$4\,Au + 16\,Cl^- + 3\,O_2 + 12\,H^+ = 4\,AuCl_4^- + 16\,H_2O \quad . \tag{52}$$

Gold chloride complexes migrate, and precipitate pure elemental gold (53). On the other hand, goethite forms by hydrolysis in the mottled zone after its upward ascent and near-surface enrichment of iron—see Figure 52. The gold precipitation is thought to be due to reduction of $AuCl_4^-$ with ferrous iron (Mann, 1984).

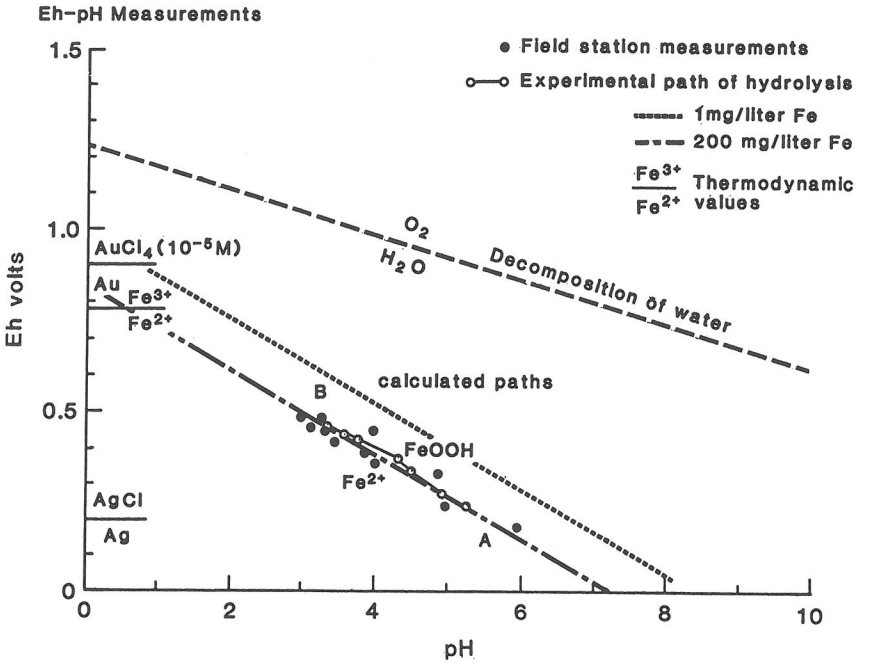

Figure 50. Eh-Ph diagram showing experimental data on weathering laterites where ferrolysis is occurring. From Mann (1984). Computed path is shown for comparison using 200 milligrams dissolved iron per liter.

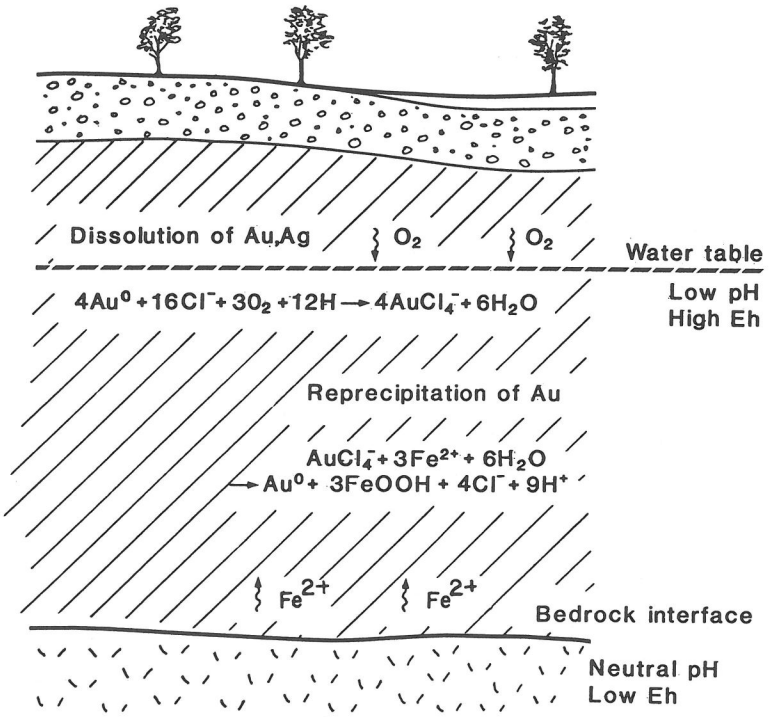

Figure 51. Chemical model for the redistribution of gold from a primary lode system by weathering in a lateritic profile. From Mann (1984).

$$AuCl_4^- + 3\,Fe^{2+} + 6\,H_2O = Au + 3\,FeOOH + 4\,Cl^- + 9\,H^+ \quad . \qquad (53)$$

The mass balance model for hypogene chemical weathering is identical to supergene in form, but the direction of transport is inverted. Many of the same limiting factors are expected to control enrichment: thickness of the leached zone in relation to the thickness of the zone of enrichment, density ratios of the enriched and leached zones with respect to protore density, and concentration in the leached zone.

Internal factors

Weathering paths in physical properties. Primary permeability in a protolith before chemical weathering has been viewed as a controlling factor of water percolating through rocks (Samana, 1986), and thus a major internal factor of oxidative weathering. Measurements of permeability of weathered rocks are presently quite rare, but a mounting data base of porosity measurements exists (Brimhall and Dietrich, 1987) which suffices to illustrate the limitations of the role of permeability in surficial environments. The results are surprising.

Figure 53 shows that there is little correlation between the initial porosity of a protolith and the final porosity after intense weathering. Bulk density and average density serve a useful purpose in providing a comparative framework for viewing weathering paths in diverse protoliths on a uniform basis regardless of the bulk composition of the rock. Bulk density varies both with the density of constituent minerals and the abundance and size of voids, and thus responds to dissolution and precipitation reactions as well as deformation. Grain density is simply the average density of the constituent mineral assemblage and is therefore a mineralogic effect. The two densities combine to give porosity. In Figure 53, five protoliths are depicted: disseminated sulfide deposits, granites, ultramafic rocks, massive sulfide deposits, and granular material such as beach sand. These parent material are converted to leached capping, bauxite, laterites, gossans, and podzols respectively. For example, ultramafic rocks with very low porosity can be converted to laterites with porosities of almost 0.8 (80 %) while beach sands with an initial porosity of 0.35 (35 %) can weather to podzols with a porosity of only 0.6 (60 %). Many other factors play a role besides porosity, including the amount of deformation, particularly collapse due to weathering, which can be as high as 50%. Also, secondary precipitation in voids can reduce porosity.

Primary permeability. Rather than consider porosity and permeability as primary factors controlling and limiting chemical weathering, it may be more accurate to consider them as being, to a large extent, consequences of chemical weathering. The principal role of permeability in the context of thermodynamic modeling may be as an important aspect of initial conditions which are rapidly modified once hydrochemical processes are initiated. Such changes in permeability may ultimately be so large that they outweigh the initial differences between systems. Clearly then, a major importance of permeability is its relationship to the fluid flow regime within the full context of surface processes including rock composition and hydrological patterns, especially the interface between unsaturated and saturated conditions. The capillary rise of water under tension saturation in the capillary fringe varies inversely with average pore radius, making a hydrology, lithology, and pore structure complexly intertwined, even at the start of chemical weathering. The selection of one controlling factor such as permeability is misleading in this respect.

Available sulfur. Another factor of major importance in oxidative weathering systems such as supergene enrichment of primary copper ores is available sulfur. Here the major effect is in the production of sulfuric acid from the oxidation of pyrite. Once hydrogen ion is formed, hydrolysis reactions proceed which modify the protolith extensively. Depending upon the pyrite to copper sulfide ratio, oxidation may be total or incomplete (Samana, 1986). In the simplest sense, chalcopyrite has a sulfur to total metal ratio S/M of 1 which means it can be extensively oxidized. Chalcocite is sulfur deficient in this respect, S/M = 0.5, requiring 1 mole of sulfur from another source for it to be oxidized. Pyrite (S/M = 2) can provide sulfur for the oxidation of other sulfide minerals. These sulfur to metal ratios are the minimum required for total oxidation since the analysis does not include the

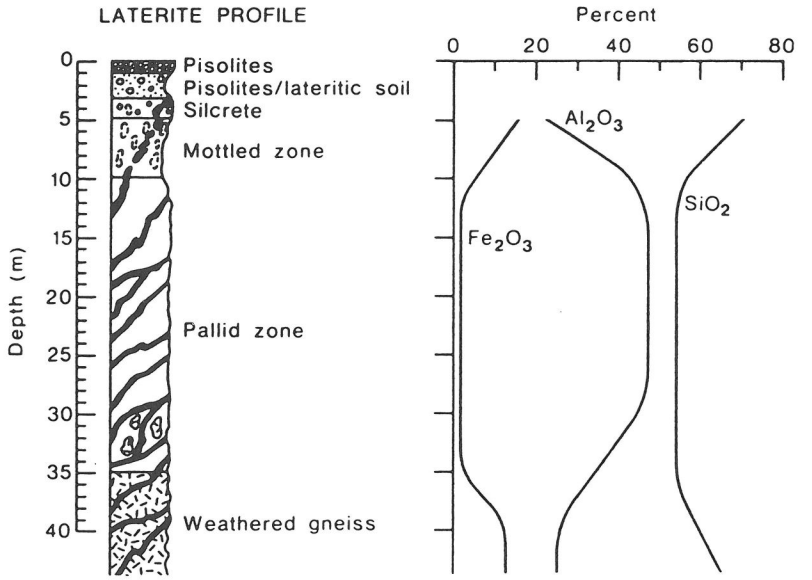

Figure 52. Chemical profiles showing iron, aluminum, and silica variation with depth. From Webster and Mann (1984).

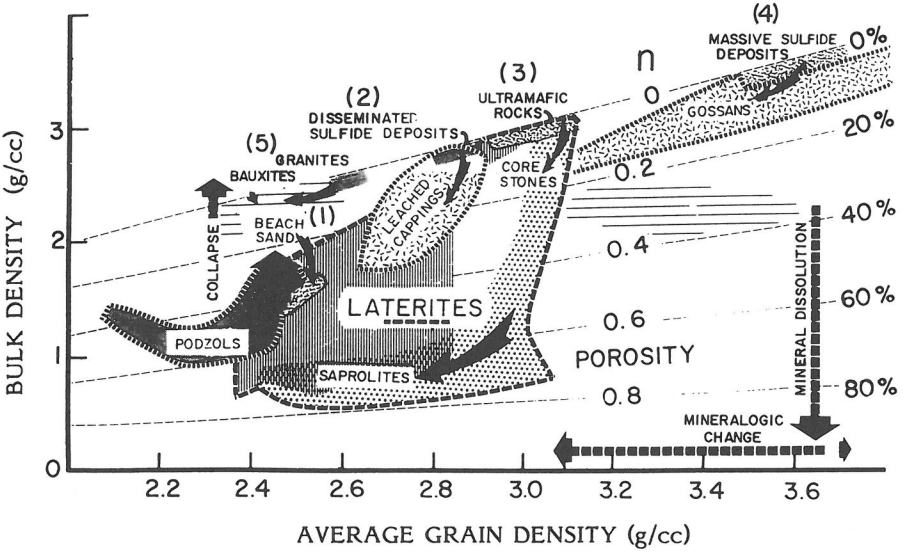

Figure 53. Comparison of physical weathering paths in terms of bulk density and average grain density for five parent materials: beach sand, porphyry copper ores, ultramafic rocks, massive sulfide deposits, and granites. These weather to podzols, leached cappin, laterites, gossans, and bauxites, respectively. From Brimhall and Dietrich (1987).

reactivity of gangue minerals. These are based primarily on the sulfide-oxide-silicate buffer assemblages, and the capacity of the rock to neutralize strong acids. It is thought that a pyrite to copper sulfide ratio of four is optimal for oxidation and secondary enrichment. Chalcocite enrichment blankets may be stable partly because of the relatively low pyrite to copper sulfide ratio, and the inhibition of oxidation-leaching processes. Perched enrichment blankets may result from lowering of the ground water table, and the relative slow rates of sulfide oxidation.

External factors

Geomorphic conditions are of major importance in surficial weathering, especially the evolution in time as changes have particularly marked effects on the ground water table and the rates of erosion in relation to rates of chemical weathering. In this respect, the single most important external factor seems to be climate, as it relates to rainfall, infiltration rates, the nature of runoff, temperature, and biota such as bacteria which catalyze pyrite oxidation. Tectonic factors contribute to the uplift rate which is complexly related to hydrology through fluvial processes.

Optimal conditions for secondary enrichment and preservation

Steady state versus transient flow effects. The downward cumulative enrichment which characterizes supergene transport is optimized in a transient fluid flow regime in which the ground water table descends exposing increasing column heights of sulfides to oxidizing conditions above the ground water table (Brimhall et al., 1985; Samana, 1986). Similar conclusions have been reached about the importance of water table recession during the onset of arid climates favoring deep zones of bleached clays and duricrusts (Butt, 1981). There is a distinct asymmetry in the effects produced by changes in the position of the ground water table. Descent enhances supergene enrichment. Ascent simply submerges sulfide enrichment blankets putting them in a temporary state of preservation through reduction as pores previously filled with air in the unsaturated zones are filled with water. Therefore, seasonal fluctuations only produce significant supergene transport during the descent phase.

The preservation of such secondarily enriched products over geological periods of time depends either upon chance events such as burial of leached capping beneath a capping conglomerate as at San Manuel-Kalamazoo, Arizona (Lowell and Guilbert, 1970) or some other effects. Enrichment blankets developed in porphyry copper deposits are so common that it seems therefore highly unlikely that such chance events are the main cause of preservation of these enriched states. It seems more likely that preservation is somehow intrinsically related to the fundamental processes of enrichment so that their preservation would be expected and not simply an aberration.

It is clear that optimal development of supergene enrichment processes is due to a balance of rates of ground water table descent, mechanical erosion, and sulfide oxidation (Alpers and Brimhall, 1988a,b). With excessively high erosion rates, leached capping is stripped away and ultimately enriched blanket material is removed. If the rate of ground water descent is much higher than the equivalent rate at which sulfides are oxidized, then leaching is incomplete, and the enrichment processes is inefficient. If the ground water table is static, then an enrichment system may become stagnant, and downward cumulative enrichment ceases, as in the case of ascent of the groundwater table.

Dynamic evolution of supergene metal transport systems has been demonstrated in the Atacama Desert of northern Chile (Alpers and Brimhall, 1988a,b). This chemical and hydrological evolution was quite likely in direct response to transient groundwater flow during Tertiary climatic desiccation with uplift of the Andes which produced an essentially monotonic decline of the ground water table. Related to this hydrologic trend are surficial processes which were similarly changing during the Tertiary. Long-term average rates of erosion decreased markedly from approximately 0.1 mm/year during primary hydrothermal hypogene mineralization in the La Escondida porphyry copper deposit. During supergene enrichment the rate slowed to 0.04 mm/year and subsequent to this enrichment, 0.009

mm/year. Therefore, optimal conditions for supergene enrichment were simultaneously accompanied by a major decrease in the rate of erosion, providing a simple mechanism for insuring the long-term preservation of the enrichment system. This coupling of surficial rates, migration of the ground water table, sulfide oxidation, and erosion is only one example of mutually enhancing effects in transport processes which operate with chemical, thermodynamic, and fluid mechanical aspects.

ACKNOWLEDGMENTS

First we thank Joan Bossart and Jan Dennie for their considerable patience and word processing skills in assembling this document. We thank Mary Yang, Remy Hennet, Gregor M. Anderson, Charles Alpers, Jay Ague, and Aric Cunningham for kindly letting us use their unpublished data. D.A.C. particularly thanks Jacques Schott and the Laboratoire de Géochimie, Université Paul Sabatier, Toulouse for the stimulating scientific and cultural environment in which this was written, and C.N.R.S., France, for financial support. L'inspiration gastronomique de cet article a été fournie gracieusement par Messieurs Lucien Vanel (Toulouse), Yves Thuries (Cordes sur Ciel), André et Arnaud Daguin (Auch), Alain Chapel (Mionnay) et beaucoup d'autres artistes. Financial support came from NSF grants EAR-8517254 to D.A.C. and EAR-8416790 to G.H B.

REFERENCES

Ague, J.J. and Brimhall, G.H (1987) Granites of the batholiths of California: Products of local assimilation and regional-scale crustal contamination. Geology 15, 63-66.

Ague, J.J. and Brimhall, G.H (1988a) Regional variations in bulk chemistry, mineralogy, and the compositions of mafic and accessory minerals in the batholiths of California. Geol. Soc. Amer. Bull. (submitted).

Ague, J.J. and Brimhall, G.H (1988b) Diverse regional controls on magmatic arc asymmetry and distribution of anomalous plutonic belts in the batholiths of California: Effects of assimilation, cratonal rifting, and depth of crystallization. Geol. Soc. Amer. Bull. (submitted).

Ahrland, S. (1968) Thermodynamics of complex formation between hard and soft acceptors and donors. Struct. Bonding 5, 118-149.

Ahrland, S. (1973) Thermodynamics of stepwise formation of metal-ion complexes in aqueous solution. Struct. Bonding 15, 167-188.

Alpers, C.N. and Brimhall, G.H. (1988a) Tertiary climatic dessication and erosion rates in the Atacama Desert, Northern Chile: Optimal Conditions for the Supergene Enrichment and Preservation of Ore Deposits. Submitted to Geol. Soc. Amer. Bull.

Alpers, C.N. and Brimhall, G.H (1988b) Dynamic evolution of supergene metal transport systems in response to transient groundwater flow: Results from La Escondida, Chile. Submitted to Econ. Geol.

Ananthaswany, J. and Atkinson, G. (1982) Thermodynamics of concentrated electrolyte mixtures. I. Activity coefficients in aqueous $NaCl$-$CaCl_2$ at 25°C. J. Solution Chem. 11, 509-527.

Anderson, G.M. (1975) Precipitation of Mississippi Valley-type ores. Econ. Geol. 70, 937-942.

Anderson, J.A. (1982) Characteristics of leached capping and techniques of appraisal. In: Advances in the Geology of Porphyry Copper Deposits, Southwestern North America. S.R. Titley, ed., University of Arizona Press, Tucson, p. 275-295.

Baes, C.F., Jr. and Mesmer, R.E. (1976) The Hydrolysis of Cations. Wiley-Interscience, New York, 489 pp.

Baes, C.F., Jr. and Mesmer, R.E. (1981) The thermodynamics of cation hydrolysis. Amer. J. Sci. 281, 935-962.

Barnes, H.L. (1975) Zoning of ore deposits: Types and causes. Trans. Royal Soc. Edinburgh 69, 295-310.

Barnes, H.L. (1979) Solubilities of ore minerals. In: Geochemistry of Hydrothermal Ore Deposits, 2nd ed. H.L. Barnes, ed., Wiley-Interscience, New York, p. 404-460.

Barnes, H.L. (1981) Measuring thermodynamically interpretable solubilities at high pressures and temperatures. In: Chemistry and Geochemistry of Solutions at High Temperatures and Pressures. D. Rickard and F. Wickman, eds., Physics and Chemistry of the Earth, v. 13/14, Pergamon Press, New York, p. 321-343.

Barnes, H.L. and Ernst, W.G. (1963) Ideality and ionization in hydrothermal fluids: The system $MgO-H_2O-NaOH$. Amer. J. Sci. 261, 129-150.

Barnes, H.L. and Kullerud, G. (1961) Equilibria in sulfur-containing aqueous solutions, in the system Fe-S-O, and their correlation during ore deposition. Econ. Geol. 56, 648-688.

Barrett, T.J. and Anderson, G.M. (1987) The solubility of sphalerite and galena in 1-5 M NaCl solution to 300°C. Geochim. Cosmochim. Acta, in press.

Barton, M.D. (1983) Metallogenesis. Reviews in Geophys. and Space Physics 21, 1407-1419.

Barton, M.D. (1987) Lithophile-element mineralization associated with Late Cretaceous two-mica granites in the Great Basin. Geology 15, 337-340.

Barton, P.B., Jr., Bethke, P.M. and Roedder, E. (1977) Environment of ore deposition in the Creede mining district, San Juan Mountains, Colorado: Part III. Progress toward interpretation of the chemistry of the ore-forming fluid for the OH vein. Econ. Geol. 72, 1-24.

Barton, P.B., Jr. and Skinner, B.J. (1979) Sulfide mineral stabilities. In: Geochemistry of Hydrothermal Ore Deposits, 2nd ed. H.L. Barnes, ed., Wiley-Interscience, New York, p. 278-403.

Bateman, A.M. (1950) Economic Mineral Deposits. John Wiley, New York, p. 245-287.

Bischoff, J.L. and Seyfried, W.E. (1978) Hydrothermal chemistry of seawater from 25°C to 350°C. Amer. J. Sci. 278, 838-860.

Blain, C.F. and Andrew, R.L. (1977) Sulfide weathering and the evaluation of gossans in mineral exploration. Mineral Sci. Eng. 9, 119-149.

Bockris, J.O'M. and Reddy, A.K.N. (1970) Modern Electrochemistry, v. 1. Plenum, New York, 622 pp.

Born, M. (1920) Volumen und Hydrationswärme der Ionen. Zeit. Physik. 1, 45-48.

Boles, J., Crerar, D., Grissom, G. and Key, T. (1987) Aqueous thermal degradation and diagenesis of naturally occurring aromatic acids. Geochim. Cosmochim. Acta, in press.

Bowers, T.S., Jackson, K.J. and Helgeson, H.C. (1984) Equilibrium Activity Diagrams. Springer-Verlag, New York, 397 pp.

Bowers, T.S., Von Damm, K.L. and Edmond, J.M. (1985) Chemical evolution of mid-ocean ridge hot springs. Geochim. Cosmochim. Acta 49, 2239-2252.

Braithwaite, J.W. (1976) Simulated deep solution mining of chalcopyrite and chalcocite. Unpublished thesis, University of Utah.

Brantley, S.L. (1986) The Chemistry and Thermodynamics of Natural Brines and the Kinetics of Dissolution-Precipitation Reactions of Quartz and Water. Ph.D. dissertation, Princeton University, p. 39-62.

Brantley, S.L., Rowe, G., Fernandez, J.F., Reynolds, J.R., and Borgia, A. (1987) Acid crater lake brine of Poás volcano, Costa Rica. Nature, in press.

Brimhall, G.H (1977) Early fracture-controlled disseminated mineralization at Butte, Montana. Econ. Geol. 72, 37-59.

Brimhall, G.H (1979) Lithologic determination of mass transfer mechanisms of multiple-stage porphyry copper mineralization at Butte, Montana: Vein formation by hypogene leaching and enrichment of potassium silicate protore. Econ. Geol. 74, 556-589.

Brimhall, G.H (1980) Deep hypogene oxidation of porphyry copper potassium-silicate protore at Butte, Montana: A theoretical evaluation of the copper remobilization hypothesis. Econ. Geol. 75, 384-407.

Brimhall, G.H, Jr. (1987a) Metallogenesis. Reviews in Geophys. and Space Physics 25, 1079-1088.

Brimhall, G.H (1987b) Preliminary fractionation patterns of ore metals through earth history. Chem. Geol. 64, 1-16.

Brimhall, G.H, Agee, C., and Stoffregen, R. (1985) The hydrothermal conversion of hornblende to biotite. Canadian Mineral. 23, 369-379.

Brimhall, G.H and Ague, J.J. (1988) Granite systems. In: Hydrothermal Processes—Applications to Ore Genesis. H.L. Barnes and H. Ohmoto, eds., Reidel Publishers, Dordrecht, Holland, 33 pp. (in press).

Brimhall, G.H, Alpers, C.N., and Cunningham, A.B. (1985) Analysis of supergene ore-forming processes and ground water solute transport processes using mass balance principles. Econ.

Geol. 80, 1227-1256.
Brimhall, G.H and Dietrich, W.E. (1987d) Constitutive mass balance relations between chemical composition, volume, density, porosity, and strain in metasomatic hydrochemical systems: Results on weathering and pedogenesis. Geochim. Cosmochim. Acta 51, 567-587.
Brimhall, G.H and Ghiorso, M.S. (1983) Origin and ore-forming consequences of the advanced argillic alteration process in hypogene environments by magmatic gas contamination of meteoric fluids. Econ. Geol. 78, 73-90.
Brinkman, R. (1977) Surface-water gley soils in Bangladesh: Genesis. Geoderma 17, 111-144.
Buback, M. (1981) Spectroscopic investigations of fluids. In: Chemistry and Geochemistry of Solutions at High Temperatures and Pressures. D. Rickard and F. Wickman, eds., Physics and Chemistry of the Earth, v. 13/14, Pergamon Press, New York, p. 345-360.
Buback, M., Crerar, D. and Vogel, L. (1987) Vibrational and electronic spectroscopy of hydrothermal systems. In: Hydrothermal Experimental Techniques. G.C. Ulmer and H.L. Barnes, eds., Wiley-Interscience, New York, Ch. 14, in press.
Burnham, C.W. (1975) Water and magmas; a mixing model. Geochim. Cosmochim. Acta 39, 1077-1084.
Burnham, C.W. (1979) Magmas and hydrothermal fluids. In: Geochemistry of Hydrothermal Ore Deposits, 2nd ed. H.L. Barnes, ed., Wiley-Interscience, New York, p. 71-136.
Burnham, C.W. (1981) Physiochemical constraints on porphyry mineralization. In: Relations of Tectonics to Ore Deposits in the Southern Cordillera. W.R. Dickenson and W.D. Payne, eds., Arizona Geol. Soc. Digest 14, p. 71-77.
Burnham, C.W. (1985) Energy release in subvolcanic environments: Implications for breccia formation. Econ. Geol. 80, 1515-1522.
Burnham, C.W. and Davis, N.F. (1971) The role of H_2O in silicate melts. I. P-V-T relations in the system $NaAlSi_3O_8$-H_2O. Amer. J. Sci. 270, 54-79.
Burnham, C.W., Holloway, J.R. and Davis, N.F. (1969) Thermodynamic Properties of Water to 1000°C and 10,000 bars. Geol. Soc. Amer. Special Paper 132, 96 pp.
Burnham, C.W. and Ohmoto, H. (1980) Late-stage processes of felsic magmatism. In: Granitic Magmatism and Related Mineralization. S. Ishihara and S. Takenouchi, eds., The Soc. of Mining Geologists of Japan, Tokyo, p. 1-12.
Butt, C.R.M. (1981) The nature and origin of the lateritic weathering mantle with particular reference to Western Australia. In: Geophysical Prospecting in Deeply-Weathered Terranes. J.E. Glober and D.F. Groves, eds., Univ. Western Australia Extension Service Pub. No. 66, p. 11-29.
Butt, C.R.M. and Nickel, E.H. (1981) Mineralogy and geochemistry of ore weathering of the disseminated nickel sulfide deposit at Mt. Keith, Western Australia. Econ. Geol. 76, 1736-1751.
Candela, P.A. and Holland, H.D. (1984) The partitioning of copper and molybdenum between silicate melts and aqueous fluids. Geochim. Cosmochim. Acta 48, 373-380.
Candela, P.A. and Holland, H.D. (1984) A mass transfer model for Cu and Mo in magmatic hydrothermal systems: The origin of porphyry-type ore deposits. Econ. Geol. 81, 1-19.
Candela, P.A. (1986) The evolution of vapor from silicate melts: Effect on oxygen fugacity. Geochim. Cosmochim. Acta 50, 1205-1211.
Carmichael, I.S.E., Turner, F.J. and Verhoogen, J. (1974) Igneous Petrology. McGraw-Hill, New York, 739 pp.
Carothers, W.W. and Kharaka, Y.K. (1980) Stable carbon isotopes of HCO_3 in oil-field waters—implications for the origin of CO_2. Geochim. Cosmochim. Acta 44, 323-332.
Carron, J.P. and Lagache, M. (1980) Etude experimentale du fractionnement des élements Rb, Cs, Sr et Ba entre feldspaths alcalins, solutions hydrothermales et liquides silicates dans le système Q.Ab.Or.H_2O à 2 kbar entre 700 et 800°C. Bull. Mineral. 703, 571-578.
Cathles, L.M. (1977) An analysis of the cooling of intrusives by ground-water convection which includes boiling. Econ. Geol. 72, 804-826.
Chou, I-Ming and Eugster, H.P. (1977) Solubility of magnetite in supercritical chloride solutions. Amer. J. Sci. 277, 1296-1314.
Christiansen, E.C. and Lee, D.E. (1986) Fluorine and chlorine in granitoids from the Basin and Range Province, western United States. Econ. Geol. 81, 1481-1494.
Crerar, D.A. (1973) The estimation of activity coefficients of electrolyte solutions and related thermodynamic models. Rpt., available from Dept. Geol. and Geophys. Sci. Library, Princeton

University, Princeton, NJ, 195 pp.
Crerar, D.A. and Barnes, H.L. (1976) Ore solution chemistry—V. Solubilities of chalcopyrite and chalcocite assemblages in hydrothermal solution at 200-350°C. Econ. Geol. 71, 722-794.
Crerar, D.A., Susak, N.J., Borcsik, M. and Schwartz, S. (1978) Solubility of the buffer assemblage pyrite + pyrrhotite + magnetite in NaCl solutions from 200 to 350°C. Geochim. Cosmochim. Acta 42, 1427-1437.
Crerar, D., Wood, S., Brantley, S. and Bocarsly, A. (1985) Chemical controls on solubility of ore-forming minerals in hydrothermal solutions. Canadian Mineral. 23, 333-352.
Cumberlidge, J.T. and Chase, M.C. (1968) Geology of the Nickel Mountain Mine, Riddle, Oregon. In: Ore Deposits of the United States, 1933-1967. J.D. Ridge, ed., Graton-Sales, New York, pp. 1650-1672.
Cunningham, A.B. (1984) Geologically constrained hydrologic and geochemical modeling of supergene weathering processes using physical rock parameters, geochemical profiles, and modal data. Unpublished M.S. thesis, University of California, Berkeley, 122 p.
Czamanske, G.K., Ishihara, S., and Atkin, S.A. (1981) Chemistry of rock-forming minerals of the Cretaceous-Paleocene batholith in southwestern Japan and implications for magma genesis. J. Geophys. Res. 86, 10431-10469.
Davy, R. and El-Ansary, M. (1986) Geochemical patterns in the laterite profile at the Boddington Gold Deposit, Western Australia. J. Geochem. Expl. 26, 119-144.
Decker, R. and Decker, B. (1981) The eruptions of Mount St. Helens. Sci. Amer. 244, 68-83.
De Donder, Th. (1928) L'Affinité. Gauthier-Villars, Paris.
De Donder, Th. and Rysselberghe, P.V. (1936) Affinity. Stanford University Press, Stanford, CA, 142 pp.
Drude, P. and Nernst, W. (1894) Über Elektrostriktion durch freie Ionen. Zeit. Phys. Chem. 15, 79-85.
Drummond, S.E. and Ohmoto, H. (1985) Chemical evolution and mineral deposition in boiling hydrothermal systems. Econ. Geol. 80, 126-147.
Drummond, S.E. and Palmer, D.A. (1986) Thermal decarboxylation of acetate—Part II. Boundary conditions for the role of acetate in the primary migration of natural gas and the transportation of metals in hydrothermal systems. Geochim. Cosmochim. Acta 50, 825-833.
Dunn, T.M., McClure, D.S. and Pearson, R.G. (1965) Some Aspects of Crystal Field Theory. Harper and Row, New York, 115 pp.
Eisenberg, D. and Kauzmann, W. (1969) The Structure and Properties of Water. Oxford Press, New York, 296 pp.
Ellis, A.J. (1979) Explored geothermal systems. In: Geochemistry of Hydrothermal Ore Deposits, 2nd ed. H.L. Barnes, ed., Wiley-Interscience, New York, p. 632-737.
Ellis, A.J. and Mahon, W.A.J. (1977) Chemistry and Geothermal Systems. Academic Press, New York, 392 pp.
Eugster, H.P. (1985) Granites and hydrothermal ore deposits: A geochemical framework. Mineral. Mag. 49, 7-23.
Eugster, H.P. (1986) Minerals in hot water. Amer. Mineral. 71, 655-673.
Eugster, H.P. and Wones, D.R. (1962) Stability relations of the ferruginous biotite, annite. J. Petrol. 3, 82-125.
Fehn, U. (1986) The evolution of low-temperature convection cells near spreading centers: A mechanism for the formation of the Galapagos mounds and similar manganese deposits. Econ. Geol. 81, 1396-1407.
Fehn, U. and Cathles, L.M. (1986) The influence of plate movement on the evolution of hydrothermal convection cells in the oceanic crust. Tectonophys. 125, 289-312.
Feiss, P.G. (1978) Magmatic sources of copper in porphyry copper deposits. Econ. Geol. 73, 397-404.
Figgis, B.N. (1966) Introduction to Ligand Fields. Wiley-Interscience, New York, 351 pp.
Flynn, R.T. and Burnham, C.W. (1978) An experimental determination of rare earth partition coefficients between a chloride-containing vapor phase and silicate melts. Geochim. Cosmochim. Acta 42, 685-701.
Franck, E.U. (1981) Survey of selected non-thermodynamic properties and chemical phenomena of fluids and fluid mixtures. In: Chemistry and Geochemistry of Solutions at High Temperatures and Pressures. D. Rickard and F. Wickman, eds., Physics and Chemistry of the Earth, v.

13/14, Pergamon Press, New York, p. 65-88.
Franks, F. (1972) Introduction—Water, the unique chemical. In: Water. A Comprehensive Treatise. F. Franks, ed., Plenum, New York, p. 1-20.
Franks, F. (1973) The solvent properties of water. In: Water. A Comprehensive Treatise, v. 2. F. Franks, ed., Plenum, New York, p. 1-54.
Franks, F., ed. (1982) Water. A Comprehensive Treatise, v. 7. Plenum, New York, 484 pp.
Frantz, J.D. and Marshall, W.L. (1984) Electrical conductances and ionization constants of salts, acids, and bases in supercritical aqueous fluids: I. Hydrochloric acid from 100° to 700°C and at pressures to 4000 bars. Amer. J. Sci. 284, 651-667.
Frantz, J.D., Popp, R.K. and Boctor, N.Z. (1981) Mineral-solution equilibria. V. Solubilities of rock-forming minerals in supercritical fluids. Geochim. Cosmochim. Acta 45, 69-77.
Fyfe, W.S. and Henley, R.W. (1973) Some thoughts on chemical transport processes with particular reference to gold. Minerals Sci. Eng. 5, 295-298.
Fyfe, W.S. and Kerrich, R. (1984) Gold: Natural concentration processes. In: Gold '82, the Geology, Geochemistry, and Genesis of Gold Deposits. R.P. Foster, ed., Geol. Soc. Zimbabwe Spec. Publ. 1, p. 99-128.
Garrels, R.M. and Christ, C.L. (1965) Solutions, Minerals and Equilibria. Harper and Row, New York, 450 pp.
Giordano, T.H. (1985) A preliminary evaluation of organic ligands and metal-organic complexing in Mississippi Valley-type ore solutions. Econ. Geol. 80, 96-106.
Giordano, T.H. and Barnes, H.L. (1981) Lead transport in Mississippi Valley-type ore solutions. Econ. Geol. 76, 2200-2211.
Golightly, J.P. (1979) Nickeliferous laterites: A general description. In: International Laterite Symposium. D.J.I. Evans and R.S. Shoemaker, eds., Soc. Mining Engineers, New York, pp. 3-23.
Golightly, J.P. (1981) Nickeliferous laterite deposits. In: Econ. Geol. 75th Anniv. Vol. (1905-1980). B.J. Skinner, ed., pp. 710-734.
Grubb, P.L.C. (1970) Mineralogy, geochemistry, and genesis of the bauxite deposits on the Gove and Mitchell Plateaus, northern Australia. Mineralia Deposita 5, 248-272.
Grubb, P.L.C. (1971) Genesis of the Weipa bauxite deposits, N.E. Australia. Mineralia Deposita 5, 265-274.
Grubb, P.L.C. (1979) Genesis of bauxite deposits in the lower Amazon basin and Guianas coastal plain. Econ. Geol. 74, 735-750.
Gunow, A.J., Ludington, S., and Munoz, J.L. (1980) Fluorine in micas from the Henderson molybdenite deposit, Colorado. Econ. Geol. 75, 1127-1137.
Gurney, R.W. (1962) Ionic Processes in Solution. Dover, New York, 275 pp.
Gustafson, L.B. and Hunt, J.P. (1975) The porphyry copper deposit at El Salvador, Chile. Econ. Geol. 70, 857-912.
Hamann, S.D. (1981) Properties of electrolyte solutions at high pressures and temperatures. In: Chemistry and Geochemistry of Solutions at High Temperatures and Pressures. D. Rickard and F. Wickman, eds., Physics and Chemistry of the Earth, v. 13/14, Pergamon Press, New York, p. 89-111.
Haselton, H.T., Jr. and D'Angelo, W.M. (1986) Tin and tungsten solubilities (500-700°C, 1 kbar) in the presence of a synthetic quartz monzonite [abs]. Amer. Geophys. Union, EOS 67, 388.
Heald, P., Foley, N.K. and Hayba, D.O. (1987) Comparative anatomy of volcanic-hosted epithermal deposits: Acid-sulfate and adularia-seriate types. Econ. Geol. 82, 1-26.
Helgeson, H.C. (1967) Thermodynamics of complex dissociation in aqueous solution at elevated temperatures. J. Phys. Chem. 71, 3121-3136.
Helgeson, H.C. (1968) Evaluation of irreversible reactions in geochemical processes involving minerals and aqueous solutions—I. Thermodynamic relations. Geochim. Cosmochim. Acta 32, 853-877.
Helgeson, H.C. (1969) Thermodynamics of hydrothermal systems at elevated temperatures and pressures. Amer. J. Sci. 267, 729-804.
Helgeson, H.C. (1981) Prediction of the thermodynamic properties of electrolytes at high temperatures and pressures. In: Chemistry and Geochemistry of Solutions at High Temperatures and Pressures. D. Rickard and F. Wickman, eds., Physics and Chemistry of the Earth, v. 13/14, Pergamon Press, New York, p. 133-177.

Helgeson, H.C., Delany, J.M., Nesbitt, H.W., and Bird, D.K. (1978) Summary and critique of the thermodynamic properties of rock-forming minerals. Amer. J. Sci. 278-A, 1-229.

Helgeson, H.C. and Kirkham, D.H. (1974) Theoretical prediction of the thermodynamic behavior of aqueous electrolytes at high pressures and temperatures: I. Summary of the thermodynamic/electrostatic properties of the solvent. Amer. J. Sci. 274, 1089-1198.

Helgeson, H.C. and Kirkham, D.H. (1974) Theoretical prediction of the thermodynamic behavior of aqueous electrolytes at high pressures and temperatures: II. Debye-Hückel parameters for activity coefficients and relative partial molal properties. Amer. J. Sci. 274, 1199-1261.

Helgeson, H.C. and Kirkham, D.H. (1976) Theoretical prediction of the thermodynamic properties of aqueous electrolytes at high pressures and temperatures: III. Equation of state for aqueous species at infinite dilution. Amer. J. Sci. 276, 97-240.

Helgeson, H.C., Kirkham, D.H. and Flowers, G.C. (1981) Theoretical prediction of the thermodynamic behavior of aqueous electrolytes at high pressures and temperatures: IV. Calculation of activity and osmotic coefficients and apparent molal and standard and relative partial molal properties to 600°C and 5 kb. Amer. J. Sci. 281, 1249-1493.

Helgeson, H.C. and Lichtner, P. (1987) Fluid flow and mineral reactions at high temperatures and pressures. J. Geol. Soc. London 144, 313-326.

Hemley, J.J. (1959) Some mineralogical equilibria in the system K_2O-Al_2O_3-SiO_2-H_2O. Amer. J. Sci. 257, 241-270.

Hemley, J.J., Cygan, G.L. and d'Angelo, W.M. (1986) Effect of pressure on ore mineral solubilities under hydrothermal conditions. Geol. 14, 377-379.

Hemley, J.J., Hostetler, P.B., Gude, A.J., and Mountjoy, W.T. (1969) Some stability relations of alunite. Econ. Geol. 64, 599-612.

Hemley, J.J. and Jones, W.R. (1964) Chemical aspects of hydrothermal alteration with emphasis on hydrogen metasomatism. Econ. Geol. 59, 538-569.

Hemley, J.J., Montoya, J.W., Marinenko, J.W. and Luce, R.W. (1980) Equilibria in the system Al_2O_3-SiO_2-H_2O and some general implications for alteration/mineralization processes. Econ. Geol. 75, 210-228.

Henley, R.W. (1985) The geothermal framework of epithermal deposits. In: Geology and Geochemistry of Epithermal Systems. B.R. Berger and P.M. Bethke, eds., Reviews in Econ. Geol. v. 2, Econ. Geol. Publ. Co., El Paso, Texas, p. 1-24.

Henley, R.W. and Brown, K.L. (1985) A practical guide to the thermodynamics of geothermal fluids and hydrothermal ore deposits. In: Geology and Geochemistry of Epithermal Systems. B.R. Berger and P.M. Bethke, eds., Reviews in Econ. Geol. v. 2, Econ. Geol. Publ. Co., El Paso, Texas, p. 25-44.

Henley, R.W. and Ellis, A.J. (1983) Geothermal systems ancient and modern: A geochemical review. Earth Sci. Rev. 19, 1-50.

Henley, R.W. and McNabb, A. (1978) Magmatic vapor plumes and ground-water interaction in porphyry copper emplacement. Econ. Geol. 73, 1-20.

Henley, R.W., Norris, R.J. and Paterson, C.J. (1976) Multistage ore genesis in the New Zealand geosyncline—A history of post-metamorphic lode emplacement. Mineralium Deposita 11, 180-196.

Henley, R.W., Truesdell, A.H., Barton, P.B., Jr. and Whitney, J.A. (1984) Fluid-Mineral Equilibria in Hydrothermal Systems. Reviews in Econ. Geol. v. 1, Econ. Geol. Publ. Co., El Paso, Texas, 267 pp.

Hennet, R. (1987) The effect of organic complexing and CO_2 partial pressure on metal transport in low-temperature hydrothermal systems. Ph.D. Dissertation, Princeton Univ., 308 pp.

Holland, H.D. (1959) Some applications of thermochemical data to problems of ore deposits. I. Stability relations among the oxides, sulfides, sulfates and carbonates of ore and gangue minerals. Econ. Geol. 54, 184-233.

Holland, H.D. (1965) Some applications of thermochemical data to problems of ore deposits. II. Mineral assemblages and the composition of ore-forming fluids. Econ. Geol. 60, 1101-1166.

Holland, H.D. (1972) Granites, solutions, and base metal deposits. Econ. Geol. 67, 281-301.

Holland, H.D. and Malinin, S.D. (1979) Solubility and occurrence of non-ore minerals. In: Geochemistry of Hydrothermal Ore Deposits, 2nd ed. H.L. Barnes, ed., Wiley-Interscience, New York, p. 461-508.

Hollister, V.F. (1978) Geology of the Porphyry Copper Deposits of the Western Hemisphere. American Institute of Mining, Metallurgy and Petroleum Engineers, New York, pp. 29-137.

Hollister, L.S. and Crawford, M.L., eds. (1981) Short Course in Fluid Inclusions: Applications to Petrology. Mineral. Assoc. Canada, Short Course Handbook, v. 6, Toronto, 304 pp.
Horne, R.H. (1969) Marine Chemistry: The Structure of Water and the Chemistry of the Hydrosphere. Wiley-Interscience, New York, 568 pp.
Horne, R.A., ed. (1972) Water and Aqueous Solutions. Wiley-Interscience, New York, 837 pp.
Huebner, J.S. (1971) Buffering techniques for hydrostatic systems at elevated pressures. In: Research Techniques for High Pressure and High Temperature. G.C. Ulmer, ed., Springer-Verlag, New York, p. 123-178.
Huheey, J.E. (1978) Inorganic Chemistry, 2nd ed. Harper and Row, New York, 889 pp.
Hutchinson, R.W. (1981) Mineral deposits as guides to supracrustal evolution. In: Evolution of the Earth. R.J. O'Conel and W.S. Fyfe, eds., Amer. Geophys. Union 5, p. 120-132.
Irish, D.E. and Brooker, M.H. (1976) Raman and infrared spectral studies of electrolytes. In: Advances in Infrared and Raman Spectroscopy, v. 2. R.J.H. Clark and R.E. Hester, eds., Heyden, London, p. 212-311.
Irvine, T.N., Keith, D.W., and Todd, S.G. (1983) The J-M platinum and palladium reef of the Stillwater Complex, Montana. II. Origin by double diffusive convection magma mixing and applications for the Bushveld Complex. Econ. Geol. 78, 1287-1334.
Ishihara, S. (1977) The magnetite-series and ilmenite-series rocks. Mining Geol. 27, 293-305.
Ishihara, S., Sawata, H., Arpornsuwan, S., Busaracombe, P., and Bungbrakearti, N. (1979) The magnetite-series and ilmenite-series granitoids and their bearing on tin mineralization, particularly of the Malay Peninsula region. Geol. Soc. Malaysia Bull. 11, 103-110.
Jackson, K.S., Jonasson, I.R. and Skippen, G.B. (1978) The nature of metals-sediment-water interactions in freshwater bodies, with emphasis on the role of organic matter. Earth Sci. Rev. 14, 97-146.
Jackson, S.A. and Beales, F.W. (1967) An aspect of sedimentary basin evolution: The concentration of Mississippi Valley-type ores during late stages of diagenesis. Bull. Can. Petroleum Geol. 15, 383-433.
Jacobs, D.C. and Parry, W.T. (1979) Geochemistry of biotite in the Santa Rita porphyry copper deposit, New Mexico. Econ. Geol. 74, 860-887.
Kesler, S.E. (1973) Copper, molybdenum, and gold abundances in porphyry copper deposits. Econ. Geol. 68, 106-112.
Kharaka, Y.K., Carothers, W.W. and Rosenbauer, R.J. (1983) Thermal decarboxylation of acetic acid: Implications for origin of natural gas. Geochim. Cosmochim. Acta 47, 397-402.
Khodakovskiy, I.L. and Yelkin, A. Ye. (1975) Measurement of the solubility of zincite in aqueous NaOH at 100, 150 and 200°C. Geochem. Int. 12, 127-133.
Kilinc, I.A. (1969) Experimental Metamorphism and Anatexis of Shales and Graywackes. Ph.D. dissertation, Pennsylvania State University, State College, PA.
Kilinc, I.A. and Burnham, C.W. (1972) Partitioning of chloride between a silicate melt and coexisting aqueous phase from 2 to 8 kilobars. Econ. Geol. 67, 231-235.
Kwak, T.A.P., Brown, W.M., Abeysinghe, P.B. and Tan, T.H. (1986) Fe solubilities in very saline hydrothermal fluids: Their relation to zoning in some ore deposits. Econ. Geol. 81, 447-465.
Lacy, W.C. and Hosmer, H.L. (1956) Hydrothermal leaching in central Peru. Econ. Geol. 51, 69-79.
Lehmann, B. (1982) Metallogeny of tin: Magmatic differentiation versus geochemical heritage. Econ. Geol. 77, 50-59.
Lewis, G.N. and Randall, M. (1961) Thermodynamics, 2nd ed. Revised by K.S. Pitzer and L. Brewer, McGraw-Hill, New York, 723 pp.
Lichtner, P.C. (1985) Continuum model for simultaneous chemical reactions and mass transport in hydrothermal system. Geochim. Cosmochim. Acta 49, 779-800.
Lindsay, W.T. (1980) Estimation of concentration quotients for ionic equilibria in high temperature water: The model substance approach. Proceedings, 41st Int'l. Water Conference, Pittsburgh, PA, p. 284-294.
Lowell, J.D. and Guilbert, J.M. (1970) Lateral and vertical zoning in porphyry ore deposits. Econ. Geol. 65, 373-408.
Macqueen, R.W. and Powell, T.G. (1983) Organic geochemistry of the Pine Point lead-zinc ore field and region, Northwest Territories, Canada. Econ. Geol. 78, 1-25.
Mann, A.W. (1984) Mobility of gold and silver in lateritic weathering profiles: Some observations from western Australia. Econ. Geol. 79, 38-49.

Mann, A.W. and Ollier, C.D. (1985) Chemical diffusion and ferricrete formation, Catena Supplement, 6, 152-157.

Manning, D.A.C. (1981) The effect of fluorine on liquidus phase relationships in the system Qz-Ab-Or with excess water at 1 kb. Contrib. Mineral. Petrol. 76, 206-215.

Marshall, W.L. (1972) A further description of complete equilibrium constants. J. Phys. Chem. 76, 720-731.

Meyer, C., and Hemley, J.J. (1967) Wall rock alteration. In: Geochemistry of Hydrothermal Ore Deposits. H.L. Barnes, ed., Holt, Rinehart and Winston, New York, p. 166-235.

Meyer, C. (1985) Ore metals through geological history. Science 227, 1421-1428.

Meyer, C., Shea, E., Goddard, C.C., Zeihen, L.G., Guilbert, J.M., Miller, R.N., McAleer, J.F., Brox, G.B., Ingersoll, R.G., Burns, G.J., and Wigal, T. (1968). In: Ore Deposits in the United States 1933/1967. J.D. Ridge, ed., American Institute of Mining, Metallurgy and Petroleum Engineers, New York, p. 1373-1416.

Millero, F.J. (1971) The partial molal volumes of electrolytes in aqueous solutions. In: Water and Aqueous Solutions. R.A. Horne, ed., Wiley, New York, p. 519-564.

Montoya, J.W. and Hemley, J.J. (1975) Activity relations and stabilities in alkali feldspar and mica alteration reactions. Econ. Geol. 70, 577-594.

Morel, F.M.M. (1983) Principles of Aquatic Chemistry. Wiley-Interscience, New York, 446 pp.

Munoz, J.L. (1984) F^-OH and Cl^-OH exchange in micas with applications to hydrothermal ore deposits: Micas. In: S.W. Bailey, ed., Reviews in Mineralogy, 13, 469-494.

Munoz, J.L. and Swenson, A. (1981) Chloride-hydroxl exchange in biotite: An estimation of relative HCl/HF activities in hydrothermal fluids. Econ. Geol. 766, 2212-2221.

Narasimhan, T.N., Witherspoon, P.A., and Edwards, E.A. (1978) Numerical model for saturated-unsaturated flow in deformable porous media, 2. The algorithm. Water Resources Research 14, 255-261.

Nancollas, G.H. (1970). The thermodynamics of metal complex and ion-pair formation. Coord. Chem. Rev. 5, 379-415.

Neilson, G.W. and Enderby, J.E., eds. (1986) Water and Aqueous Solutions. Adam Hilger, Bristol, England, 349 pp.

Nissenbaum, A. and Swaine, D.J. (1976) Organic matter-metal interactions in recent sediments: The role of humic substances. Geochim. Cosmochim. Acta 40, 809-816.

Nordstrom, D.K. and Munoz, J.L. (1985) Geochemical Thermodynamics. Benjamin/Cummings, Inc., Menlo Park, CA, 477 pp.

Norton, D. (1978) Sourcelines, sourceregions, and pathlines for fluids in hydrothermal systems related to cooling plutons. Econ. Geol. 73, 21-28.

Norton, D.L. (1984) Theory of hydrothermal systems. Ann. Rev. Earth Planet. Sci. 12, 155-177.

Norton, D. and Knight, J. (1977) Transport phenomena in hydrothermal systems: Cooling plutons. Amer. J. Sci. 277, 937-981.

Ohmoto, H. (1972) Systematics of sulfur and carbon isotopes in hydrothermal ore deposits. Econ. Geol. 67, 551-579.

Ohmoto, H., and Kerrick, D. (1977) Devolatilization equilibria in graphitic systems. Amer. J. Sci. 277, 1013-1044.

Ohmoto, H. and Rye, R.O. (1979) Isotopes of sulfur and carbon. In: Geochemistry of Hydrothermal Ore Deposits, 2nd ed. H.L. Barnes, ed., Wiley-Interscience, New York, p. 509-567.

Pearson, R.G. (1963) Hard and soft acids and bases. J. Amer. Chem. Soc. 85, 3533-3539.

Pitzer, K.S. (1979) Theory: Ion interaction approach. In: Activity Coefficients in Electrolyte Solutions, v. I. R.M. Pytkowicz, ed., CRC Press, Boca Raton, Florida, p. 157-208.

Pollard, P.J., Taylor, R.G., and Cuff, C. (1983) Metallogeny of tin: Magmatic differentiation versus geochemical heritage—A discussion. Econ. Geol. 78, 543-545.

Prigogine, I. (1955) Introductiion to Thermodynamics of Irreversible Processes. John Wiley, New York, 119 p.

Quist, A.S. and Marshall, W.L. (1968) Electrical conductances of aqueous sodium chloride solutions from 0 to 800° C and at pressures to 4000 bars. J. Phys. Chem. 72, 684-703.

Reuter, J.H. and Perdue, E.M. (1977) Importance of heavy metal-organic matter interactions in natural waters. Geochim. Cosmochim. Acta 41, 325-334.

Ringwood, A.E. (1979) Origin of the Earth and Moon. Springer, New York, 295 p.

Roedder, E. (1979) Fluid inclusions as samples of ore fluids. In: Geochemistry of Hydrothermal Ore Deposits, 2nd ed. H.L. Barnes, ed., Wiley-Interscience, New York, p. 684-737.

Rose, A.W. and Burt, D.M. (1979) Hydrothermal alteration. In: Geochemistry of Hydrothermal Ore Deposits, 2nd ed. H.L. Barnes, ed., Wiley-Interscience, New York, p. 173-235.

Ruaya, J.R. and Seward, T.M. (1986) The stability of chlorozinc (II) complexes in hydrothermal solutions up to 350°C. Geochim. Cosmochim. Acta 50, 651-661.

Rye, R.O. and Ohmoto, H. (1974) Sulfur and carbon isotopes and ore genesis: A review. Econ. Geol. 69, 826-842.

Sadleir,. S.B. and Gilkes, R.J. (1976) Bauxite in relation to parent material. J. Geol. Soc. Australia 23, 333-344.

Samana, J.C. (1986) Ore Fields and Continental Weathering. Van Nostrand-Reinhold, New York, 124-129.

Sangameshwar, S.R. and Barnes, H.L. (1983) Supergene processes in zinc-lead-silver sulfide ores in carbonates. Econ. Geol. 78, 1379-1397.

Sawkins, F.J. (1984) Metal Deposits in Relation to Plate Tectonics. Springer Verlag, Berlin, 330 pp.

Seward, T.M. (1973) Thio complexes of gold and the transport of gold in hydrothermal ore solutions. Geochim. Cosmochim. Acta 37, 379-399.

Seward, T.M. (1976) The stability of chloride complexes of silver in hydrothermal solutions up to 350°C. Geochim. Cosmochim. Acta 40, 1329-1341.

Seward, T.M. (1981) Metal complex formation in aqueous solutions at elevated temperatures and pressures. In: Chemistry and Geochemistry of Solutions at High Temperatures and Pressures. D. Rickard and F. Wickman, eds., Physics and Chemistry of the Earth, v. 13/14, Pergamon Press, New York, p. 113-132.

Seward, T.M. (1983) The transport and deposition of gold in hydrothermal systems. In: Gold '82: The Geology, Geochemistry and Genesis of Gold Deposits. R.P. Foster, ed., Geol. Soc. Zimbabwe, Spec. Publ. No. 1, p. 165-181.

Seward, T. (1984) The formation of lead (II) chloride complexes to 300°C: A spectrophotometric study. Geochim. Cosmochim. Acta 48, 121-134.

Shanks, W.C. and Bischoff, J.L. (1977) Ore transport and deposition in the Red Sea geothermal system: A geochemical model. Geochim. Cosmochim. Acta 41, 1507-1519.

Sillitoe, R.H. (1972) A plate tectonic model for the origin of porphyry copper deposits. Econ. Geol. 76, 184-197.

Skinner, B.J. (1979) The many origins of hydrothermal mineral deposits. In: Geochemistry of Hydrothermal Ore Deposits, 2nd ed. H.L. Barnes, ed., Wiley-Interscience, New York, p. 1-21.

Slack, J.F. (1980) Multistage vein ores of the Lake City district, western San Juan Mountains, Colorado. Econ. Geol. 75, 963-991.

Smith, R.M. and Martell, A.E. (1976) Critical Stability Constants, v. 4: Inorganic Complexes. Plenum, New York, 257 pp.

Sohn, M.L. and Hughes, M.C. (1981) Metal ion formation constants of some sedimentary humic acids with Zn (II), Cu (II), and Cd (II). Geochim. Cosmochim. Acta 45, 2393-2399.

Stoffregen, R. (1986) Observations on the behavior of gold during supergene oxidation at Summitville, Colorado, U.S.A., and implications for electron stability in the weathering environment. Appl. Geochem. 1, 549-558.

Stumm, W. and Morgan, J.J. (1981) Aquatic Chemistry, 2nd ed. Wiley-Interscience, New York, 780 pp.

Susak, N. and Crerar, D. (1982) Factors controlling mineral zoning in hydrothermal ore deposits. Econ. Geol. 77, 476-482.

Susak, N. and Crerar, D. (1985) Spectra and coordination changes of transition metals in hydrothermal solutions: Implications for ore genesis. Geochim. Cosmochim. Acta 49, 555-564.

Sverjensky, D.A. (1986) Genesis of Mississippi Valley-type lead-zinc deposits. Ann. Rev. Earth Planet. Sci. 14, 177-199.

Tardy, I. and Nahon, D. (1985) Geochemistry of laterites, stability of Al-goethite, Al-hematite, and Fe^{3+}-Kaolinite in bauxites and ferricretes: An approach to the mechanism of concretion formation. Amer. J. Sci. 285, 865-903.

Taylor, H.P. (1979) Oxygen and hydrogen isotope relationships in hydrothermal mineral deposits. In: Geochemistry of Hydrothermal Ore Deposits, 2nd ed. H.L. Barnes, ed., Wiley-Interscience, New York, p. 236-277.

Taylor, R.G. (1979) Geology of Tin Deposits. Elsevier, Amsterdam, 543 pp.
Taylor, S.R. and McClennan, S.M. (1985) The continental crust: Its composition and evolution. An Examination of the Geochemical Record Preserved in Sedimentary Rocks. Blackwell Scientific Publications, Oxford, 301 pp.
Titley, S.R. and Beane, R.E. (1981) Porphyry copper deposits. In: Econ. Geol. 75th Anniv. Vol., B.J. Skinner, ed., p. 214-269.
Titley, S.R., Thompson, R.C., Haynes, F.M., Manske, S.L., Robinson, L.C., and White, J.L. (1986) Evolution of fractures and alteration in the Sierrita-Espernanza hydrothermal system, Pima Country, Arizona. Econ. Geol. 81, p. 343-370.
Tremaine, P.R., Sway, K. and Barbero, J.A. (1986) The apparent molar heat capacity of aqueous hydrochloric acid from 10 to 140°C. J. Sol. Chem. 15, 1-22.
Troeh, G., Jabro, J.D., and Kirkham, D. (1982) Gaseous diffusion equations for porous materials. Geoderma 27, 239-253.
Turcotte, D.L. and Schubert, T. (1973) Frictional heating on the descending lithosphere. J. Geophys. Res. 78, 5876-5886.
Vogel, L.M., McClure, D.S. and Crerar, D.A. (1987) A spectroscopic study of iron (II) chloro complexes in LiCl-DCl-D_2O solutions. Inorg. Chem. 26, 308-313.
Von Damm, K.L., Edmond, J.M., Grant, B., Measures, C.I., Walden, B. and Weiss, R.F. (1985a) Chemistry of submarine hydrothermal solutions at 21° N, East Pacific Rise. Geochim. Cosmochim. Acta 49, 2197-2220.
Von Damm, K.L., Edmond, J.M., Measures, C.I. and Grant, B. (1985b) Chemistry of submarine hydrothermal solutions at Guaymas Basin, Gulf of California. Geochim. Cosmochim. Acta 49, 2221-2238.
Wallace, A.B. (1979) Possible signatures of buried porphyry-copper deposits in middle to late Tertiary volcanic rocks of western Nevada. In: Proceedings of the Fifth Quadrennial IAGOD Symposium. J.D. Ridge, ed., University of Nevada-Mackay School of Mines, Reno, Vol. 2, p. 69-76.
Wallace, S.R., Muncaster, N.K., Jonson, D.C., MacKenzie, W.B., Bookstrom, A.A., and Surface, V.E. (1968) Multiple intrusion and mineralization at Climax, Colorado. In: Ore Deposits in the United States 1933/1967. J.D. Ridge, ed., American Institute of Mining, Metallurgy and Petroleum Engineers, New York, p. 605-640.
Walther, J.V. and Wood, B.J. (1986) Mineral-fluid reaction rates. In: Fluid-rock interactions during metamorphism. J.V. Walther and B.J. Wood, eds., Advances in Physical Geochemistry, v. 5, Springer-Verlag, New York, p. 194-213.
Wanke, H.G., Dreibus, G.D., and Jagoutz, E. (1984) Mantle chemistry and accretion history of the earth. In: Archean History of the Earth. A. Kroner, ed., Springer-Verlag, Berlin, p. 1-22.
Webster, E.A. and Holloway, J.R. (1980) The partitioning of REE'S, Sc, Rb and Cs between a silicic melt and a Cl fluid. EOS Amer. Geophys. Union Trans. 61, 1152.
Webster, J.G. (1986) The solubility of gold and silver in the system Au-Ag-S-O_2-H_2O at 25°C and 1 atm. Geochim. Cosmochim. Acta 50, 1837-1845.
Webster, J.G. and Mann, A.W. (1984) The influence of climate, geomorphology and primary geology on the supergene migration of gold and silver, J. Geochem. Expl. 22, 21-42.
Weissberg, B.G., Browne, P.L. and Seward, T.M. (1979) Ore metals in active geothermal systems. In: Geochemistry of Hydrothermal Ore Deposits, 2nd ed. H.L. Barnes, ed., Wiley-Interscience, New York, p. 738-780.
White, W.H., Bookstrom, A.A., Kamilli, R.J., Ganster, M.W., Smith, R.P., Ranta, D.E., and Steininger, R.C. (1981) Character and origin of Climax-type molybdenum deposits. Econ. Geol. 75th Anniv. Vol. B.J. Skinner, ed., p. 270-316.
Whitney, J.A. (1975) Vapor generation in a quartz monzonite magma: A synthetic model with application to porphyry copper deposits. Econ. Geol. 70, 346-358.
Whitney, J.A., Hemley, J.J. and Simon, F.O. (1985) The concentration of iron in chloride solutions equilibrated with synthetic granitic compositions: The sulfur-free system. Econ. Geol. 80, 444-460.
Wiersma, E.L. and Rimstidt, J.D. (1984) Rates of reaction of pyrite and marcasite with ferric iron at pH: 2. Geochim. Cosmochim. Acta 48, 85-92.
Willey, L.M., Kharaka, Y.K., Presser, T.S., Rapp, J.B. and Barnes, I. (1975) Short chain aliphatic acid anions in oil field waters and their contribution to the measured alkalinity. Geochim.

Cosmochim. Acta 39, 1707-1711.
Wilson, G.A. and Eugster, H.P. (1984) Cassiterite solubility and tin-chloride speciation in supercritical solutions [abs]. Geol. Soc. Amer. Abstr. Program 16, 696.
Wolery, T.J. (1979) Calculation of chemical equilibrium between aqueous solution and minerals: The EQ3/6 soft-wares package. Univ. California Lawrence Livermore Lab. Bull. 526658, 31 p.
Wones, D.R. and Eugster, H.P. (1965) Stability of biotite: Experiment, theory and applications. Amer. Mineral. 50, 1228-1272.
Wood, S.A. and Crerar, D.A. (1985) A numerical method for obtaining multiple linear regression parameters with physically realistic signs and magnitudes: Applications to the determination of equilibrium constants from solubility data. Geochim. Cosmochim. Acta 49, 165-172.
Wood, S.A., Crerar, D.A. and Borcsik, M.P. (1987) Solubility of the assemblage pyrite-pyrrhotite-magnetite-sphalerite-galena-gold-stibnite-bismuthinite-argentite-molybdenite in H_2O-NaCl-CO_2 solutions from 200° to 350°C. Econ. Geol. 81, in press.
Wood, S., Crerar, D., Brantley, S. and Borcsik, M. (1984) Mean molal stoichiometric activity coefficients of alkali halides and related electrolytes in hydrothermal solutions. Amer. J. Sci. 284, 668-705.
Wood, B.J. and Walther, J.V. (1983) Rates of hydrothermal reactions. Science 222, 413-415.
Woodward, L.A. (1986) Tectonic origin of fractures for fissure vein emplacement in the Boulder batholith and adjacent rocks, Montana. Econ. Geol. 81, 1387-1395.